

**SYNTHESIS AND STUDIES OF  $\pi$ -EXTENDED  
SQUARAINES AND CATION PROBES DERIVED FROM  
CONJUGATED BISPYRROLES**

THESIS SUBMITTED TO  
**THE UNIVERSITY OF KERALA**  
FOR THE DEGREE OF  
**DOCTOR OF PHILOSOPHY**  
IN CHEMISTRY  
UNDER THE FACULTY OF SCIENCE

*By*  
**PRIYA CAROL**



**PHOTOSCIENCES AND PHOTONICS GROUP  
CHEMICAL SCIENCES AND TECHNOLOGY DIVISION  
NATIONAL INSTITUTE FOR INTERDISCIPLINARY SCIENCE AND TECHNOLOGY  
CSIR, TRIVANDRUM - 695019  
KERALA, INDIA**

DECEMBER 2008

## DECLARATION

I hereby declare that the matter embodied in the thesis entitled: **“Synthesis and Studies of  $\pi$ -Extended Squaraines and Cation Probes Derived from Conjugated Bispyrroles”** is the result of the investigations carried out by me at the Photosciences and Photonics Group, Chemical Sciences and Technology Division, National Institute for Interdisciplinary Science and Technology (NIIST), CSIR, Trivandrum, under the supervision of Dr. A. Ajayaghosh and the same has not been submitted elsewhere for any other degree.

In keeping with the general practice of reporting scientific observations, due acknowledgement has been made wherever the work described is based on the findings of other investigators.

  
Priya Carol

**National Institute for Interdisciplinary Science and Technology  
(NIIST)**

*(Formerly Regional Research Laboratory)*



**Council of Scientific & Industrial Research  
(CSIR)**

Industrial Estate P.O., Trivandrum - 695 019  
Kerala, INDIA



A. Ajayaghosh, F. A. Sc.  
Scientist  
Photosciences and Photonics Section  
Chemical Sciences and Technology  
Division

Tel: 91-471-2515 306  
Fax: +91-471-2491 712  
E-mail: [ajayaghosh62@gmail.com](mailto:ajayaghosh62@gmail.com)

December 5, 2008

**CERTIFICATE**

This is to certify that the work embodied in the thesis entitled:  
**“Synthesis and Studies of  $\pi$ -Extended Squaraines and Cation Probes  
Derived from Conjugated Bispyrroles”** has been carried out by Ms. Priya  
Carol under my supervision at the Photosciences and Photonics Group of the  
National Institute for Interdisciplinary Science and Technology (NIIST), CSIR,  
Trivandrum and the same has not been submitted elsewhere for a degree.

A. Ajayaghosh  
(Thesis Supervisor)

## ACKNOWLEDGEMENTS

*It is with great pleasure that I extend my deep sense of gratitude to Dr. A. Ajayaghosh, my thesis supervisor, for suggesting the research problem, for his constant guidance, support and encouragement, leading to the successful completion of this work.*

*I would like to express my gratitude to Prof. M. V. George for his constant encouragement and inspiration during my stay at the National Institute for Interdisciplinary Science and Technology (NIIST).*

*I wish to thank Professor T. K. Chandrashekar, Dr. G. Vijay Nair and Professor Javed Iqbal former Directors and Dr. B. C. Pai, acting Director of NIIST, Trivandrum for providing necessary facilities and infrastructure of the laboratory for carrying out the work.*

*I would like to thank Dr. K. Radhakrishnan, Director, Dr. K. N. Ninan, former Deputy Director, PCM, Sri. N. Raveendran Pillai, GD, QRPG and Dr. N. S. Babu, PPEG, of Vikram Sarabhai Space Center, Thiruvananthapuram for supporting my research activities.*

*My Sincere thanks are also due to:*

- *Dr. Suresh Das, Head, Chemical Sciences and Technology Division, Dr. K. R. Gopidas, Dr. D. Ramaiah and Dr. K. George Thomas, scientists of the Photosciences and Photonics Group, for their help and valuable suggestions.*
- *Dr. Joby Eldo, Dr. E. Arunkumar and Ms. P. Chithra former members of the Photosciences and Photonics Group for their help and advice.*
- *Mr. S. Sreejith, Ms. K. P. Divya and other members of Photosciences and Photonics Group for their help and cooperation.*
- *Mr. Robert Philip and Mrs. Sarada Nair for general help.*
- *Mrs. Saumini Mathew for NMR spectra, Mrs. S. Viji for HRMS and Elemental Analysis, Ms. Priya A. Nair for GC-MS and IR spectra, Dr. U. Shyamaprasad and Mr. P. Guruswamy for XRD.*
- *Members of the Organic Chemistry Section and Polymer Chemistry for general help.*
- *CSIR and DST for financial assistance.*

*Priya Carol*

## PREFACE

Exploring the chemistry of functional dyes to the design of materials with tunable optical and electrical properties is a promising area in the field of advanced material research. Understanding of the structure-property relationship in these systems is essential for the development of advanced materials with better properties. Functional dyes have contributed significantly to the development of materials for photon based technologies. Squaraine dyes, with unique optical and electronic properties are a class of dyes which are being increasingly explored in this aspect. The first chapter of the thesis touches a few areas where the optical and electronic properties of squaraine dye based systems are made use of. The chapter is an overview of the literature of squaraine dye based  $\pi$ -extended near infrared (NIR) dyes, low band gap polymers and ion probes.

The second chapter describes the role of aromatic bridging units on the optical and electronic properties of a few  $\pi$ -extended squaraine dyes and the corresponding polysquaraines derived from conjugated bispyrroles. The absorption spectra of polysquaraines and the corresponding NIR dyes showed dependence on the nature of the aromatic bridging unit. The shift in the absorption spectra of the polymers from the NIR region for the dialkoxydivinylbenzene bridged squaraine dyes to the visible region for dialkoxydivinylnaphthalene bridged dye indicates lesser degree of conjugation and planarity of the conjugated backbone in the latter case. The solution state band gaps were around 1.01 to 1.52 eV and the conductivities varied from  $2 \times 10^{-5}$  to  $2 \times 10^{-9} \text{ Scm}^{-1}$ .

The third chapter of the thesis deals with the solution state and solid-state aggregation properties of  $\pi$ -extended near-IR dyes derived from the dialkoxydivinylbenzene bridged bispyrroles. Interesting changes were observed in binary solvent systems such as DMSO-water and THF-water. The UV-vis spectra of the  $\pi$ -extended dyes in binary solvent systems showed more than one absorption maximum, the intensities of which vary with solvent composition and temperature indicating the existence of interchain aggregates of the dye

molecules. In solid-state, the absorption spectra are broad and further shift towards the longer wavelength region. The optical properties of the dyes showed considerable dependence on the length and nature of the alkyl side chains and the position of attachment of these side chains to the chromophore backbone. The existence of stable H- and J-type aggregates in solution was supported by concentration dependent and temperature dependent studies.

The fourth chapter describes the synthesis and cation sensing properties of 5,5'-divinyl-2,2'-bipyridine bridged bispyrroles. Specific detection of  $Zn^{2+}$ , the spectroscopically silent  $d^{10}$  transition metal ion, in presence of other metal ions such as  $Ca^{2+}$ ,  $Mg^{2+}$ ,  $Na^+$ ,  $K^+$  has been achieved. The emission of the bipyridine bridged bispyrroles at 537 nm was significantly quenched by  $Cu^{2+}$ ,  $Ni^{2+}$ ,  $Hg^{2+}$ ,  $Co^{2+}$ , and  $Mn^{2+}$  whereas the titration of  $Zn^{2+}$  resulted in a strong orange-red emission at 635 nm ( $\Delta E_{em} = 97$  nm) through an isoemissive point at 601 nm. The spectral changes enabled the visual detection of the metal ion. The Job plot revealed a 1:1 complexation between the fluorophore and the metal ion. The Benesi-Hildebrand plot gave a binding constant of  $1.23 \times 10^5$  for  $Zn^{2+}$ . Addition of  $Zn^{2+}$  into the nonemissive bispyrrole- $Cu^{2+}$  resulted in strong orange-red emission of bispyrrole- $Zn^{2+}$  complex thereby unambiguously proving the selectivity of the molecules to the sensing of  $Zn^{2+}$ . Bispyrrole with a polyether side chain allowed the detection of  $Zn^{2+}$  under aqueous physiological conditions.

In conclusion the present thesis deals with a systematic investigation on the synthesis and studies of a few bispyrroles with different divinylaryl bridges and their use in the design of NIR dyes, polysquaraines and  $Zn^{2+}$  sensors.

## CONTENTS

	Page
Declaration	i
Certificate	ii
Acknowledgements	iii
Preface	iv
<b>Chapter 1 Squaraine Based Near-IR Dyes, Low Band Gap Systems and Cation Sensors: An Overview</b>	<b>1-34</b>
1.1 Introduction	1
1.2 Squaraine Based $\pi$ -Extended Near-IR Dyes	3
1.3 Squaraine Based Low Band Gap Polymers	12
1.4 Squaraine Based Ion Probes (Chemosensors)	20
1.5 Objectives of the Present Investigation	27
1.6 References	28
<b>Chapter 2 Low Band Gap Squaraine Dyes and Polysquaraines: Role of Aromatic Bridging Units in Optical and Conducting Properties</b>	<b>35-81</b>
2.1 Abstract	35
2.2 Introduction	36
2.3 Results and Discussion	42
2.3.1 Synthesis and Characterization of Bispyrroles <b>1a-e</b>	42
2.3.2 Photophysical Properties of the Bispyrroles <b>1a-e</b>	45
2.3.3 Synthesis and Characterization of Polysquaraines ( <b>2a-e</b> ) and $\pi$ -Extended Squaraine Dyes ( <b>3a-d</b> )	48
2.3.4 Electronic Absorption Spectra of Polysquaraines <b>2a-e</b>	52
2.3.5 Electronic Absorption Spectra of the $\pi$ -Extended Squaraine Dyes <b>3a-d</b>	54
2.3.6 Electronic Absorption Spectra of Polysquaraines and the Model Dyes in Mixed Solvent Systems: Aggregation Properties	55
2.3.7 Solid-State Absorption Spectra	61
2.3.8 Conductivity studies	63
2.3.9 X-ray Diffraction Study	64
2.4 Conclusions	66
2.5 Experimental	67

2.6	References	79
<b>Chapter 3</b>	<b>Control of Optical and Aggregation Properties of a few Bispyrrole Derived Squaraine Dyes: Effect of Alkoxy Chains of the Aromatic Bridging Moiety</b>	81-122
3.1	Abstract	82
3.2	Introduction	83
3.3	Results and Discussion	89
3.3.1	Synthesis and Characterization	89
3.3.2	Electronic Absorption Spectra of the $\pi$ -Extended Squaraine Dyes <b>2a-c</b>	91
3.3.3	Aggregation	92
3.3.3.1	Aggregation Behavior of Dyes <b>2a-c</b> in DMSO-water	92
3.3.3.2	Aggregation behavior of Dyes <b>2a-c</b> in THF-water	103
3.3.4	Solid-State Absorption Properties	111
3.3.5	X-ray Diffraction Studies	114
3.4	Conclusions	116
3.5	Experimental	117
3.6	References	120
<b>Chapter 4</b>	<b>2,2'-Bipyridine Bridged Bispyrroles: New Ratiometric Fluorescence Probes for the Selective Sensing of Zn<sup>2+</sup></b>	123-159
4.1	Abstract	123
4.2	Introduction	124
4.3	Results and Discussion	136
4.3.1	Synthesis	136
4.3.2	Optical Properties	136
4.3.3	Cation Binding Properties of <b>1a-d</b>	138
4.3.4	Cation Binding Properties of <b>1d</b> : A Selective Sensor for Zn <sup>2+</sup> under Aqueous Conditions	145
4.4	Conclusion	152
4.5	Experimental	152
4.6	References	157
	<b>List of publications</b>	160

## Chapter 1

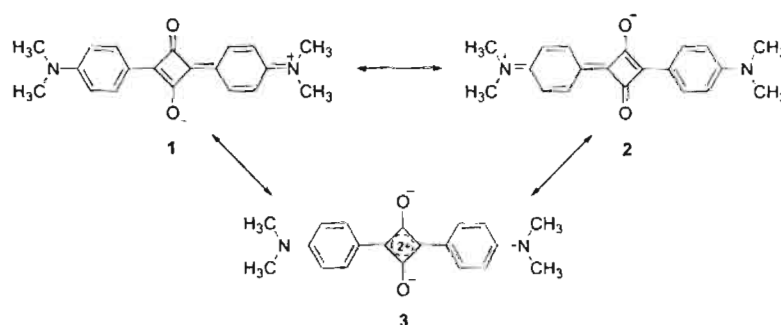
### Squaraine Based Near-IR Dyes, Low Band Gap Systems and Cation Sensors: An Overview

---

#### 1.1. Introduction

The demand for new and novel technological innovations is never ending, which ensures the design of advanced materials with new or improved properties for optimum device performance. The chemistry of functional organic dyes have made significant contributions to the development of electronic devices of the modern times, particularly in the area of photon based technologies such as optical data storage, imaging and communications.<sup>1</sup> Squaraines are one of the extensively studied class of organic dyes which are used for wide-ranging applications such as imaging,<sup>2,3</sup> nonlinear optics,<sup>4-6</sup> photovoltaics,<sup>7-9</sup> biological labeling<sup>10</sup> and photodynamic therapy.<sup>11-13</sup> Squaraine dyes typically contain an electron-deficient central four membered ring and two electron-donating groups in a donor-acceptor-donor (D-A-D) form. The intense absorption and emission properties of squaraines, which are associated with the donor-acceptor-donor type charge-transfer interaction, is suitable for applications related to photosensitization phenomenon.<sup>3,14</sup> Thus, in the past several decades, squaraine chemistry is at the center stage of research both from fundamental and technological viewpoints.

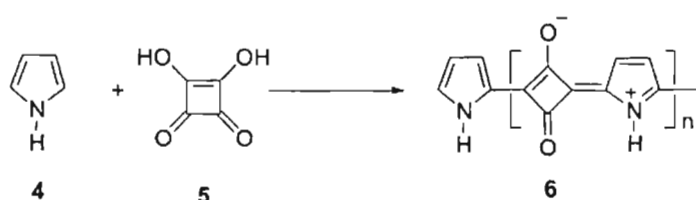
Squaraines belong to the class of polymethyne dyes with a resonance stabilized zwitterionic structure, a classical example of which is shown in Scheme 1.1. The genesis of squaraine dyes can be traced back to 1965 in a report of Triebs and Jacob, which pertains to the formation of an insoluble product **6** (Scheme 1.2) when pyrrole was reacted with 3,4-dihydroxy-3-cyclobutene-1,2-dione (squaric acid).<sup>15</sup> Later, several reports on condensation of squaric acid with electron rich aromatic or heterocyclic compounds such as *N,N*-dialkyl anilines, benzothiazoles, phenols, azulenes and pyrroles started appearing in the literature giving birth to a novel class of intensely colored and technologically important organic dyes.<sup>16-19</sup>



**Scheme 1.1**

Schmidt coined the widely accepted name 'squaraines' for this class of zwitterionic dyes.<sup>20</sup> Access to the synthesis of a variety of electron rich aromatic and heterocyclic systems, which react with squaric acid paved the way for the design of a variety of symmetrical and unsymmetrical squaraines with tunable optical properties from visible to the near-IR region. In the solid-state, due to strong intermolecular interactions and aggregation, the absorption of these dyes

becomes broad and red-shifted ( $\epsilon > 10^5 \text{ L mol}^{-1} \text{ cm}^{-1}$ ) to the near-IR region. Squaraines in general have strong absorption in the visible region and are photostable. Most of these dyes emit in the visible to near-IR region. These properties of squaraines have generated considerable interests to the design of squaraine based near-IR dyes that have potential application in photonic devices.



Scheme 1.2

## 1.2. Squaraine Based $\pi$ -Extended Near-IR Dyes

Near-IR absorbing organic dyes are important in optical recording devices based on gallium-arsenide diode lasers (780-803 nm), Nd-YAG lasers (1064 nm) and in the imaging of biological specimens. A large number of squaraines are known, which absorb and emit in the visible to the near-IR region. Two ways to achieve near-IR absorption in squaraines are the introduction of strong electron-donating groups or increasing the conjugation length. Attempts to design near-IR dyes by increasing the electron-donating ability of the amino donor group of the *N,N*-diaryl amines are known in the literature (Chart 1.1).<sup>21</sup> When the lone pair orbital of the amino donor group is forced into greater overlap with the rest of the chromogen, as in the case of the dye **8a**, the absorption maximum is shifted by 30 nm to the longer wavelength region ( $\lambda_{\text{max}} = 670 \text{ nm}$ ) when compared to the parent

dye **7** ( $\lambda_{\text{max}} = 640 \text{ nm}$ ) in the same solvent. Introduction of a hydroxyl group *ortho* to the cyclobutane ring, as in **8b**, causes an additional bathochromic shift of 4 nm with an increase in the molar absorption coefficient.

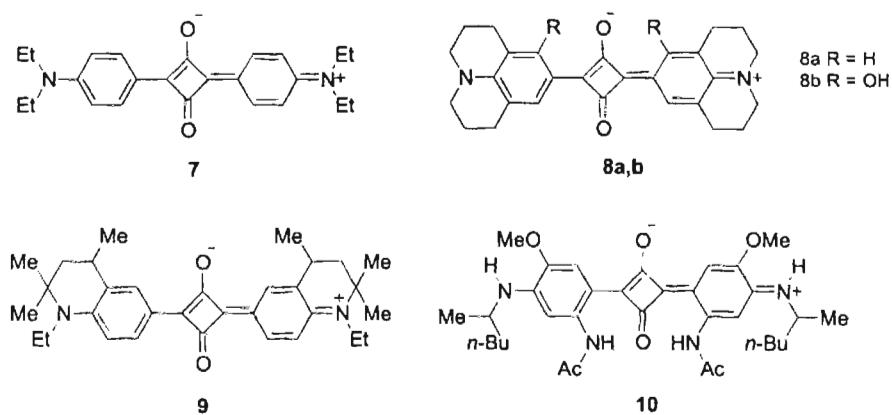


Chart 1.1

In dye **9**, there is enhanced overlap between the lone pair orbital on nitrogen and the  $\pi$ -electron system of the molecule, resulting in a further shift of the absorption to 700 nm when compared to that of **8a**. Dye **10** demonstrates clearly how increasing the number of electron-donating groups of the arylamine ring can cause a pronounced bathochromic shift of the absorption band. This dye absorbs at 708 nm in dichloromethane. This large shift when compared to **7** is due to the presence of two electron-donating groups at positions 2 and 5 relative to the electron acceptor ring. This is the first recorded arylamino squarylium dye that absorbs beyond 700 nm. Theoretical calculations confirm the high bathochromic character of the dyes and their exceptionally high absorption intensities. The

calculation also predicts the strong bathochromic effect of the 2-acylamino-4-amino-5-methoxy electron donor system, as noted for the dye **10**.

One of the major contributions to the design of squaraine based near-IR dyes come from Meier *et al.* who have reported a variety of stilbenoid (**11-17**) squaraines (Chart 1.2).<sup>22-26</sup> These stilbene-squaraine conjugates exhibit intense and sharp absorption bands with maxima between 650-900 nm ( $\epsilon > 250000 \text{ L mol}^{-1} \text{ cm}^{-1}$ ). For the series **11a-d**, it turned out that the extension of conjugation leads first to a bathochromic shift. Further extension caused a hypsochromic shift.<sup>24</sup> Enhancement of donor strength by introducing two more dialkylamino groups as in **18** or two alkoxy chains as in **19** shifted the absorption maxima of the dyes above 900 nm and showed improved solubility (Chart 1.3).<sup>27</sup> Spin coated films of the dye **19** showed red-shifted absorption bands due to J-type aggregates. The squaraine dye **19** is reported to be potentially useful for the design of optical switches operating in the infrared region.

The near-IR dye **20** with amino thiazolyl groups showed improved solubility and long wavelength absorption maximum over 900 nm.<sup>28</sup> Near-IR absorbing squaraine dyes **21** and **22** (Chart 1.4) based on perimidine<sup>29</sup> and pyrylium<sup>30</sup> derivatives respectively, absorb in the range of 700-800 nm. These dyes have potential application as photoreceptors for diode lasers and are useful in laser optical recording, laser printing, photolabelling, DNA sequencing etc.

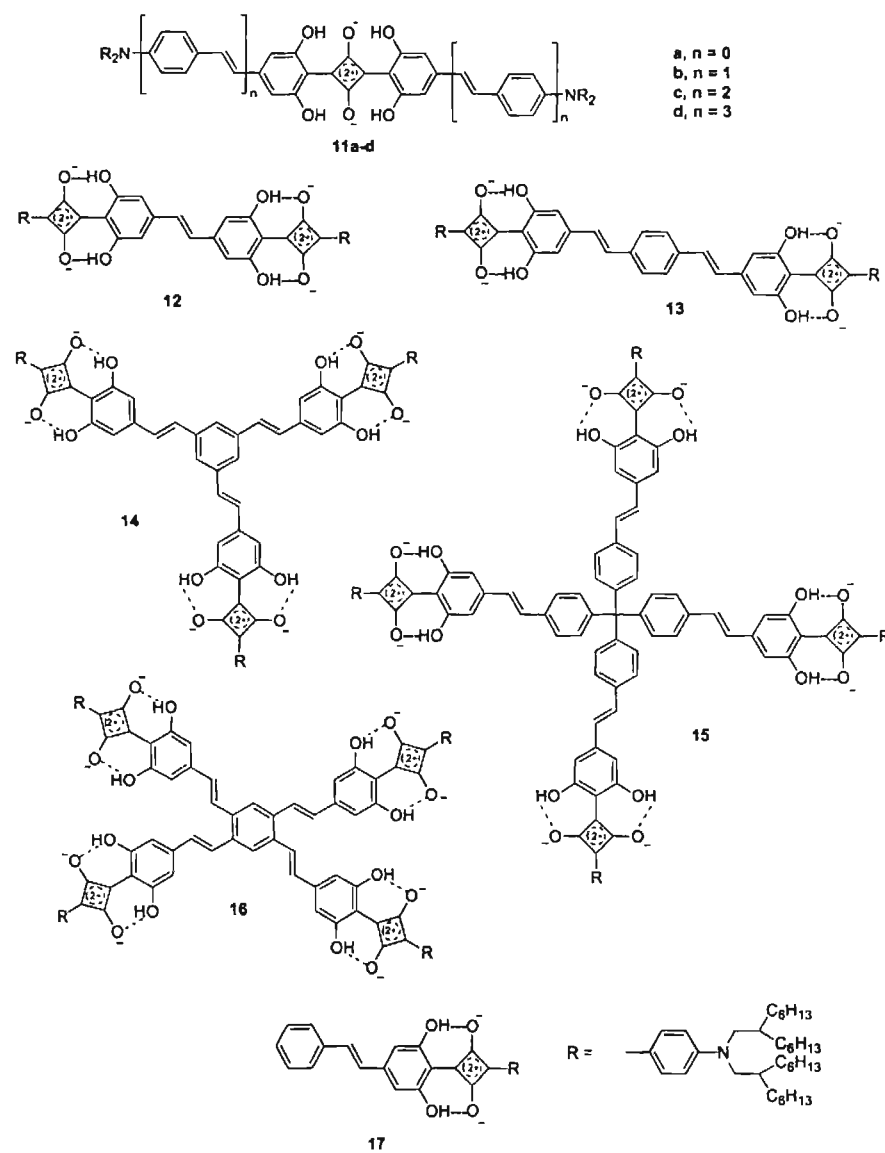


Chart 1.2

Pham and co-workers reported a non-fluorescent azulenyl squaraine dye **23** that absorbs around 750-800 nm region.<sup>31,32</sup> This molecule is expected to be an

efficient FRET quencher for a number of available near-IR fluorochromes for biological quenching assays.

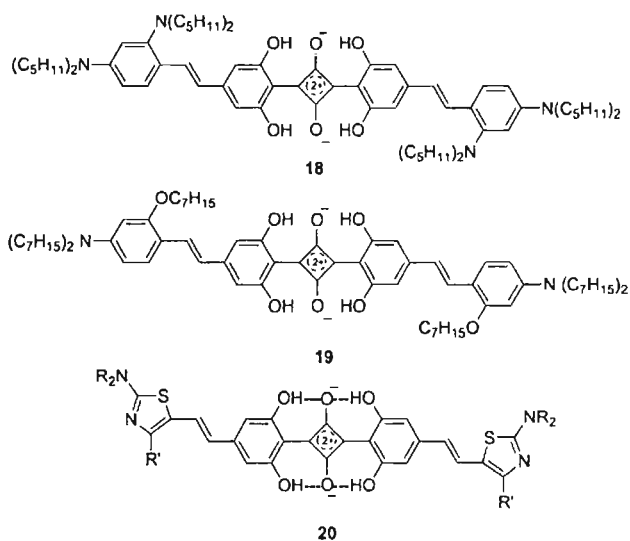


Chart 1.3

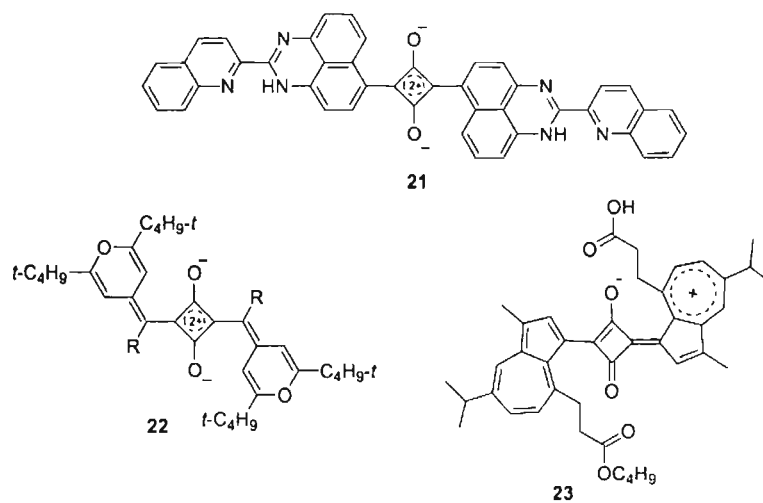
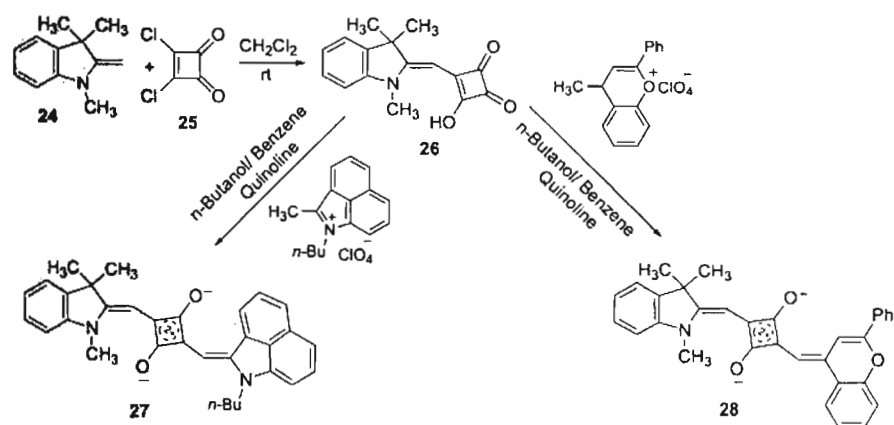
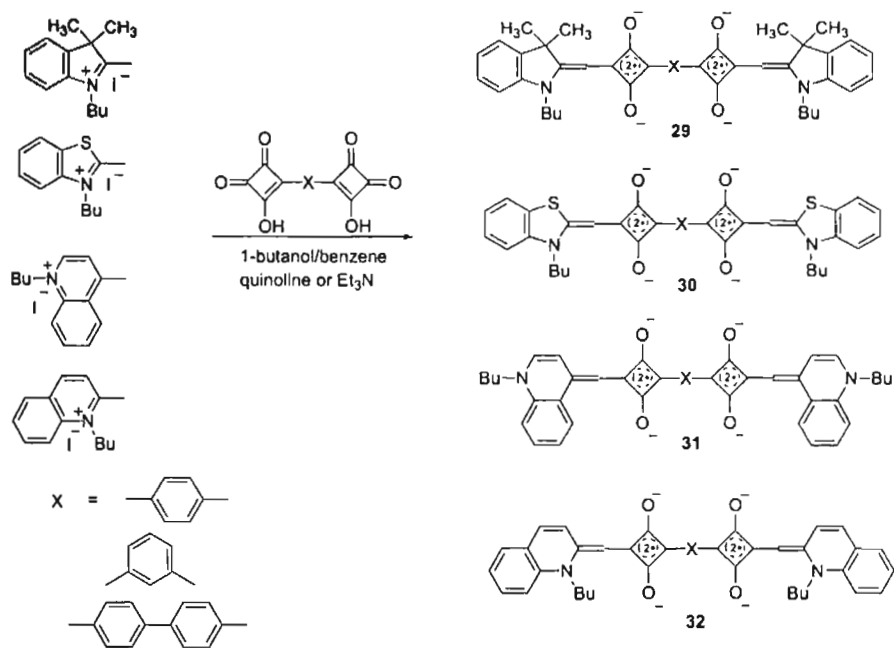


Chart 1.4

Nakazumi and coworkers have reported the synthesis of several unsymmetrical near-IR absorbing squaraine dyes by a stepwise procedure via the intermediate **26**. Reaction of **26** with the electron-donating components benz[c,d]indoline or benz[b]pyran moieties gave the squaraine dyes **27** and **28** which absorb around 739-821 nm region with large molar absorption coefficients ( $\log \epsilon = 4.96-5.18$ ) in chloroform (Scheme 1.3).<sup>33</sup> Subsequently, they have reported the synthesis of a variety of bis-squaraine dyes with extensively conjugated  $\pi$ -electron systems.<sup>34,35</sup> Condensation of a series of bis-squaric acids with heterocyclic methyl quaternary salts in 1-butanol/benzene in the presence of a small amount of quinoline or triethylamine afforded the bis-squaraine dyes **29-32** in 8-90 % yields (Scheme 1.4). The two squaryl moieties in these dyes are bridged by aromatic units, which produce significant perturbation of the absorption and emission spectra in comparison with analogous symmetrical mono-squaraine dyes. Varying the combination of the aromatic spacers and heterocyclic moieties led to the formation of squaraine dyes with extended conjugation. These dyes showed absorption and emission ranging from visible to the near-IR region and are potentially useful as red-emitting layers or dopands in electroluminescent devices.



Scheme 1.3



Scheme 1.4

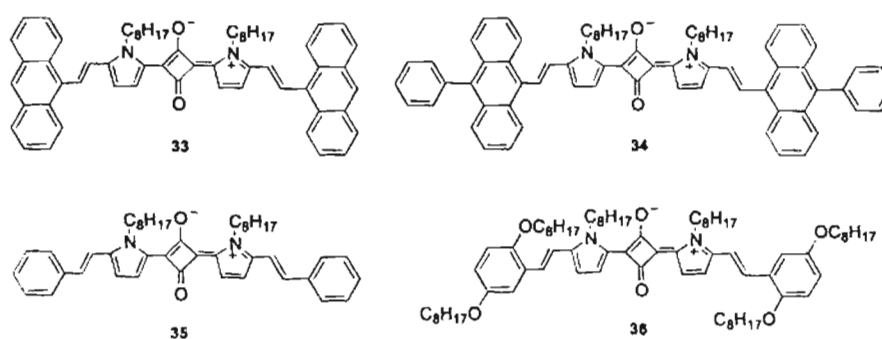
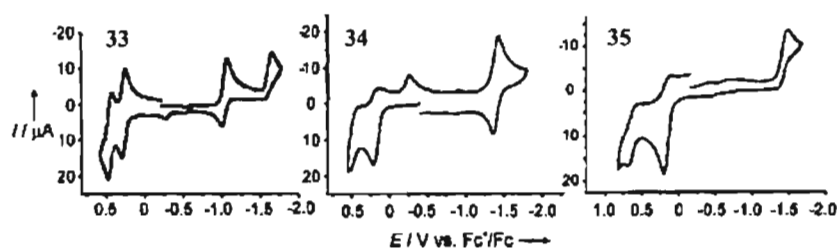


Chart 1.5

The pyrrole derived  $\pi$ -extended squaraine dyes **33-36** (Chart 1.5) show interesting optical and redox properties.<sup>36</sup> Incorporation of two vinylbenzene moieties to the simple *N*-alkylpyrrole based squaraine dye resulted in the formation of **35** that show a red-shift in the absorption maximum from 547 nm to 687 nm in toluene. The dye **36** exhibits a further red shift of 13-20 nm in toluene depending on the length of side chains. In the solid-state, they show broad absorption around 600-1000 nm range.



**Figure 1.1.** Cyclic voltammograms of **33-36** in dichloromethane using 0.1 M tetrabutylammonium hexafluorophosphate as supporting electrolyte; scan rate-250 mV/s.

Cyclic voltammograms of these dyes shown in Figure 1.1 reveal that the squaraine **34** possesses the maximum reversibility indicating the role of the phenylanthracenyl unit in the stabilization of the radical ions and dication. The squaraine dye **34** could be reversibly oxidized to the radical cation and dication whereas reduction showed limited electrochemical but full chemical reversibility (Figure 1.2). The radical cation of **34** showed an absorption band at 1000 nm and a 'two-band' feature at 1600 nm. It is assumed that oxidation leads to an electronic situation at the mixed valent radical cation stage in which the positive charge is localized primarily on the vinylpyrrole subunits.

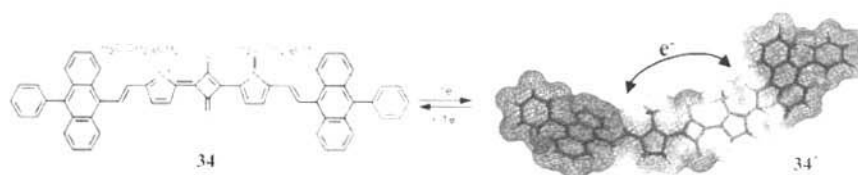


**Figure 1.2.** Redox behavior of **34** and the calculated charge distribution of **34'**.

One of the properties of squaraine dyes that have increasingly been addressed is their aggregation in heterogeneous environment, which tends to change their absorption and excited state properties. The research groups of McKerrow,<sup>37,38</sup> Whitten<sup>39-41</sup> and Das<sup>42</sup> have carried out extensive studies on the aggregation behavior of squaraine dyes. The excited state properties of squaraine dyes have been a topic of significant interest to researchers.<sup>42-44</sup> The promising optical and redox properties of squaraine dyes which can be modulated by

structural modification, are of great significance to squaraines as building blocks to the design of oligomers and polymers with intrinsic semiconducting properties.

### 1.3. Squaraine Based Low Band Gap Polymers

Design of  $\pi$ -conjugated polymers with low optical band gaps are important due to intrinsic semiconducting properties.<sup>45</sup> Oligomers and polymers based on organic dye molecules are ideal candidates as low band gap intrinsic semiconductors. Use of organic dyes with inherently low HOMO-LUMO energy gap as building blocks for conjugated polymers will lead to strong absorption in the near-IR region which is a signature of the low optical band gap. Though a variety of near-IR absorbing organic dyes are known,  $\pi$ -conjugated polymers that absorb in the near-IR region are rarely known.<sup>46,47</sup> Squaraines, due to the favorable optical properties and immense flexibility for synthetic manipulation, stand suitable for the design of polymers with low optical band gaps. This is supported by the theoretical calculations of Brocks and Tol who predicted low band gaps in polysquaraines.<sup>48</sup> In this context, the optical properties of squaraines have prompted researchers to explore the possibility of using them as building blocks for the synthesis of conjugated oligomers and polymers. Bifunctional heterocyclic aromatic compounds such as pyrrole, carbazole and benzothiazoles are suitable substrates, which on polycondensation with squaric acid form either oligomers or polymers with squaraine dye backbones. Extension of conjugation in squaraines to the level of oligomers and polymers are expected to improve the

optical and the electronic conducting properties. As mentioned earlier, the first attempt to the synthesis of polysquaraines resulted in the formation of insoluble materials (**6**).<sup>15</sup> Later Chen *et al.* have reported the formation of an insoluble polymer **37** derived from *N*-alkylcarbazoles (Chart 1.6).<sup>49</sup> Havinga and coworkers have made significant contributions to the synthesis and studies of several polysquaraines based on benzobisthiazoles and benzobis-pyrrolines.<sup>50-52</sup> Condensation of benzobisthiazoles and benzobis-pyrrolines with squaric acid resulted in the formation of polysquaraines (**38-40**) with low optical band gap (Chart 1.6). The polysquaraine **38** showed an optical band gap of 1.2 eV, with conductivity in the range of  $10^{-6}$ - $10^{-5}$  Scm<sup>-1</sup>. The water soluble polysquaraine **39** and **40** showed low band gaps of 0.7 and 1.2 eV, respectively which equal the photoconductivity band gaps. The low band gap in these polymers is due to the fact that the conjugated main chain with alternation of strong electron-withdrawing and electron-donating moieties represents the one dimensional analogue of an n-i-p-i semiconductor super lattice structure in which the valence and the conduction bands are curved by space charge effects.

Condensation of squaric acid with aromatic primary diamines such as *p*-phenylenediamine is known to form polyamides of squaric acid.<sup>53-58</sup> Neuse and Green have carried out extensive studies on the synthesis of polyamides of squaryl esters and dianilines, which are composed of both the 1,2- and 1,3-oriented cyclobutenone repeat units as in **41** (Chart 1.7).<sup>59,60</sup> However, these condensation reactions differ from the usual squaraine dye formation and hence the product do

not have any properties of squaraine dyes. Certain non-conjugated squaraine polymers containing repeat units of squaraine and long alkyl chains are also known in the literature.<sup>62</sup> The reaction of diethyl squarate with a quinolidine bis-quaternary salt yielded polysquaraine (42) with a non-conjugated structure (Chart 1.7).

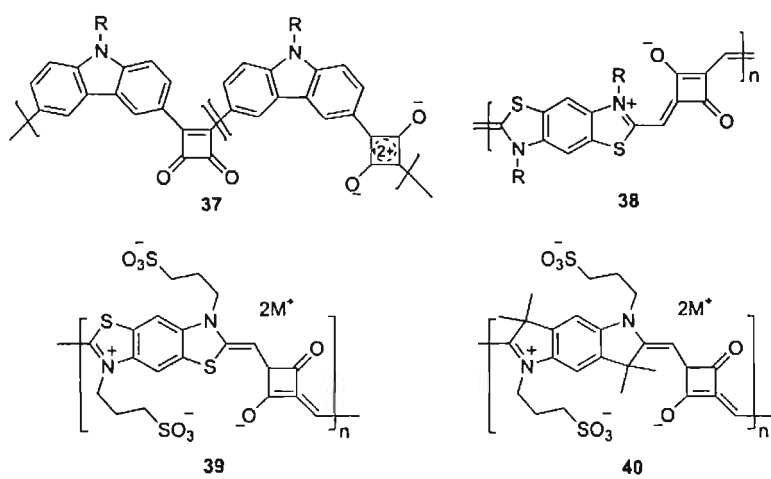


Chart 1.6

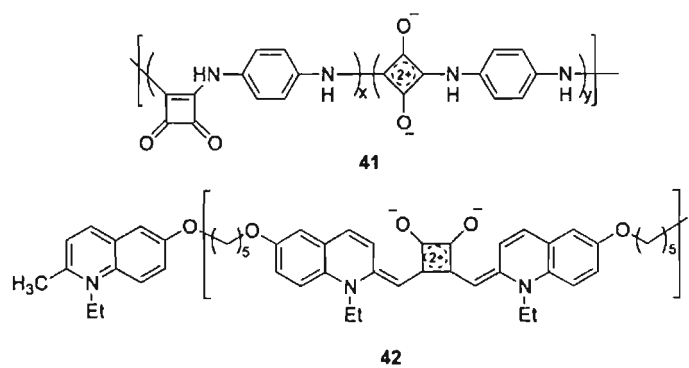


Chart 1.7

Pyrrole derivatives have been extensively used for the synthesis of polysquaraines for their use as intrinsic organic semiconductors and near-IR absorbers.<sup>63-65</sup> Lynch *et al.* have synthesized a series of polysquaraines from oligo(1-methylpyrroles) to investigate their electrical conduction properties.<sup>66-68</sup> In this series, only the tetramer-derived polysquaraine showed electric conduction ( $2 \times 10^{-7} \text{ Scm}^{-1}$ ), whereas the dimer and trimer derived polysquaraines are insulators with a dielectric breakdown of 1.0-0.05  $\text{cm}^{-1}$ .

Reaction of *N*-alkyl or 3-alkyl substituted pyrroles with squaric acid results in polysquaraines 43-46 (Chart 1.8), structures and properties of which vary depending upon reaction conditions. The water soluble copolymer 47 prepared by the reaction of squaric acid with a mixture of pyrrole and pyrrole-*N*-propanesulphonate showed conductivities in the range of  $10^{-5} \text{ Scm}^{-1}$  depending upon the copolymer composition.

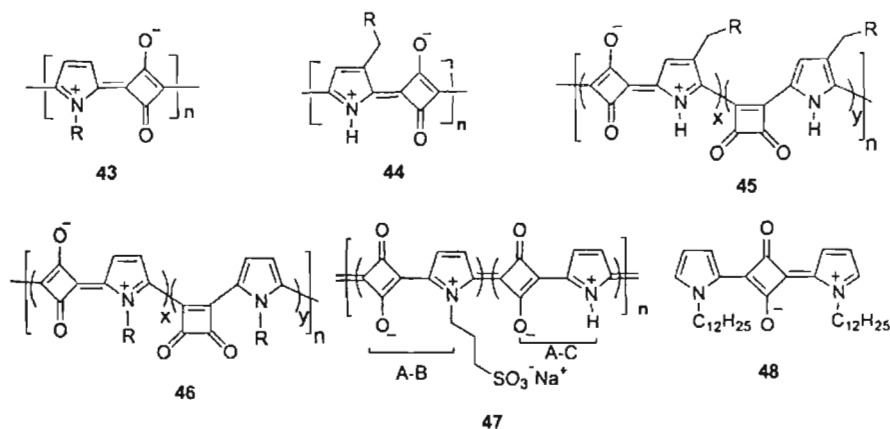
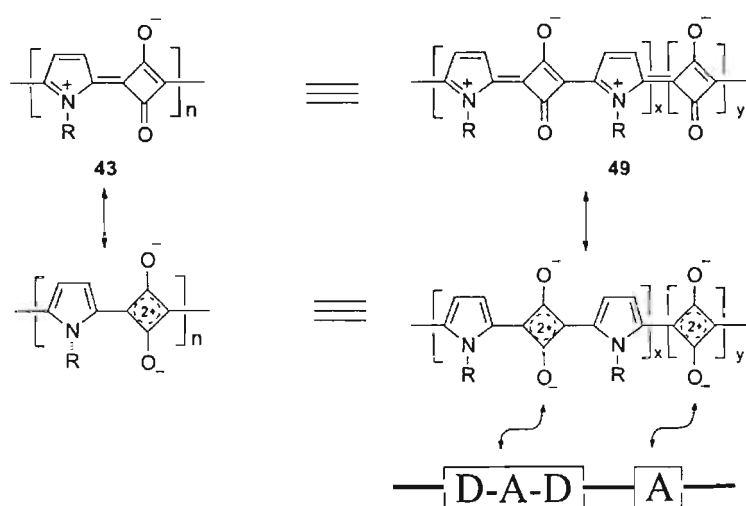


Chart 1.8

Although, pyrrole based polysquaraines were expected to have near-IR absorption and low optical band gaps, their absorption maxima were not much different from the corresponding monomeric dye units. For example, the squaraine dye **48** has an absorption maximum of 547 nm whereas the corresponding polysquaraine **43** has an absorption maximum of 580 nm. This observation revealed that a mere extension of conjugation in these systems is not sufficient to lower the band gaps. This is rationalized by rearranging the structure of the polysquaraine **43** as a copolymer of the donor-acceptor-donor (D-A-D) type squaraine dye repeating unit, as shown in **49**, which is bridged through an electron deficient cyclobutene unit (A) (Figure 1.3).



**Figure 1.3.** A pyrrole based polysquaraine represented as a copolymer of D-A-D squaraine dye and an electron deficient cyclobutene diolate dianion unit.

The presence of an electron deficient cyclobutene acceptor unit after every squaraine moiety may facilitate in reducing the D-A-D interactions of the squaraine unit, which in turn influence upon the optical properties. From this viewpoint, it is reasonable to argue that introduction of an electron rich bridging group may significantly improve the optical and electronic properties of the resulting polymers as depicted in Figure 1.4.

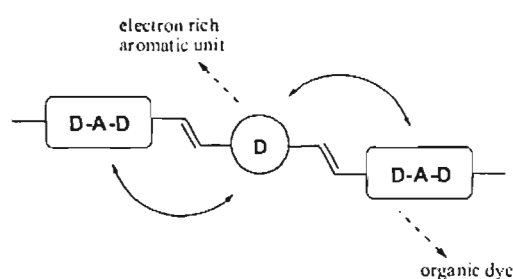


**Figure 1.4.** Design strategy for a D-A-D dye based low band gap polymer.

A direct approach to the implementation of the above strategy starting from squaraine dye is not viable due to the difficulties associated with the direct functionalization of squaraine dyes. A rational approach to the problem is the use of a bifunctional monomer (M) with two reaction sites for squaric acid which are connected to an electron rich conjugated bridging unit D as shown in Figure 1.5. Reaction of such a monomer with squaric acid can lead to a polysquaraine through the *in situ* generation of squaraine dye units (SQ) at definite positions of the polymer backbone. This is successfully illustrated using a variety of bispyrroles, bridged with electron rich dialkoxydivinylbenzene moiety as the building block. Polycondensation of bispyrroles of the general structure **51** with squaric acid

resulted in the formation of a series of corresponding polysquaraines **52** (Scheme 1.5) with strong near-IR absorption, which indicate low optical band gap in these polymers.<sup>69-71</sup>

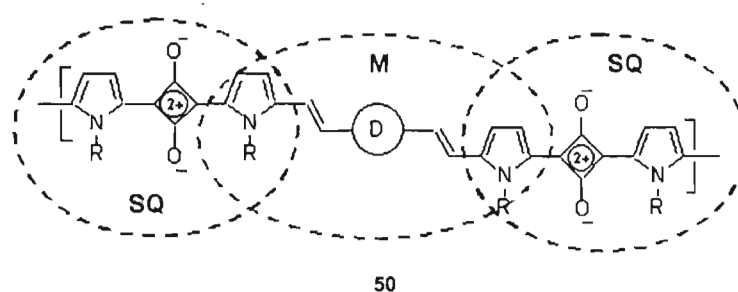
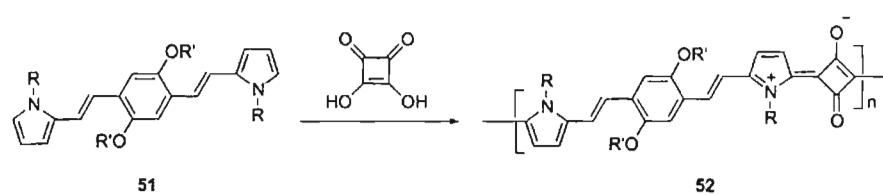
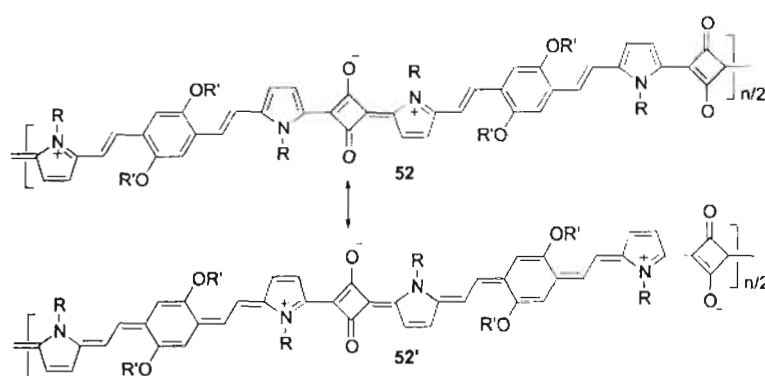


**Figure 1.5.** Structure of a polysquaraine with low optical band gap.



**Scheme 1.5**

The absorption spectra of polysquaraines are strongly influenced by the length of the aliphatic side chains of the polymer backbone. Polysquaraines with short side chains (methyl) on the pyrrole nitrogen atom showed a broad electronic absorption spectra with different absorption maxima and those with long side chains (dodecyl) showed relatively narrow spectra. The strong donor-acceptor interaction in these polymers may facilitate the resonance-stabilized quinoid structures,<sup>72,73</sup> which may be responsible for the observed long wavelength optical absorption (Scheme 1.6).



Scheme 1.6

The relative intensities of the different absorption maxima vary with the difference in side chains. The solution and solid-state band gaps of polymers, which are calculated from the onset of the absorption bands, are in the range of 0.7-1.1 eV. The intrinsic conductivities measured by two-probe method were in the order of  $10^{-4}$ - $10^{-7}$   $\text{Scm}^{-1}$ . The salient observation of the study is that, though the band gaps of the polysquaraines are very close to each other, the intrinsic conductivities showed considerable variation. This is explained based on the length of the side chains, which has considerable influence on the solid-state molecular packing of the polymer chains which revealed that among polysquaraines of comparable band gaps, conductivity can be tuned by the proper tailoring of the side chains. This is established by the powder X-ray diffraction data that showed interdigitated packing, the spacing of which varied with the length of the side chains.

Apart from the applications of polysquaraines as near-IR absorbers and organic semiconductors, Lynch and coworkers have recently reported the use of poly(1-methylpyrrolyl squaraine) for the preparation of sub-micrometer silica shells. The silica shells produced are able to encapsulate organic dyes upon soaking of the shells in chloroform solution of the dyes.<sup>74</sup>

#### 1.4. Squaraine Based Ion Probes (Chemosensors)

Selective sensing of metal ions is a topic of considerable interest due to their importance in different fields such as chemistry, biology, medicine and environmental studies. A chemosensor is a molecular system for which the physicochemical properties change upon interaction with a chemical species in such a way as to produce a detectable signal. The usual design of a chemosensor consists of an ionophore unit integrated to a reporter unit. The sensor must produce a perceptible signal upon the selective binding of the analyte. The binding of an analyte can be realized by using hosts such as cyclodextrins,<sup>75</sup> crown ethers,<sup>76,77</sup> aza-macrocycles,<sup>78-80</sup> chelates,<sup>81</sup> calixarenes,<sup>82,83</sup> cyclophanes<sup>84-86</sup> etc. In order to report on the analyte interactions, such groups are further functionalized with groups that are perturbed by the analyte binding. This perturbation is recorded by a change in the reduction potential, or a modification of the optical properties such as absorption or emission of the reporter. Even though all these techniques can provide information on analyte binding, techniques based on

absorption and emission properties of chromophores/fluorophores are preferred<sup>87,88</sup>

Organic dyes are extensively used as the signaling units in chemosensor design due to their intense absorption and emission properties, which are sensitive to external inputs.<sup>89</sup> Squaraine dyes are ideally suited for this purpose due to their favorable optical properties associated with the peculiar zwitterionic structure, which gets perturbed with the polarity, temperature and other additives. Binding of substrates to an ionophore which is integrated to a squaraine dye can signal the binding event in the form of a measurable change in the absorption or emission properties. A variety of squaraine based sensors are known in the literature, the selectivity and sensitivity of which are relatively low when compared to several of the other class of chemosensors.

The azacrown containing squaraine fluoroionophores **53** shows considerable changes in fluorescence quantum yield and redox properties.<sup>90</sup> The cationic squaraine dye **54** is capable of detecting trace amounts of transition elements and lanthanide ions in aqueous solution (Chart 1.9).<sup>91</sup>

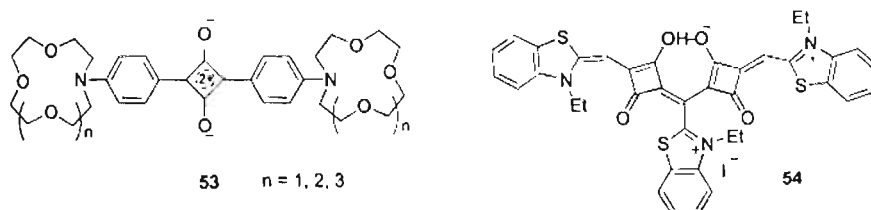


Chart 1.9

Akkaya and coworkers have reported a series of metal ion sensors based on squaraine fluorophores. The azacrown appended squaraine dyes **55** and **56** are sensitive to alkali and alkaline earth metals (Chart 1.10).<sup>92,93</sup> Dye **56** is selective to  $\text{Na}^+$ . The 1,2-bis(2'-aminophenoxy) ethanetraacetic acid based squaraine dye (**57**) is specific to  $\text{Ca}^{2+}$  ions.<sup>94</sup> The 2,3,3-trimethyl 3H-indole derived squaraine dye (**58**) showed three levels of signals based on the concentration of  $\text{Zn}^{2+}$  ions.<sup>95</sup> In addition, a few other reports on the use of squaraine dyes for the detection of various metal ions are also known in the literature.<sup>96-98</sup>

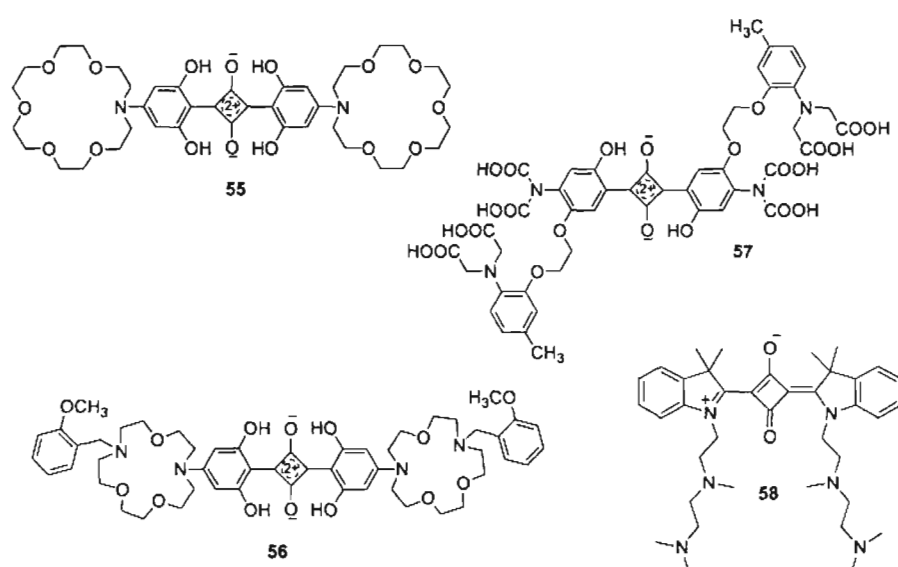


Chart 1.10

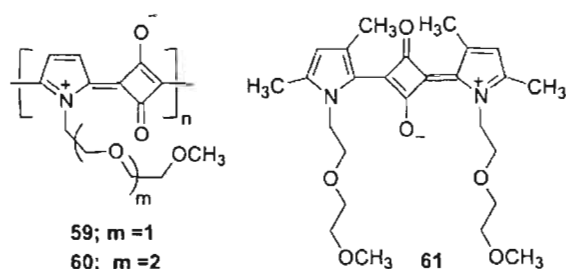
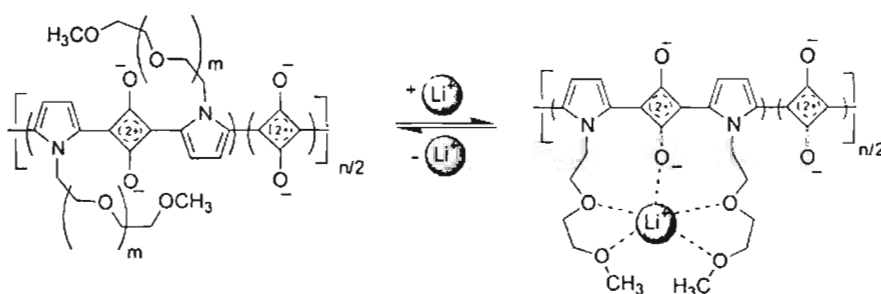
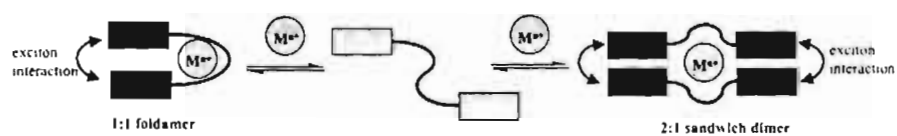


Chart 1.11

Swager's concept of molecular wire-based signal amplification<sup>99</sup> has been reported to have strong effect on the analyte sensitivity of polysquaraines.<sup>100,101</sup> This is illustrated using the polysquaraines 59 and 60 and a model dye 61 containing flexible oxyethylene chains (Chart 1.11). The polysquaraine 59 showed enhanced sensitivity and selectivity to  $\text{Li}^+$  over  $\text{Na}^+$  and  $\text{K}^+$ . Although there is no change in the absorption maximum of the polymer, considerable enhancement in the fluorescence emission is observed upon  $\text{Li}^+$  binding which could be due to the restricted rotation of the polymer backbone (Figure 1.6). However, the model squaraine dye 61 showed a weak response to  $\text{Li}^+$  revealing the crucial role of the polysquaraine backbone in the signal amplification.

Figure 1.6. Schematic representation  $\text{Li}^+$  binding of the polysquaraine 59.

Signal transduction in chemosensors are usually achieved by the change in the absorption or emission properties associated with electron transfer, energy transfer or charge-transfer interactions or by conformational restrictions. Unfortunately, the analyte induced changes in the absorption and emission properties associated with the above phenomena are weak in the case of squaraine based sensors. Therefore, alternate approach toward selective and sensitive signaling in squaraine based sensors has significance. Squaraines are known to form 'H' (blue shift) and 'J' (red-shift) aggregates in certain solvents. In majority of the cases, they favor the blue shifted H-aggregates with strong quenching of the emission. These changes in the absorption and emission are due to exciton interaction in squaraine aggregates, which can be a potential signaling pathway for a specific cation binding event. This could be achieved by a cation-induced folding of the dye-linked podands to form complexes similar to the H-aggregates. Exciton interaction in the bound complex produces measurable changes in the optical properties as shown in Figure 1.7.



**Figure 1.7.** Schematic representation of a squaraine based chemosensor based on cation driven exciton interaction.

The above concept has been successfully illustrated with the help of a number of squaraine tethered bichromophoric podands of the general structure **62**

and analogous monochromophores of the general structure **63** by changing the alkyl groups and the length of the oxyethylene spacer. (Chart 1.12).<sup>102,103</sup> The bichromophores **62a-e** exhibit strong perturbation in the absorption and emission spectra with high selectivity toward alkaline earth metal cations, particularly to  $\text{Mg}^{2+}$  and  $\text{Ca}^{2+}$ , whereas no optical response was noticed against alkali metal ions.

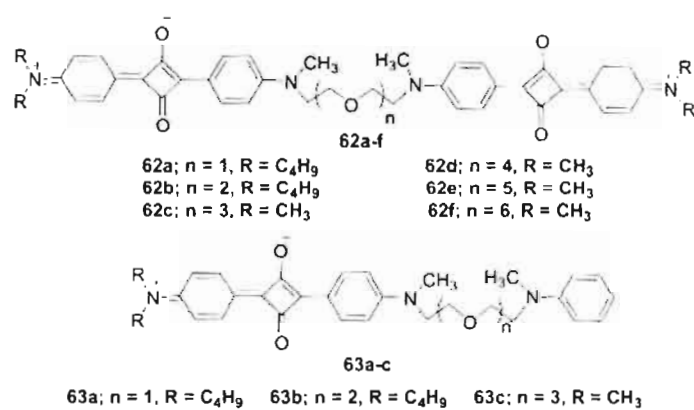


**Chart 1.12**

However, the bichromophore **62e** with five oxygen atoms in the podand chain is selective to  $\text{Ca}^{2+}$  and the binding is visible to naked eyes due to the color change from light blue to deep purple blue (Figure 1.8). Addition of EDTA which is a strong complexing agent for  $\text{Ca}^{2+}$  reinstated the original absorption spectrum of the dye indicating the decomplexation of the cation. On the other hand, the monochromophores **63a-c** preferentially form complexes having Head-Tail-Tail-Head arrangements. They have similar properties to that of the H-aggregates of squaraines where the exciton interaction between the chromophore results in the

blue shift of the absorption bands. Thus, using squaraines it could be possible to control and express the binding of specific cations, invoking exciton interaction as the mode of signaling, which is different from other known signaling mechanisms resulting in a novel class of cation sensors.

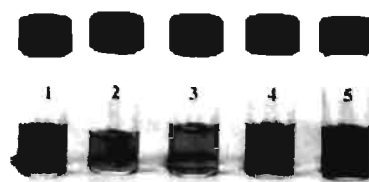


**Figure 1.8.** Visible color change of the bicromophore **62e** ( $n = 5$ ) in acetonitrile upon addition of  $\text{Ca}^{2+}$ . (1) in the absence of metal salts, (2)  $\text{Mg}^{2+}$ , (3)  $\text{Na}^+$ , (4)  $\text{K}^+$  and (5)  $\text{Ca}^{2+}$ .

Block and coworkers have recently used this concept for ion responsive polymers **64** and **65** (Chart 1.13) wherein the binding event is translated to a shift in the unimer to dimer equilibrium that can be visualized by UV-vis and fluorescence spectroscopy.<sup>104</sup>

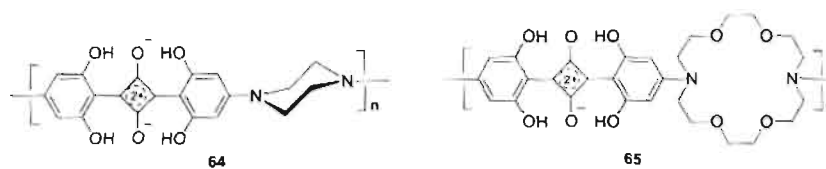
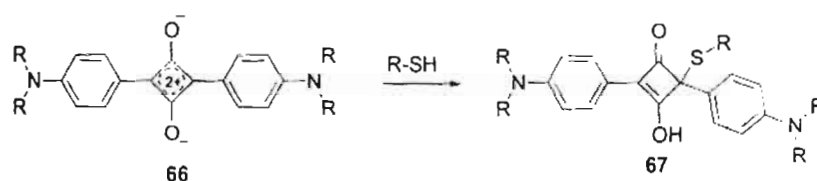


**Chart 1.13**

Recently, Ros-Lis *et al.* have reported the use of squaraines for the detection of anions which is illustrated with the help of the simple squaraine **66** for  $\text{CN}^-$  ions.<sup>105</sup> Subsequently, squaraines are shown to be useful as fluoro-

chromogenic probes for thiol-containing compounds which has significance to the detection of biorelevant thiols. (Scheme 1.7).<sup>106</sup> Addition of  $\text{Hg}^{2+}$  to **67** regenerate the dye, thereby allowing the detection of  $\text{Hg}^{2+}$ . In this way the dye **66** becomes a reusable molecular probe for the detection of  $\text{Hg}^{2+}$ .<sup>107</sup> A recent application of squaraines pertains to the development of an ionically controlled nanoscopic molecular gate.<sup>108</sup> Thus, squaraines are reaching new heights with respect to the design of advanced materials with intriguing properties.<sup>109,110</sup>



**Scheme 1.7.** Proposed reaction between squaraine derivatives and thiol-containing compounds.

### 1.5. Objectives of the Present Investigation

Inspired by the recent progress in the design and study of squaraine dyes, we have planned to explore the possibility of 1,4-divinyl(aryl)bridged bispyrroles to the synthesis of  $\pi$ -extended squaraines. With this objective, a number of bispyrroles with different aromatic bridging moieties and their use as building blocks to the design of near-IR polymers were envisaged. Studies were planned to investigate their aggregation behavior in solution and in solid-state. The role of alkyl side chains on the optical properties and on the aggregation behavior of these polymers was studied. In order to have a better understanding, a variety of model

dyes were synthesized and their aggregation properties were investigated. Another objective of the present investigation was to develop molecular probes based on bispyrroles. By incorporating a metal ion receptor in the bispyrrole structure, design of a visual sensor for the biologically relevant  $Zn^{2+}$  was planned. The present thesis is a systematic investigation on the synthesis and use of a variety of divinyl(aryl)bridged bispyrroles and their use to the design of  $\pi$ -extended squaraine dyes and cation probes.

## 1.6. References

1. *In proceedings of the second international symposium on chemistry of functional dyes*; Yohida, Z.; Shirota, Y. Eds.; Mita Press: Tokyo, 1993, Vol.2.
2. Tam, A. C. *Appl. Phys. Lett.* **1980**, *37*, 979.
3. Law, K. -Y. *Chem. Rev.* **1993**, *93*, 449.
4. Dirk, C. W.; Herndon, W. C.; Cervantes, -L. F.; Selnau, II.; Martinez, S.; Kalamegham, P.; Tan, A.; Campos, G.; Velez, M.; Zyss, I.; Ledoux, I.; Cheng, L. -T. *J. Am. Chem. Soc.* **1995**, *117*, 2214.
5. Ashwell, G. J.; Jefferies, G.; Hamilton, D. G.; Lynch, D. E.; Roberts, M. P. S.; Bahra, B. S.; Brown, C. R. *Nature* **1995**, *375*, 385.
6. Furuki, M.; Pu, L. S.; Sasaki, F.; Kobayashi, S.; Tani, T. *Appl. Phys. Lett.* **1998**, *21*, 2648.
7. Iwamoto, M.; Shidoh, S.; *Jpn. J. Appl. Phys.* **1990**, *29*, 2031.
8. Merrit, V. Y.; Hovel, H. J. *Appl. Phys. Lett.* **1976**, *29*, 414.
9. Morel, D. L.; Ghosh, A. K.; Feng, T.; Stogryn, E. L.; Purwin, P.E.; Shaw, R. F.; Fishman, C. *Appl. Phys. Lett.* **1978**, *32*, 495.

10. Ghazarossian, V.; Pease, J. S.; Ru, M. W. L.; Loneey, M.; Tarnowski, T. L. *Chem. Abstr.* **1990**, *113*, 61319j.
11. Ramaiah, D.; Joy, A.; Chandrashekar, N.; Eldho, N. V.; Das, S.; George, M. V.; *Photochem. Photobiol.* **1997**, *65*, 783.
12. Bonnett, R. *Chemical Aspects of Photodynamic Therapy*; Gordon and Breach: Amsterdam, 2000.
13. Ramaiah, D.; Eckert, I.; Arun, K. T.; Weidenfeller, L.; Epe, B. *Photochem. Photobiol.* **2002**, *76*, 672.
14. Das, S.; Thomas, K. G.; George, M. V. In *Molecular and Supramolecular Photochemistry*; Ramamurthy, V.; Schanze, K. S., Eds.; Marcel Dekker Inc: NewYork, 1997; chapter 11, pp 467.
15. Treibs, A.; Jacob, K. *Angew. Chem., Int. Ed.* **1965**, *4*, 694.
16. Ziegenbein, W.; Sprenger, H. -E. *Angew. Chem., Int. Ed.* **1966**, *5*, 893.
17. Sprenger, H. -E.; Ziegenbein, W. *Angew. Chem., Int. Ed.* **1966**, *5*, 894.
18. Sprenger, H. -E.; Ziegenbein, W. *Angew. Chem., Int. Ed.* **1967**, *6*, 553.
19. Sprenger, H. -E.; Ziegenbein, W. *Angew. Chem., Int. Ed.* **1968**, *7*, 530.
20. Schmidt, H. A. *Synthesis* **1980**, 961.
21. Bello, K. A.; Ajayi, J. O. *Dyes Pigm.* **1996**, *31*, 79.
22. Meier, H.; Dullweber, U. *Tetrahedron Lett.* **1996**, *37*, 1191.
23. Meier, H.; Dullweber, U. *J. Org. Chem.* **1997**, *62*, 4821.
24. Meier, H.; Petermann, R.; Gerold, J. *Chem. Commun.* **1999**, 977.
25. Meier, H.; Petermann, R. *Tetrahedron Lett.* **2000**, *41*, 5475.
26. Gerold, J.; Holzenkamp, U.; Meier, H. *Eur. J. Org. Chem.* **2001**, 2757.
27. Petermann, R.; Tian, M.; Tatsuura, S.; Furuki, M. *Dyes Pigm.* **2003**, *57*, 43.
28. Meier, H.; Petermann, R. *Helv. Chim. Acta* **2004**, *87*, 1109.
29. Kim, S. -H.; Kim, J. -H.; Cui, J.-Z.; Gal, Y.-S.; Jin, S.-H.; Koh, K. *Dyes Pigm.* **2002**, *55*, 1.
30. Chen, J. -G.; Huang, D. -Y.; Li, Y. *Dyes Pigm.* **2000**, *46*, 93.

31. Pham W.; Weissleder, R.; Tung, C. H. *Angew. Chem.; Int. Ed.* **2002**, *41*, 3659.
32. Pham W.; Weissleder, R.; Tung, C. H. *Tetrahedron Lett.* **2003**, *44*, 3975.
33. Yagi, S.; Hyodo, Y.; Matsumoto, S.; Takahashi, N.; Kono, H.; Nakazumi, H. *J. Chem. Soc., Perkin Trans. 1* **2000**, *4*, 599.
34. Hyodo, Y.; Nakazumi, H.; Yagi, S.; Nakai, K. *J. Chem. Soc., Perkin Trans. 1* **2001**, 2823.
35. Yagi, S.; Murayama, S.; Hyodo, Y.; Fujie, Y.; Hirose, M.; Nakazumi, H. *J. Chem. Soc., Perkin Trans. 1* **2002**, 1417.
36. Büschel, M.; Ajayaghosh, A.; Arunkumar, E.; Daub, J. *Org. Lett.* **2003**, *5*, 2957.
37. Buncel, E.; McKerrow, A. J.; Kazmaier, P. M. *J. Chem. Soc. Chem. Commun.* **1992**, 1242.
38. McKerrow, A. J.; Buncel, E.; Kazmaier, P. M. *Can. J. Chem.* **1995**, *73*, 1605.
39. Chen, H.; Herkstroeter, W. G.; Perlstein, J.; Law, K. -Y.; Whitten, D. G. *J. Phys. Chem.* **1994**, *98*, 5138.
40. Liang, K.; Law, K. -Y.; Whitten, D. G. *J. Phys. Chem.* **1994**, *98*, 13379.
41. Chen, H.; Farahat, M. S.; Law, K. -Y.; Whitten, D. G. *J. Am. Chem. Soc.* **1996**, *118*, 2584.
42. Das, S.; Thanulingam, L. T.; Thomas, K. G.; Kamat, P. V.; George, M. V. *J. Phys. Chem.* **1993**, *97*, 13620.
43. Das, S.; Thomas, K. G.; Thomas, K. J.; Kamat, P. V.; George, M. V. *J. Phys. Chem.* **1994**, *98*, 9291.
44. Thomas, K. G.; Thomas, K. J.; Das, S.; George, M. V. *Chem. Commun.* **1997**, 597.
45. Ajayaghosh, A. *Chem. Soc. Rev.* **2003**, *32*, 181.
46. Tsuda, A.; Osuka, A. *Science* **2001**, *293*, 79.

47. Cho, H. S.; Jeong, D. H.; Cho, S.; Kim, D.; Matsuzaki, Y.; Tanaka, K.; Tsuda, A.; Osuka, A. *J. Am. Chem. Soc.* **2002**, *124*, 14642.
48. Brocks, G.; Tol, A. *J. Phys. Chem.* **1996**, *100*, 1838.
49. Chen, Y. -Y.; Hall, Jr. H. K. *Polym. Bull.* **1986**, *16*, 419.
50. Havinga, E. E.; ten Hoeve, W.; Wynberg, H. *Polym. Bull.* **1992**, *29*, 119.
51. Havinga, E. E.; ten Hoeve, W.; Wynberg, H. *Synth. Met.* **1993**, *55*, 299.
52. Havinga, E. E.; Pomp, A.; ten Hoeve, W.; Wynberg, H. *Synth. Met.* **1995**, *69*, 581.
53. Manecke, G.; Gauger, J. *Makromol. Chem.* **1969**, *125*, 231.
54. Gauger, J.; Manecke, G. *Angew. Chem., Int. Ed. Engl.* **1969**, *8*, 898.
55. Manecke, G.; Gauger, J. *Tetrahedron Lett.* **1967**, 3509.
56. Manecke, G.; Gauger, J. *Tetrahedron Lett.* **1968**, 1139.
57. Gauger, J.; Manecke, G. *Chem. Ber.* **1970**, *103*, 2696.
58. Gauger, J.; Manecke, G. *Chem. Ber.* **1970**, *103*, 3553.
59. Neuse, E. W.; Green, B. R. *Leibigs Ann. Chem.* **1973**, 619.
60. Neuse, E. W.; Green, B. R. *Leibigs Ann. Chem.* **1973**, 633.
61. Neuse, E. W.; Green, B. R. *Polymer* **1974**, *15*, 339.
62. Yu, L.; Chen, M.; Dalton, L. R. *Polymer* **1991**, *32*, 1369.
63. Ajayaghosh, A.; Chenthamarakshan, C. R.; Das, S.; George, M. V. *Chem. Mater.* **1997**, *9*, 644.
64. Chenthamarakshan, C. R.; Ajayaghosh, A. *Chem. Mater.* **1998**, *10*, 1657.
65. Chenthamarakshan, C. R.; Eldo, J.; Ajayaghosh, A. *Macromolecules* **1999**, *32*, 251.
66. Lynch, D. E.; Geissler, U.; Kwiatkowski, J.; Whittaker, A. K. *Polym. Bull.* **1997**, *38*, 493.
67. Lynch, D. E.; Geissler, U.; Peterson, I. R.; Floersheimer, M.; Terbrack, R.; Chi, L. F.; Fuchs, H.; Calos, N. J.; Wood, B.; Kennard, C. H. L.; Langley, G. J. *J. Chem. Soc., Perkin Trans. 2* **1997**, 827.

68. Lynch, D. E.; Peterson, I. R.; Floersheimer, M.; Essing, D.; Chi, L.-f.; Fuchs, H.; Calos, N. J.; Wood, B.; Kennard, C. H. L.; Langley, G. J. *J. Chem. Soc., Perkin Trans. 2* **1998**, 779.
69. Eldo, J.; Arunkumar, E.; Ajayaghosh, A. *Tetrahedron Lett.* **2000**, *41*, 6241.
70. Ajayaghosh, A.; Eldo, J. *Org. Lett.* **2001**, *3*, 2595.
71. Eldo, J.; Ajayaghosh, A. *Chem. Mater.* **2002**, *14*, 410.
72. Jenekhe, S. A. *Nature* **1986**, *322*, 345.
73. Brédas, J. L.; Heeger, A. J.; Wudl, F. *J. Chem. Phys.* **1986**, *85*, 4673.
74. Lynch, D. E.; Nawaz, Y.; Bostrom, T. *Langmuir* **2005**, *21*, 6572.
75. Neilssen, H. F. M.; Kercher, M.; De Cola, L.; Feiters, M. C.; Nolte, R. J. M. *Chem. Eur. J.* **2002**, *8*, 5407.
76. Beer, P.D.; Tite, E. L.; Ibbotson, A. *J. Chem. Soc. Dalton Trans.* **1991**, 1691.
77. Murphy, S. L.; Loeb, S. J.; Shimizu, G. K. H. *Tetrahedron* **1998**, *54*, 15137.
78. Liebmann, A.; Mertesdorf, C.; Plesnivý, T.; Ringsdorf, H.; Wendorff, J. H. *Angew. Chem. Int. Ed. Engl.* **1991**, *30*, 1375.
79. Blake, A. J.; Danks, J. P.; Li, W. S.; Lippolis, V.; Schroder, M. *J. Chem. Soc. Dalton Trans.* **2000**, 3034.
80. Gott, A. L.; Mc Gowan, P. C.; Podesta, T. J.; Thornton-Pett, M. *J. Chem. Soc. Dalton Trans.* **2002**, 3619.
81. Schnepfensieper, T.; Finkler, S.; Czap, A.; van Eldik, R.; Heus, M.; Nieuwenhuizen, P.; Wreesmann, C.; Abma, W. *Eur. J. Inorg. Chem.* **2001**, 491.
82. Specht, A.; Bernard, P.; Goeldner, M.; Peng, L. *Angew. Chem., Int. Ed.* **2002**, *41*, 4706.
83. Lambert, J. B.; Liu, C. Q.; Boyne, M. T.; Zhang, A. P.; Yin, Y. X. *Chem. Mater.* **2003**, *15*, 131.

84. Benniston, A. C.; Mackie, P. R.; Harriman, A. *Tetrahedron Lett.* **1997**, *38*, 3577.
85. Tobe, Y.; Utsumi, N.; Nagano, A.; Naemura, K. *Angew. Chem., Int. Ed.* **1998**, *37*, 1285.
86. Breslow, R.; Fang, Z. L. *Tetrahedron Lett.* **2002**, *43*, 5197.
87. *Chemosensors for Ion and Molecule Recognition*; Desvergne, J. P. Czarnik, A. W., Eds.; NATO Asi Series; Kluwer Academic Publishers: Dordrecht, 1997.
88. Lakowicz, J. R. *Principles of Fluorescence Spectroscopy*; Kluwer Academic/Plenum Publishers: New York, 1999.
89. de Silva, A. P.; Gunaratne, H. Q. N.; Gunnlaugsson, T.; Huxley, A. J. M.; McCoy, C. P.; Rademacher, J. T.; Rice, T. E. *Chem. Rev.* **1997**, *97*, 1515.
90. Das, S.; Thomas, K. G.; Thomas, K. J.; Kamat, P. V.; George, M. V. *J. Phys. Chem.* **1994**, *98*, 9291.
91. Thomas, K. G.; Thomas, K. J.; Das, S.; George, M. V. *Chem. Commun.* **1997**, 597.
92. Oguz, U.; Akkaya, E. U. *Tetrahedron Lett.* **1997**, *38*, 4509.
93. Oguz, U.; Akkaya, E. U. *Tetrahedron Lett.* **1998**, *39*, 5857.
94. Akkaya, E. U.; Turkyilmaz, S. *Tetrahedron Lett.* **1997**, *38*, 4513.
95. Dilek, G.; Akkaya, E. U. *Tetrahedron Lett.* **2000**, *41*, 3721.
96. Kim, S. H.; Han, S. K.; Park, S. H.; Lee, S. M.; Lee, S. M.; Koh, K. N.; Kang, S. W. *Dyes Pigm.* **1999**, *41*, 221.
97. Ock, K.; Jang, G.; Roh, Y.; Kim, S.; Kim, J.; Koh, K. *Microchem. J.* **2001**, *70*, 301.
98. Tarazi, L.; Narayan, N.; Sowell, J.; Patonay, G.; Streckowski, L. *Spectrochem. Acta* **2002**, *58*, 257.
99. Swager, T. M. *Acc. Chem. Res.* **1998**, *31*, 201.
100. Chenthamarakshan, C. R.; Ajayaghosh, A. *Tetrahedron Lett.* **1998**, *39*, 1795.

101. Chenthamarakshan, C. R.; Eldo, J.; Ajayaghosh, A. *Macromolecules* **1999**, *32*, 5846.
102. Ajayaghosh, A.; Arunkumar, E.; Daub, J. *Angew. Chem., Int. Ed.* **2002**, *41*, 1766.
103. Arunkumar, E.; Chithra, P.; Ajayaghosh, A. *J. Am. Chem. Soc.* **2004**, *126*, 6590.
104. Block, M. A. B.; Hecht, S. *Macromolecules* **2004**, *37*, 4761.
105. Ros-Lis, J. V.; Martínez-Máñez, R.; Soto, J. *Chem. Commun.* **2002**, *19*, 2248.
106. Ros-Lis, J. V.; Garcý'a, B.; Jimé'nez, D.; Martínez-Máñez, R.; Sancenon, F.; Soto, J.; Gonzalvo, F.; Valdecabres, M. C. *J. Am. Chem. Soc.* **2004**, *126*, 4064.
107. Ros-Lis, J. V.; Marcos, M. D.; Martínez-Máñez, R.; Rurack, K.; Soto, J. *Angew. Chem. Int. Ed.* **2005**, *44*, 4405.
108. Casasus, R.; Marcos, M. D.; Martínez-Máñez, R.; Ros-Lis, J. V.; Soto, J.; Villaescusa, L. A.; Amorós, P.; Beltrán, D.; Guillem, C.; Latorre, J. *J. Am. Chem. Soc.* **2004**, *126*, 8612.
109. Ajayaghosh, A. *Acc. Chem. Res.* **2005**, *38*, 449.
110. Sreejith, S.; Carol, P.; Chithra, P.; Ajayaghosh, A. *J. Mater. Chem.* **2008**, *18*, 264.

## Chapter 2

### Low Band Gap Squaraine Dyes and Polysquaraines: Role of Aromatic Bridging Units in Optical and Conducting Properties

---

#### 2.1. Abstract

*The optical properties and electronic conductivities of donor-acceptor type  $\pi$ -conjugated polymers depend upon the donor-acceptor strength and interchain interactions. In order to study the effect of different aromatic bridging units in functional dye based systems, a few  $\pi$ -extended squaraine dyes **3a-d** and the corresponding polysquaraines **2a-e** were synthesized and characterized. They were prepared from a series of bispyrrole monomers **1a-e** having different aromatic bridging units such as divinylbenzene, divinylbiphenyl, dialkoxydivinylbenzene, divinylanthracene and dialkoxydivinylnaphthalene groups by the reaction with squaric acid. Detailed absorption, conductivity and aggregation properties of these  $\pi$ -extended squaraine dyes and the corresponding polysquaraines are described. The absorption maxima of the polysquaraines and the analogous squaraine dyes are significantly influenced by the aromatic bridging moieties. The lowest absorption maxima are observed for squaraine dyes and polysquaraines with divinylanthracene as the bridging unit whereas highest absorption maxima are noticed for those with dialkoxydivinylbenzene bridging moieties. The polysquaraines **2a-e** showed broad absorption in the range of 600-*

1200 nm with band gaps ranging from 0.82-1.30 eV with intrinsic conductivities in the range of  $2.2 \times 10^{-5}$  to  $1.74 \times 10^{-9} \text{ Scm}^{-1}$ . The lowest band gap and the maximum conductivity are obtained for the polysquaraine **2c** with a dialkoxydivinylbenzene bridging moiety.

## 2.2. Introduction

$\pi$ -Conjugated oligomers and polymers are extensively used in a wide range of electro-optical and electronic devices.<sup>1</sup> One of the criterion which determines the use of these polymers for various electronic applications is the band gap energy. The vast literature available on the band gap tuning of  $\pi$ -conjugated polymers illustrates the importance of the topic.<sup>2,3</sup> For optical applications in the visible range as in light-emitting diodes, a wide band gap is suitable,<sup>4,5</sup> whereas for a number of applications such as logic elements-transistors,<sup>6</sup> diodes,<sup>7</sup> or in a heavily doped state (conductors), there are no *a priori* restrictions on the band gap. A polymer with a small band gap is bound to have much fewer doping and contacting problems.

The electronic and optical properties of conjugated polymers result from a limited number of states around the highest occupied and the lowest unoccupied levels. According to the band theory, the highest occupied band, which originates from the HOMO of each monomer unit, is referred to as the valance band and the corresponding lowest unoccupied band originating from the LUMO as the conduction band. The band gap ( $E_g$ ) of the polymer depends on the separation  $\Delta E$

between the HOMO and LUMO energy levels of the monomers and the band width  $W(\beta)$ , which is a function of hybridization ( $\beta$ ) of the monomer levels in the polymer. Schematic representation of band formation in a polymer is given in Figure 2.1. The optical absorption of polymers is usually strongly peaked around the band gap in a way which reflects the density of states typical of one-dimensional systems.<sup>8</sup> Polymers with band gaps in the range 2.0-3.5 eV, therefore, absorb strongly in the visible range. A much smaller band gap shifts the absorption peak to the infrared. The absorption in the visible region can then be relatively small, especially if the polymer is doped. This opens the possibility for the use of semiconducting polymers, after doping, as transparent conductors.

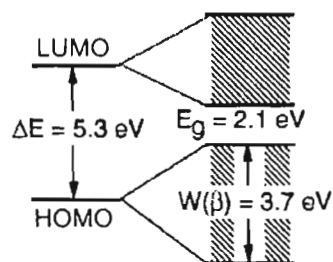


**Figure 2.1.** Schematic representation of band formation in a polymer. On the left-hand side the HOMO and LUMO energy levels of the monomer are sketched; on the right-hand side the energy bands of the polymer are shown. The numbers shown are for polythiophene (*adapted from reference 9*).

Although various routes are being used to control the band gap in conjugated polymers, a feasible strategy is the use of A-B type systems where the 'A' unit has strong electron-donating and the 'B' unit has strong electron-withdrawing moieties. The principle behind these donor-acceptor polymers is that a regular alternation of conjugated donor and acceptor moieties will stabilize the

quinonoid-like forms within the polymer backbone, thus inducing a reduction in its band gap energy.

Molecular orbital calculations have shown that the hybridization of the energy levels of the donor and the acceptor moieties result in D-A systems with unusually low HOMO-LUMO separation.<sup>9</sup> If the HOMO levels of the donor and the LUMO levels of the acceptor moiety are close in energy, the resulting band structure will show a low energy gap as depicted in Figure 2.2.

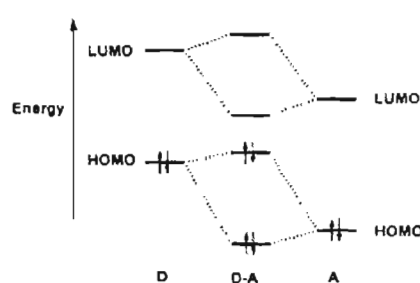


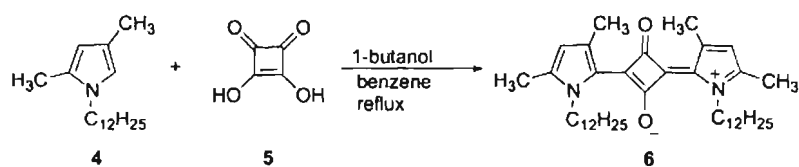
**Figure 2.2.** Molecular orbital interaction in donor (D) and acceptor (A) moieties leading to a D-A monomer with an unusually low HOMO-LUMO energy separation (*adapted from reference 3*).

During the progress of polymerization, the HOMO and LUMO levels of the repeating unit disperse into the valance and conduction bands. At each stage of monomer addition, the magnitudes of the LUMO ( $WL$ ) and the HOMO ( $WH$ ) bands increase, which strongly depend upon the degree of overlap between the aromatic orbitals in the coupling position of the monomer units. Thus,  $WL$  and  $WH$  get maximum values at an unobstructed overlap and in such a condition the molecule exists in its lowest band gap level. However, deviations from this ideal situation may occur when the steric hindrance forces the consecutive aryl units out

of plane or when the size of the atomic orbitals (AOs) at the coupling position is diminished.

Further reduction in band gap is possible by enhancing the strength of the donor and the acceptor moieties *via* strong orbital interactions. In donor-acceptor systems, the introduction of electron-withdrawing groups reduces  $E_g$  by lowering the LUMO levels whereas, the introduction of electron-donating groups reduces  $E_g$  by raising the HOMO levels. Therefore, design of extremely low  $E_g$  polymers requires strong donors and acceptors. Commonly employed electron-donating moieties are thiophene and pyrrole with various substitution patterns, which often represent the best choice since these are electron rich subunits that allow numerous chemical transformations. The most widely used electron-withdrawing groups are cyano and nitro groups.

Donor-acceptor type organic dye molecules in general have inherently low HOMO-LUMO energy gap. Extension of the conjugation length and strengthening of the donor-acceptor interaction in such dyes can generate polymers with low band gap energy and intrinsic conductivity. Squaraine dyes are the best among the different class of dyes for this purpose. They are the condensation products of 3,4-dihydroxy-3-cyclobutene-1,2-dione (squaric acid) with electron rich aromatic and heterocyclic molecules such as benzothiazoles, *N,N*-dialkylanilines, phenols, azulenes and pyrroles.<sup>10</sup> They are highly colored zwitterionic dyes, which possess intense absorption in the visible to the near infrared region. A representative example is shown in Scheme 2.1.



Scheme 2.1

Subsequent to the report of squaraine dyes in 1965, squaraine polymers have attracted much attention due to their unique and novel properties applicable to a broad area of optical and electronic technologies.<sup>11</sup> The first report on a squaraine based polymer pertains to the formation of an insoluble material upon reaction of pyrrole with squaric acid.<sup>12</sup> Electron rich heterocyclic compounds such as *N*-alkylcarbazole<sup>13</sup> and benzobisthiazoles<sup>14,15</sup> also facilitate the formation of squaraine polymers (Chart 2.1).

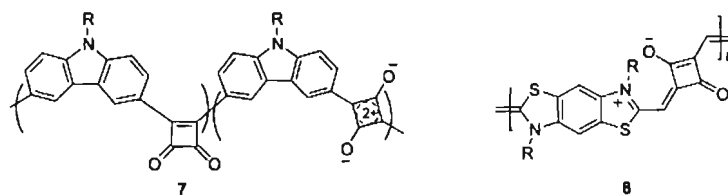
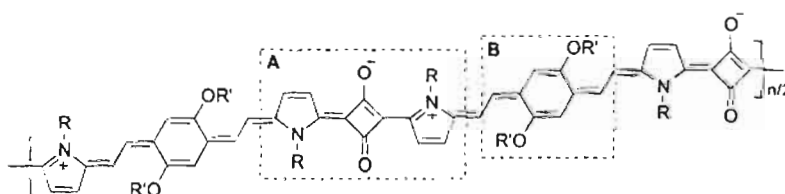


Chart 2.1

Squaric acid condenses with *N*-alkyl substituted pyrroles when both 2 and 5 positions are free to react, thereby forming partially soluble dark blue polymeric products.<sup>16-23</sup> Except for a few cases, these polymers did not show the expected low band gaps. This observation was in contrast to the theoretical prediction that extension of conjugation in squaraine dyes can lead to the formation of low band gap polymers. This could be due to the fact that in polysquaraines, the low band

gaps originated from a narrow HOMO-LUMO energy separation, typical of D-A fragments. On chain extension through polymerization of each D-A fragment, the hybridization not only raises the energy of the HOMO but also the LUMO level by a similar amount. Therefore, in polysquaraines, both HOMO and LUMO levels are shifted up equally and hence no considerable reduction in band gap is observed. If only the HOMO levels is allowed to participate in hybridization and the LUMO levels are frozen at the originally low value, a low band gap polymer can be realized.

It has been reported that incorporation of an electron rich dialkoxybenzene moiety 'B' between a squaraine dye unit 'A' significantly shifts the absorption of the resulting polymers towards near-IR region (Chart 2.2).<sup>24,25</sup> These polymers exhibit a broad window of absorption between 600-1300 nm. In view of this observation, it is important to study the effect of different aromatic bridging units on the optical and electronic properties of the resultant polysquaraines.



**Chart 2.2**

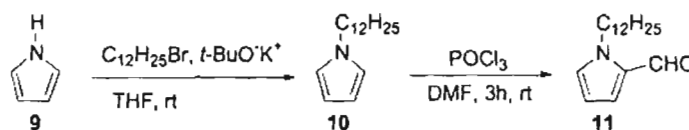
In this chapter a detailed study on the structure-property relationship existing in polysquaraines with different aromatic bridging unit is described. A series of polysquaraines were prepared by the polycondensation of bispyrrole monomers

containing divinylbenzene, divinylbiphenyl, dimethoxydivinylbenzene, divinylanthracene and dialkoxydivinylnaphthalene bridging units with squaric acid. Since the solubility of the polysquaraines is poor in organic solvents, a few monomeric dyes with better solubility were prepared which are used as the model units of the polysquaraines.

## 2.3. Results and Discussion

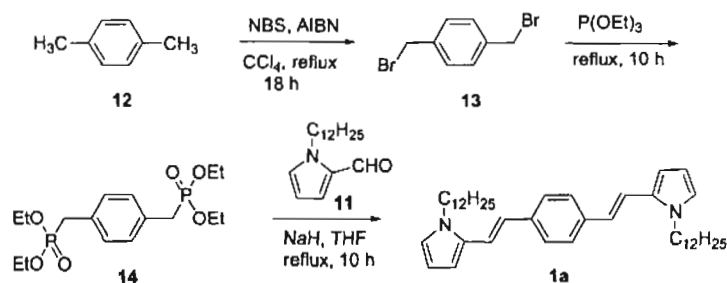
### 2.3.1. Synthesis and Characterization of Bispyrroles 1a-e

Synthesis of *N*-dodecylpyrrole-2-carboxaldehyde (**11**) was accomplished by the synthetic route shown in Scheme 2.2. The *N*-dodecylpyrrole (**10**) on Vilsmeier reaction using phosphorus oxychloride and dry *N,N*-dimethyl formamide gave the *N*-dodecylpyrrole-2-carboxaldehyde (**11**) in good yields.



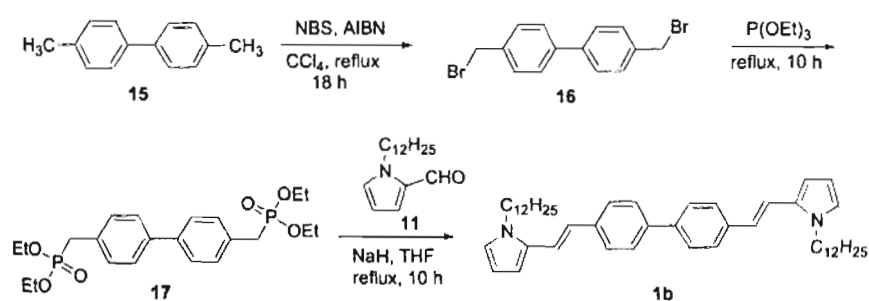
Scheme 2.2

Synthesis of the bispyrrole **1a** was started with the bromination of *p*-xylene (**12**) using *N*-bromosuccinimide to convert them to the corresponding bisbromomethyl derivative **13**. The bisphosphonate ester **14** was prepared by Michaelis-Arbuzov reaction of **13** with triethyl phosphite. The Wittig-Horner-Emmons olefination reaction of the bisphosphonate ester **14** with *N*-dodecylpyrrole-2-carboxaldehyde provided the bispyrrole **1a** in 55% yield (Scheme 2.3).<sup>26</sup>



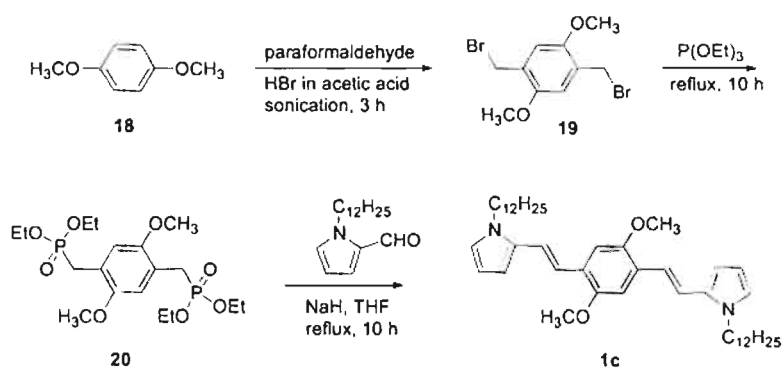
Scheme 2.3

Bispyrrole **1b** was prepared by following a similar synthetic route starting from 4,4'-dimethyl biphenyl (**15**) (Scheme 2.4).



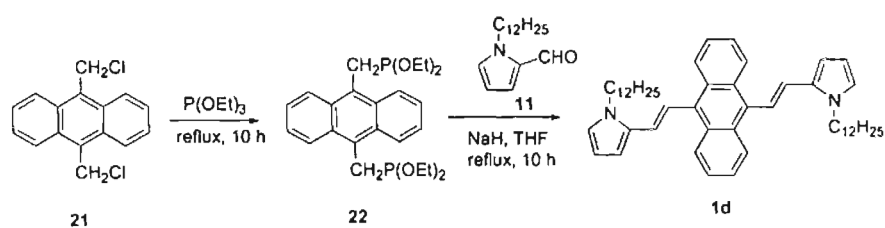
Scheme 2.4

For the preparation of the bispyrrole **1c**, 1,4-dimethoxybenzene (**18**) was converted to the corresponding bisbromomethyl derivative by sonicating with paraformaldehyde and HBr in acetic acid for 3 h. The reaction of bisbromomethyl derivative (**19**) with triethyl phosphite resulted in the formation of the corresponding bisphosphonate ester (**20**) which was then coupled with *N*-dodecylpyrrole-2-carboxaldehyde to give the bispyrrole **1c** in 70% yield. (Scheme 2.5).



Scheme 2.5

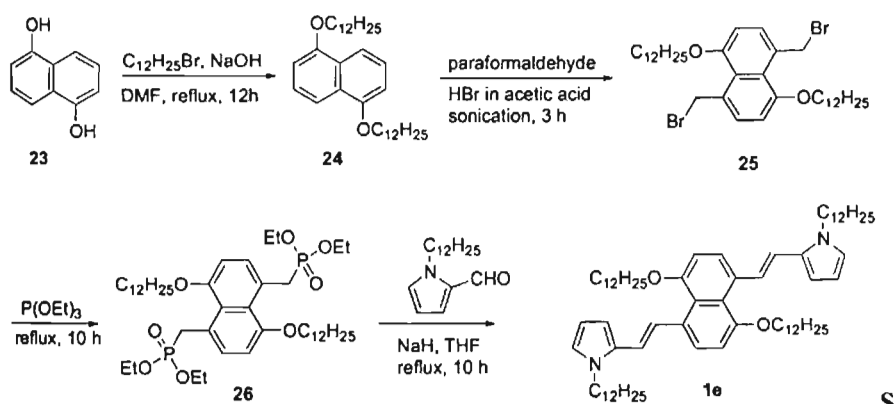
The bischloromethyl derivative of anthracene (**21**) upon conversion to the corresponding bisphosphonate ester **22** by Michaelis-Arbuzov reaction in 70% yield, followed by Wittig-Horner-Emmons olefination reaction with *N*-dodcylpyrrole-2-carboxaldehyde provided the bispyrrole **1d** in 68% yield (Scheme 2.6).



Scheme 2.6

Synthesis of the bispyrrole **1e** is shown in Scheme 2.7. Alkylation of the 1,5-dihydroxynaphthalene (**23**) with dodecylbromide in DMF gave the 1,5-didodecyloxy naphthalene derivative **24** in 65% yield. The bisbromomethyl

derivative **25** was prepared in 65% yield using a similar procedure used for the preparation of the bisbromomethyl derivative of 1,4-dimethoxybenzene **18**.



All the new compounds under study were characterized by FT-IR,  $^1\text{H}$  NMR,  $^{13}\text{C}$  NMR and HRMS analyses. The all-*trans* configuration of the monomers were confirmed from the coupling constants ( $J = 16\text{-}17$  Hz) obtained from their  $^1\text{H}$  NMR spectra.

### 2.3.2. Photophysical Properties of the Bispyrroles 1a-e

The absorption and emission spectra of **1a-e** were recorded in toluene, dichloromethane and acetonitrile. These compounds showed absorption in the range 370–450 nm and intense emission around 470–495 nm. The absorption spectra are broad without noticeable difference in spectral shape from each other. The absorption and emission spectra of the bispyrroles **1a-e** in dichloromethane are shown in Figure 2.3 and Figure 2.4, respectively. Bispyrrole **1c** with

dialkoxybenzene moiety and **1d** with anthracene group showed slight red-shift in the absorption maximum when compared to the other bispyrrole derivatives.

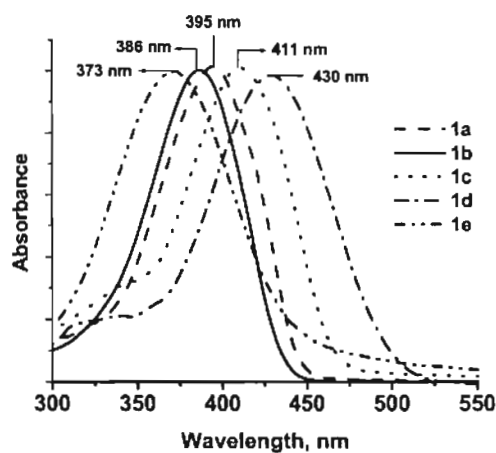


**Figure 2.3.** Normalized absorption spectra of the bispyrroles **1a-e** in dichloromethane.

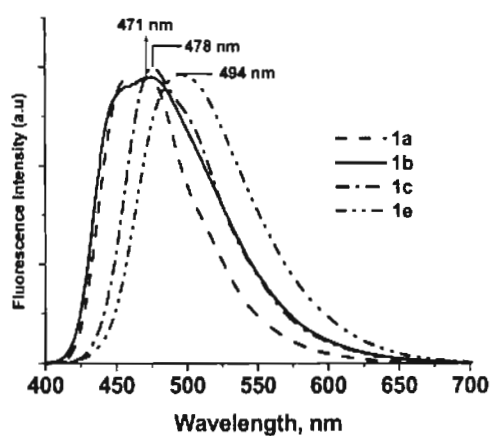


**Figure 2.4.** Emission spectra of the bispyrroles **1a-c** and **1e** in dichloromethane.

The absorption maxima of **1a-e** showed minor shift with polarity of the solvent and with nature of the aromatic bridging units whereas the emission

spectra exhibited considerably more shift. As a representative case, the absorption and emission spectra of **1b** are shown in Figure 2.5. In toluene, **1b** exhibited a structured emission with a maximum at 440 nm and shoulders at 468 and 505 nm. On the other hand, in dichloromethane, a broad emission with a maximum at 475 nm is obtained whereas in acetonitrile the emission became broad and red-shifted with maximum at 486 nm. Bispyrrole **1d** showed weak fluorescence when compared to that of the other bispyrroles. The relatively broad and red-shifted emission in acetonitrile indicates considerable charge transfer interaction at the excited state. The fluorescence quantum yields ( $\Phi_f$ ) of these monomers in toluene were determined using quinine sulfate as the standard. The  $\Phi_f$  values in toluene are found to be higher than that in dichloromethane and in acetonitrile. The optical and photophysical properties of the bispyrroles **1a-e** in toluene are summarized in Table 2.1.

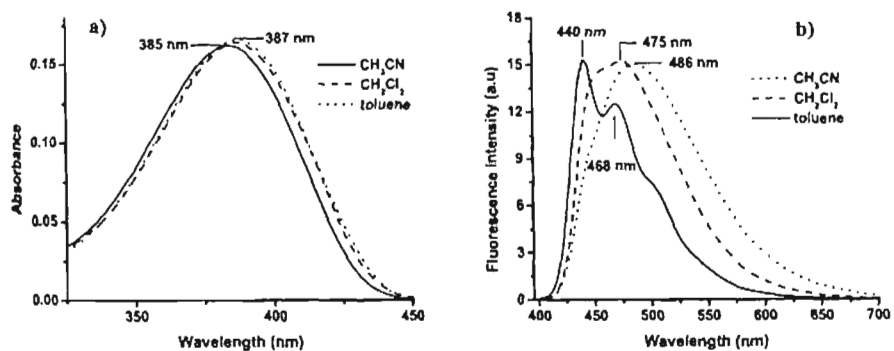


**Figure 2.5.** (a) Absorption and (b) emission spectra of the bispyrrole **1b** in various solvents.

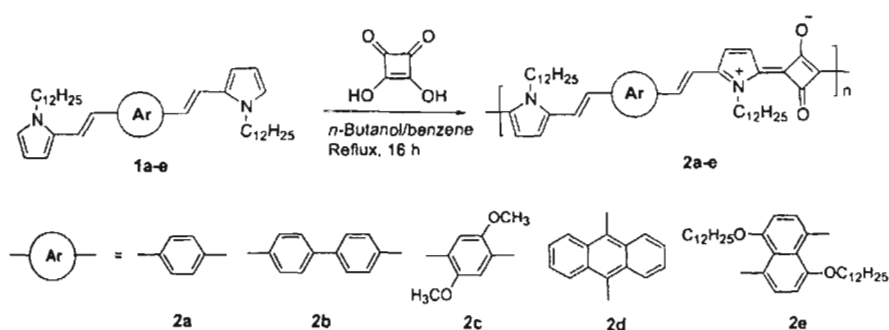
**Table 2.1.** Optical properties of the bispyrroles **1a-e** in toluene.

Bispyrrole	$\lambda_{\text{max}}$ (nm) <sup>a</sup>	$\lambda_{\text{max}}$ (nm) <sup>b</sup>	$\Phi_f$ <sup>c</sup>	$\tau_s$ (ns) <sup>d</sup>
<b>1a</b>	398	443,471	0.32	1.06
<b>1b</b>	387	440,468	0.63	1.03
<b>1c</b>	412	471	0.52	1.24
<b>1d</b>	433	563	Weak fluorescence	
<b>1e</b>	374	487	0.54	2.62

(a) Absorption maxima, (b) Emission maxima, (c) Fluorescence quantum yield determined using quinine sulfate as standard, (d) Excited state lifetime.

### 2.3.3. Synthesis and Characterization of Polysquaraines (**2a-e**) and $\pi$ -Extended Squaraine Dyes (**3a-d**)

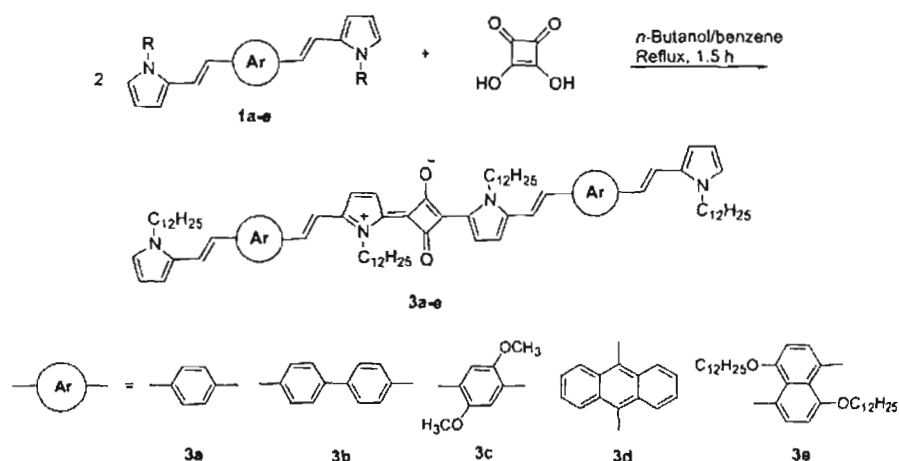
Polycondensation of the bispyrroles **1a-e** with squaric acid in 1:1 stoichiometry in a solvent mixture of *n*-butanol-benzene (1:3) under azeotropic refluxing condition resulted in the formation of intensely colored products **2a-e** (Scheme 2.8). After 16 h, the solvents were partly removed under vacuum and the products were precipitated by adding petroleum ether. The products were further washed several times with *n*-butanol and methanol to remove the unreacted squaric acid followed by washing with toluene. The precipitated products were further purified by repeated precipitation and washing using hexane. The polysquaraines with divinylbenzene and divinylbiphenyl bridging units showed poor solubility in organic solvents whereas polysquaraines with dialkoxydivinylbenzene moiety exhibited relatively better solubility in solvents such as chloroform and dichloromethane.



Scheme 2.8

Since the solubility of the polysquaraines were very low in organic solvents, it was difficult to record the NMR spectra to have a complete characterization. Therefore, for a better understanding of the structure of the polysquaraine a few analogous squaraine dyes **3a-e** were prepared by the condensation of the bispyrroles **1a-e** with squaric acid in the ratio 2:1 in *n*-butanol/benzene mixture (1:3) (Scheme 2.9). The progress of the reaction was monitored by recording the absorption spectrum of the reaction mixture at intervals. The reaction was stopped when absorption corresponding to the polymers started appearing (Figure 2.6). The reaction mixture was filtered and the solvents were partly removed under vacuum and the products were precipitated by adding methanol. The dyes **3a**, **3c** and **3d** were purified by dissolving them in chloroform and reprecipitation by adding petroleum ether. After repeated washings with petroleum ether, and column chromatography over silica gel using 50% petroleum ether-ethyl acetate mixture, the dye was obtained in 20-40% yields

in the form of deep green powder with metallic luster. These dyes were relatively more soluble in solvents, when compared to the corresponding polysquaraines.



These dyes were soluble in solvents such as chloroform, dichloromethane and tetrahydrofuran. They were characterized by FT-IR,  $^1\text{H}$  NMR,  $^{13}\text{C}$  NMR, HRMS and elemental analyses. However, the dye **3b** with the biphenyl moiety was least soluble in organic solvents and hence could not be characterized by NMR technique. All the polymers showed a strong peak between  $1621\text{-}1600\text{ cm}^{-1}$  region which corresponds to the C-O stretching frequency of the cyclobutenediylum-1,3-diolate moiety. This peak is characteristic of a resonance stabilized 1,3-cyclobutanediolate dianion moiety of the squaraine chromophore. Resonance signals of the aromatic protons were broad and weak. However, the characteristic peaks of  $-\text{NCH}_2$  protons and  $-\text{OCH}_2$  protons could be seen in the  $^1\text{H}$  NMR spectra of the soluble polysquaraines. The methyl protons of the side chain

alkyl groups appeared around  $\delta$  0.84 ppm. All the other protons of the alkyl chains were observed as broad multiplet at a region of  $\delta$  1.22 - 1.86 ppm.  $^1\text{H}$  NMR spectrum of the dyes showed strong *trans* coupling for the vinylic linkages, which was in agreement with the structure assigned to the dyes. The resonance stabilization in the dyes was indicated by strong peaks corresponding to  $^1\text{N-CH}_2$  and  $\text{N-CH}_2$  protons around  $\delta$  4.5 and 3.9 ppm, respectively. Protons of the dodecyl chains appeared as broad multiplets in the region of  $\delta$  1.82-1.25 ppm. Methyl protons of the alkyl side chains were observed as multiplet at  $\delta$  1.0-0.88 ppm.  $^{13}\text{C}$  NMR spectrum and elemental analysis of the dyes were in agreement with their structures. Elemental analyses of the polysquaraines were in agreement with their structures, which revealed the presence of a molecule of water for every repeating unit of the polymers.

(R) 541.14  
PS11

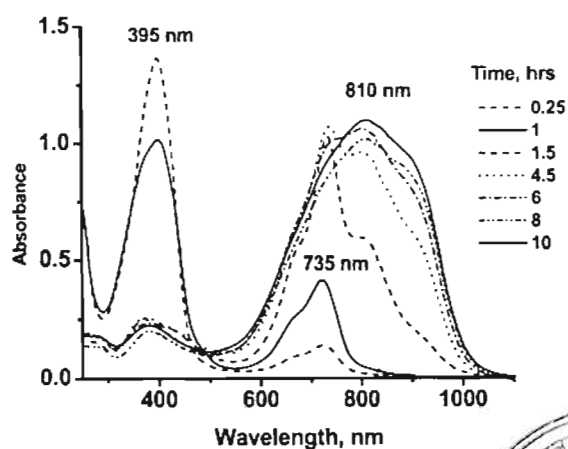
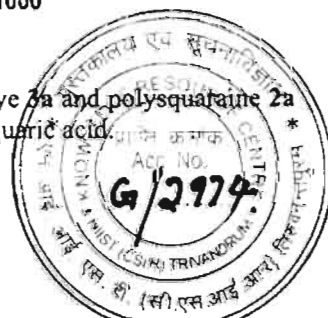


Figure 2.6. Evolution of the spectra of the squaraine dye **3a** and polysquaraine **2a** with the progress of the reaction of bispyrrole **1a** and squaric acid.



Thermogravimetric analysis (TGA) of the polysquaraines **2a-c** showed an initial weight loss around 150-250 °C due to the absorbed water molecules followed by major weight loss around 300 and 500 °C, which are due to the degradation of the side chains and the backbone (Figure 2.7).

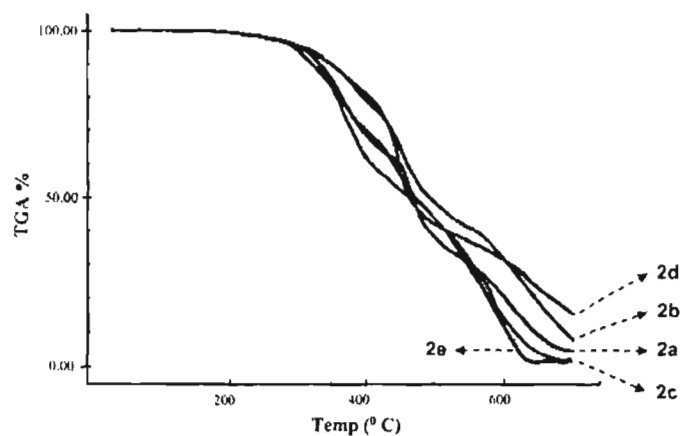
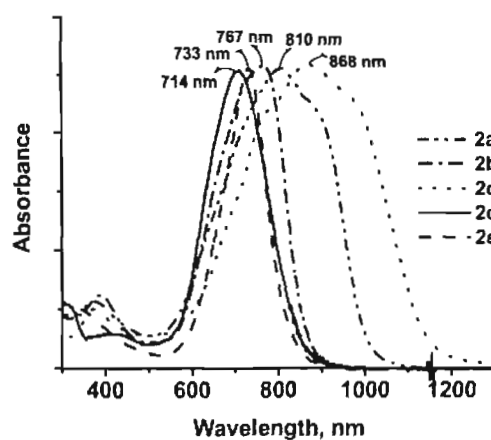


Figure 2.7. Thermogravimetric analysis (TGA) of the polymers **2a-e**

#### 2.3.4. Electronic Absorption Spectra of Polysquaraines **2a-e**

The electronic absorption spectra of the polysquaraines **2a-e** in chloroform are shown in Figure 2.8. With change in the aromatic bridging unit, the absorption spectra of **2a-e** showed considerable variations. The polysquaraine **2c** with dimethoxydivinylbenzene bridging moiety showed a broad absorption spectrum with a maximum at around 868 nm and a shoulder band at 980 nm. On the other hand, the polysquaraine **2a** with a simple divinylbenzene bridge showed a 58 nm blue shift in the absorption maximum ( $\lambda_{\text{max}} = 810$  nm) when compared to that of **2c**,



**Figure 2.8.** Normalized absorption spectra of **2a-e** in chloroform.

Interestingly, the absorption spectra of **2b**, **2d** and **2e** are relatively sharper than those of **2a** and **2c**. In the case of the biphenyl-derived polysquaraine **2b**, the twisted conformation of the biphenyl moiety may reduce the effective conjugation length, resulting in the blue shift of the absorption maximum. In the case of the anthracene and naphthalene derived polysquaraines **2d** and **2e**, relatively narrow absorption spectra were obtained. In these cases, the absorption maxima were significantly blue shifted. This is attributed to the bulkiness of the bridges that twists the polymer chain out of planarity, which reduces the effective conjugation length of the backbone. In addition, in the case of **2e**, the 1,5 double bond is not through conjugated which will also reduce the effective conjugation. In the case of **2d**, the anthracene moiety is relatively electron deficient which will reduce the charge-transfer character of the polysquaraine.

### 2.3.5. Electronic Absorption Spectra of the $\pi$ -Extended Squaraine Dyes 3a-d

Absorption spectra of the dyes **3a-d** recorded in chloroform are shown in Figure 2.9. As in the case of the polysquaraines, the different aromatic bridging units significantly influence the optical properties of these dyes. The dye **3a** without any alkoxy substituents showed absorption maximum at 739 nm. The anthracene derived dye **3d** exhibited a broad absorption with a maximum at 696 nm and the biphenyl derived dye **3b** showed absorption maximum at 707 nm. The dye **3c** had a red-shifted absorption ( $\lambda_{\text{max}} = 763$  nm) when compared to the other derivatives.

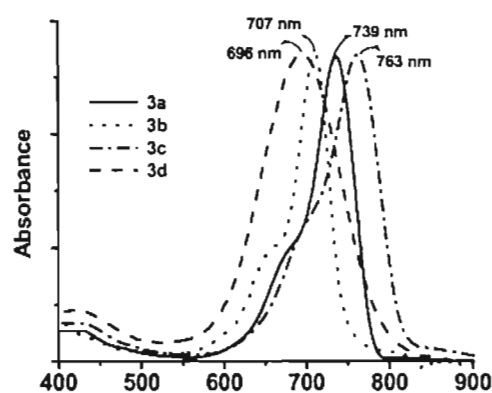
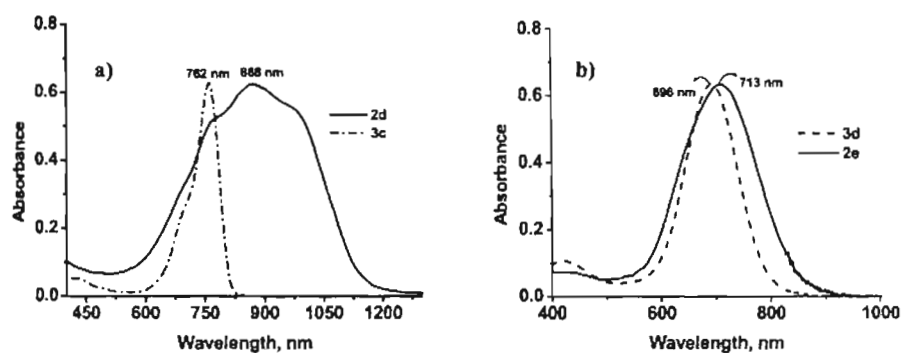


Figure 2.9. Normalized absorption spectra of **3a-d** in chloroform.

This is due to the presence of electron rich methoxy group in the aromatic bridging unit which enhances the charge-transfer interaction. A comparison of the solution state spectra of the dyes and the corresponding polysquaraines is given in Figure 2.10. In the case of **2c** and **3c**, a large difference could be observed in the absorption spectra. Dye **3c** showed a sharp absorption with  $\lambda_{\text{max}}$  at 762 nm in

chloroform. However, the corresponding polysquaraine **2c** exhibited a broad spectrum. Interestingly, such a large difference in the absorption spectra could not be observed for **2d** and **3d** having the anthracene bridging unit.



**Figure 2.10.** Comparison of the absorption spectra of the polysquaraines and the corresponding model dyes in chloroform; a) polysquaraine **2c** and the dye **3c**. b) polysquaraine **2d** and the dye **3d**.

### 2.3.6. Electronic Absorption Spectra of Polysquaraines and the Model Dyes in Mixed Solvent Systems: Aggregation Properties

The polysquaraines **2a-e** showed considerable variations in the absorption spectra in binary solvent mixtures of toluene-DMSO with varying composition, as illustrated in the case of **2a** and **2c** (Figure 2.11 and Figure 2.12). These changes could be attributed to the aggregation behavior of **2a** and **2c** in toluene-DMSO mixtures. For example, the absorption maximum of **2a** at 795 nm was decreased in intensity with increase in DMSO content in toluene. In 90% DMSO, the absorption maximum is shifted to 725 nm. Similar changes in the absorption spectrum were observed for **2c** (Figure 2.12). The absorption maximum at 865 nm was shifted to 754 nm in 90% DMSO. In both cases, the major changes in the

absorption spectra occurred only to the long wavelength side. These observations indicate similar aggregation behavior of **2a** and **2c** in toluene-DMSO mixtures. The biphenyl containing polymer **2b** could not be studied due to poor solubility in solvents. Polymers **2d** and **2e** with bulky aromatic bridging units did not show any major change in the absorption spectra in toluene-DMSO.

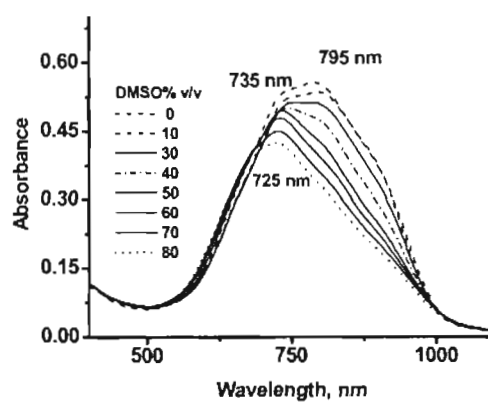


**Figure 2.11.** Absorption changes for **2a** in toluene-DMSO solvent mixtures of different DMSO content.

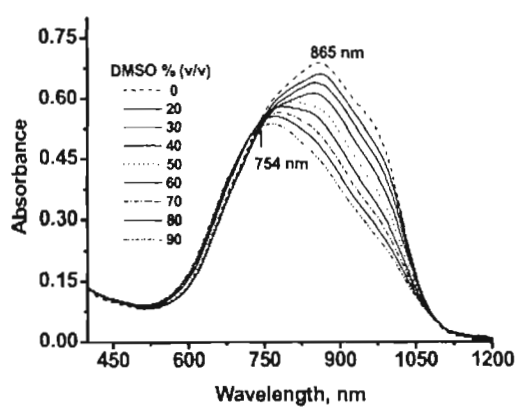


**Figure 2.12.** Absorption changes for **2c** in toluene-DMSO solvent mixtures of different DMSO content.

In contrast to the behavior of the polysquaraines, their model dyes **3a**, **3c** and **3d** failed to show any change in the absorption spectra in toluene-DMSO mixtures. This observation indicates that **3a**, **3c** and **3d** do not form aggregates in toluene-DMSO solvent mixtures. The better solubility of the dyes in these solvent mixtures may prevent the aggregation of the dyes. However, the dyes **3a** and **3c** exhibited considerable change in the absorption spectra in DMSO-water mixtures. In DMSO, the dye **3a** exhibited an absorption maximum at 739 nm. However, increasing the water content in DMSO decreased the intensity of the absorption maximum at 739 nm with the formation of a blue shifted band at 607 nm (Figure 2.13). Formation of the blue shifted band is characteristic of the H-type aggregates of squaraine dyes.

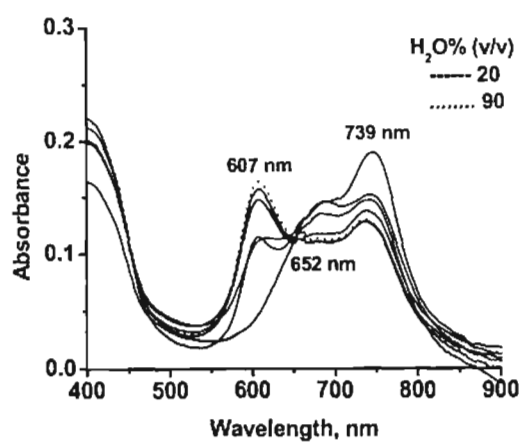


**Figure 2.13.** Changes in the absorption spectra of **3a** in DMSO-water mixtures ( $[\text{dye}] = 4.68 \times 10^{-6}\text{M}$ ).

Upon heating the solution, the intensity of the peak at 607 nm decreases while the intensity of the peak at 739 nm corresponding to the monomer is increased (Figure 2.14). Similarly, for **3c**, the sharp monomer peak at 775 is found to decrease with the formation of a new peak around 650 nm, which is attributed to the formation of H-aggregate of the dye. The solvent dependent change in the absorption spectrum of the dye **3c** in DMSO-water of varying composition is shown in Figure 2.15. In this case, aggregation is initiated with low percentage of water. For example with 8% of water, the monomer peak at 775 nm is considerably decreased and a broad spectrum with blue shifted shoulder is formed. Upon further increase in water composition, the intensity of the blue shifted peak is increased indicating the preferred formation of H-aggregates. Concentration dependent spectral changes in 88% DMSO-water mixture showed the monomer band when the concentration of the dye is low. Upon increasing the concentration, the growth of the blue shifted band corresponding to the H-aggregate is visible. Temperature dependent changes in 88% DMSO-water mixture indicate the partial dissociation of the aggregates to the monomer (Figure 2.16).

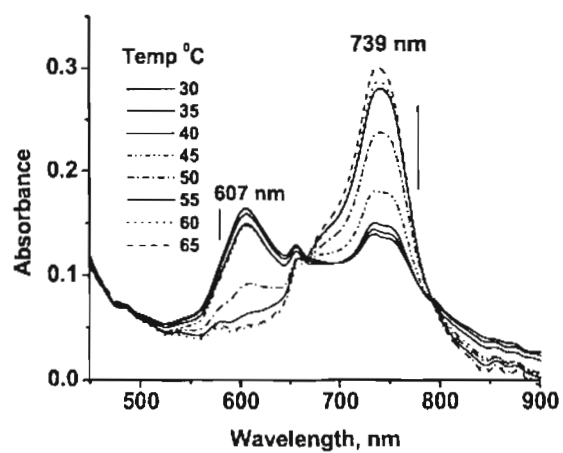


**Figure 2.14.** Temperature dependent changes of 3a in 70% DMSO-water mixture ( $[\text{dye}] = 4.68 \times 10^{-6}\text{M}$ ).

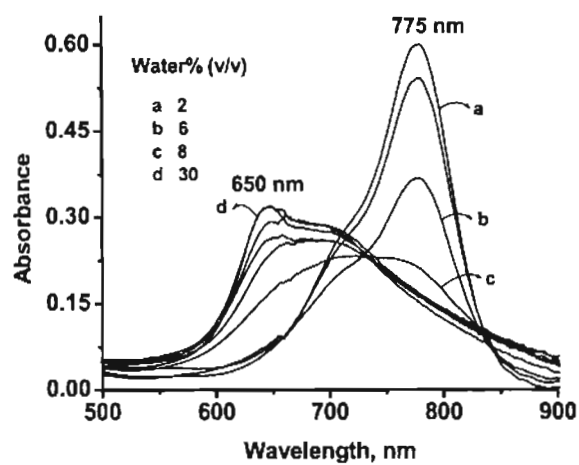


**Figure 2.15.** Absorption spectra of 3c in DMSO-water solvent mixture of different composition ( $[\text{dye}] = 4.54 \times 10^{-6}\text{M}$ ).

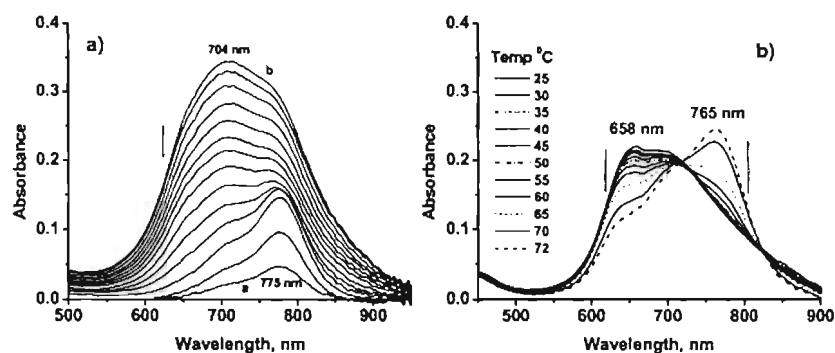


**Figure 2.16.** a) Concentration dependent spectra and b) Temperature dependent absorption spectra of **3c** in 88% (v/v) DMSO-water ( $[dye] = 4.54 \times 10^{-6}M$ ).

The dye **3d** with anthracene bridging unit exhibited an intense absorption spectrum with a maximum at 700 nm in DMSO. In contrast to the dye **3a** and **3c**, **3d** did not show any noticeable change in the absorption spectrum in DMSO-water mixtures (Figure 2.17). This observation indicates that the dye **3d** does not favor aggregation in DMSO-water mixture. This is a unique property since most of the squaraine dyes are known to form aggregates in DMSO-water mixture.

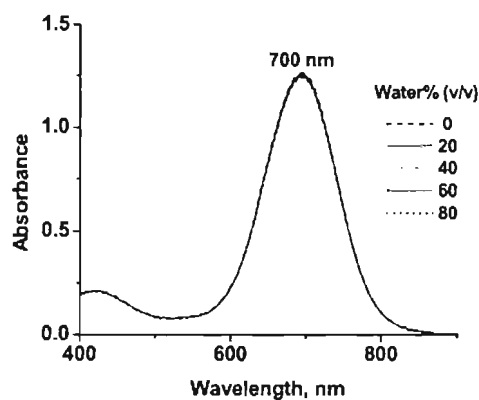


**Figure 2.17.** Absorption spectra of **3d** in DMSO-water with varying water content.

### 2.3.7. Solid-State Absorption Spectra

A comparison of the solid-state (film) absorption spectra of the polysquaraines **2a**, **2b** and **2d** on glass substrate are shown in Figure 2.18. In general, the electronic properties such as absorption and emission of conjugated polymers are considerably broad in the solid-state when compared to their solution behavior. This is mainly due to the interchain interaction and aggregation of the macromolecular backbone in the solid-state as demonstrated in the case of a variety of conjugated polymers.<sup>27-29</sup> Generally, due to strong intramolecular charge transfer interactions and aggregation, the solid-state absorption spectra of squaraine dyes are broad when compared to their solution spectra.

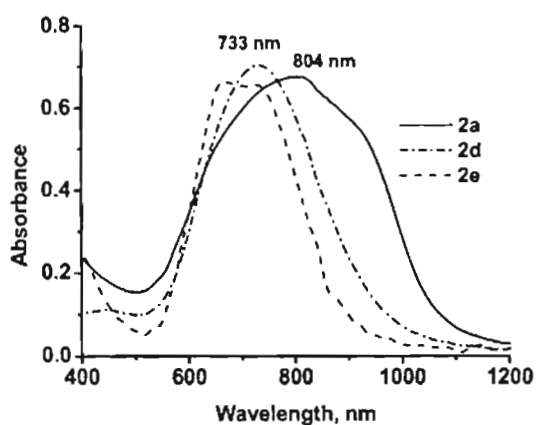
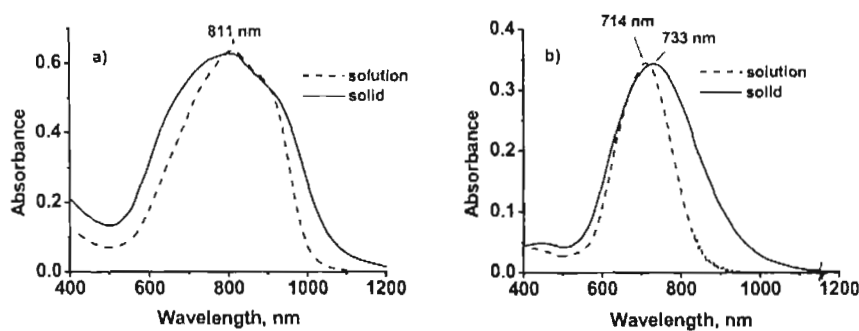


Figure 2.18. Solid-state absorption spectra of **2a**, **2d** and **2e**.

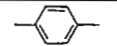
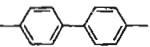
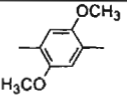
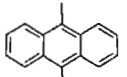
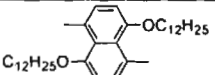
Interestingly, the solid-state absorption spectral features of the new polysquaraines are more or less identical to their solution spectra except for a marginal broadening of the shorter as well as the longer wavelength regions as

shown in the case of **2a** (Figure 2.19a). However, in the case of **2d**, the solid-state absorption exhibited a broadening towards the long wavelength region. In the shorter wavelength region, not much shift is observed (Figure 2.19b). It is likely that the marginal red-shift of the absorption maximum in the solid-state spectrum could be due to the aggregation of the polymer chains in the solid film. In the case of **2a** broadening on both lower and higher wavelength regions indicates the formation of H- as well as J-type aggregates. On the other hand, the broadening of the absorption spectrum of **2d** in the solid-state, mainly towards the long wavelength region, indicates the preferential J-type aggregation. The solid-state optical band gaps ( $E_g$ ) of the polysquaraines were calculated from the onset of the absorption spectra, which are 0.1-0.2 eV less, when compared to the band gaps calculated from the onset of the solution absorption spectra. The lowest band gap of 0.82 eV is observed for the polysquaraine **2c** and the highest band gap of 1.3 is noted for **2e**.



**Figure 2.19.** Comparison of solution and solid-state absorption spectra of **2a** and **2d**.

**Table 2.2.** Optical characteristics and intrinsic conductivity of polysquaraines (2a-g).

Polymer	Bridging unit 	Solution		Solid-state		Intrinsic conductivity (Scm <sup>-1</sup> )
		$\lambda_{\max}$ (nm)	$E_g$ (eV)	$\lambda_{\max}$ (nm)	$E_g$ (eV)	
2a		811	1.21	815	1.14	$4.32 \times 10^{-7}$
2b		715	1.41	727	1.26	$1.54 \times 10^{-8}$
2c		850	1.01	870	0.82	$2.20 \times 10^{-5}$
2d		714	1.42	733	1.29	$1.74 \times 10^{-9}$
2e		739	1.52	745	1.30	$2.40 \times 10^{-9}$

### 2.3.8. Conductivity Studies

Due to extensive conjugation and charge-transfer interaction, polysquaraines are expected to be intrinsically conducting. The absorption maxima and the  $E_g$  of the polysquaraines in the solution and solid-state along with intrinsic conductivities are shown in Table 2.2. The extremely low band gaps of these polymers indicate the possibility of intrinsic conductivity. Four probe conductivity studies showed that the intrinsic conductivities of the polysquaraines **2a-e** are in the range of  $10^{-9}$  Scm<sup>-1</sup> whereas the doped conductivities are in the order of  $10^{-6}$  Scm<sup>-1</sup>.

### 2.3.9. X-ray Diffraction Study

X-ray diffraction patterns of the polysquaraines **2a** and **2c-e** were recorded in order to get an insight into the molecular packing in the solid-state (Figure 2.20). For a better understanding of the molecular ordering of the squaraine polymers, their interchain packing distances were compared with those of the regioregular polythiophenes<sup>30,31</sup> which are reported to form lamellar packing. The reported interchain spacing of a regioregular poly(3-dodecylthiophene) is 27.19 Å. Earlier studies on a polysquaraine with *N*-dodecyl and *O*-dodecyl side chains showed an interchain distance of 21.0 Å which is 6 Å less than a regioregular poly(3-dodecylthiophene). These studies suggest an interdigitated comb like arrangement of the alkyl chains for the polysquaraines. However, the calculated interchain distance of the polysquaraine with *N*-dodecyl, chains for lamellar packing is 35 Å, which corresponds to the theoretical width of the molecules when the alkyl chains are stretched. In the case of an interdigitated packing of the alkyl chains, a packing distance of 17-19 Å should have been observed.<sup>32</sup> In the case of **2c**, a *d*-spacing of 17 Å could be observed which could be correlated to an interdigitated packing of the side chains. In addition, the broad peak corresponding to a distance of 3.8 Å to 4.4 Å indicates the existence of ordered microcrystalline domains. However, surprisingly, in the case of **2a**, **2d** and **2e**, the observed interchain *d*-spacing are 25.45, 36.99 and 36.47 Å respectively. In the wide angle region broad and weak diffraction patterns were observed indicating the absence of any long range order. Furthermore, in the case of polysquaraines **2d** and **2e** with

anthracene and naphthalene bridging units, the  $d$ -spacing is found to be nearly 11 Å greater when compared to that of **2a** with a benzene bridging unit. These observations indicate a close interchain packing in **2c** and **2a** which is very strong in **2c** leading to sidewise interdigitation of the polysquaraine backbones. Figure 2.21 and Figure 2.22 shows the interdigitated molecular packing for **2c** and the lamellar packing of **2d** respectively.

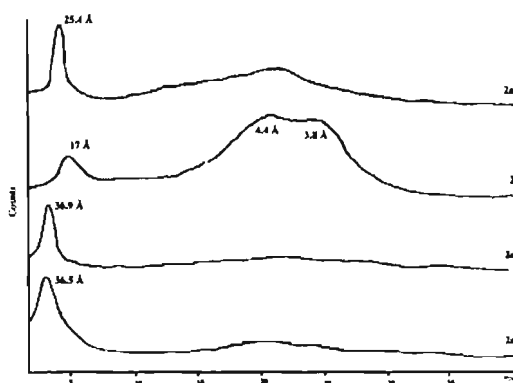


Figure 2.20. X-ray diffraction pattern of polysquaraines **2a**, **2c**, **2d** and **2e**.

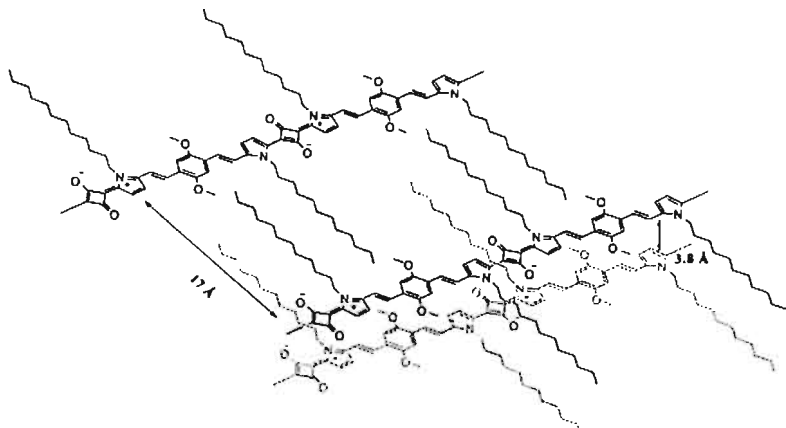


Figure 2.21. Interdigitated molecular packing diagram of the polysquaraine **2c**.

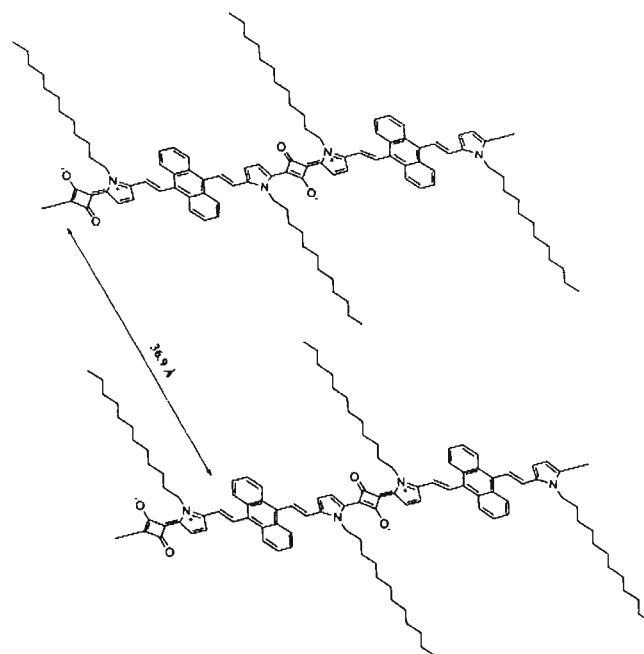


Figure 2.22. Lamellar packing diagram of the polysquaraine **2d**.

#### 2.4. Conclusions

The solution and solid-state absorption spectral properties of the polysquaraines **2a-e** are strongly influenced by the aromatic bridging units in the polymer backbone. Polysquaraines derived from divinylbenzene and dimethoxydivinylbenzene bridged bispyrroles showed broad and red-shifted absorption when compared to those polysquaraines having divinylbiphenyl or divinylanthracene or dialkoxydivinylnaphthalene bridging moieties. Polysquaraine with dimethoxydivinylbenzene bridging unit exhibited the lowest solution and solid-state band gap with maximum intrinsic conductivity. The corresponding  $\pi$ -extended model squaraine dye **3c** showed a 67 nm red-shift in the absorption

maximum when compared to the dye **3d** with a divinylanthracene bridging unit. The polysquaraines **2a** and **2c** with a divinylbenzene and dimethoxydivinylbenzene moieties, respectively showed a gradual blue-shift of the absorption maximum in toluene-DMSO mixtures whereas the corresponding model dyes **3a** and **3c** showed the characteristics of H-aggregation in DMSO-water. Interestingly, aggregation was prevented when divinylanthracene bridge was used. Squaraine dyes with strong absorption in the visible to the near-IR wavelength region that do not form aggregates may have potential application in solid-state devices.

## 2.5. Experimental

### 2.5.1. Materials

The solvents and reagents were purified and dried by usual methods prior to use. Pyrrole, 2-Ethylhexylbromide, Dodecylbromide and 3,4-Dihydroxy-3-cyclobutene-1,2-dione (squaric acid) were purchased from Sigma-Aldrich. 1,5-Dihydroxy naphthalene was purchased from Merck. Spectroscopic grade solvents purchased from Merck and used as such for spectroscopic studies. Doubly distilled deionized water was used for the studies in binary DMSO-water mixtures. Solutions for spectral measurements in mixed solvents were prepared by adding equal amount of a stock solution of the dye into a series of binary solvent mixtures with different compositions. Sufficient time was given for equilibration of the solution. For solid-state absorption studies, the film was prepared by casting a

chloroform solution of the dye on glass slides followed by slow evaporation of the solvent.

### 2.5.2. Measurements

All melting points were determined on an Aldrich Mel-Temp-II melting point apparatus.  $^1\text{H}$  NMR spectra and  $^{13}\text{C}$  NMR spectra were measured on a 300 MHz Bruker Avance DPX spectrometer. IR spectra were recorded on a Nicolet Impact 400D infrared spectrophotometer. High-resolution mass spectra were recorded on a JEOL JMS600 mass spectrometer. The UV-Vis-NIR spectra were recorded on Shimadzu UV-3101 PC NIR Scanning spectrophotometer and Agilent 8453 UV-visible Spectroscopy system. Elemental analysis was carried out using a Perkin-Elmer series-II 2400 CHN analyzer. X-ray diffraction patterns were recorded on a Philips diffractometer using Ni filtered  $\text{K}\alpha$  radiation.

### 2.5.3. Preparation of *N*-Dodecylpyrrole (10)

To a solution of potassium *tert*-butoxide (100 mmol) in 100 mL dry THF, pyrrole (95 mmol) was added and stirred at 30 °C for 3 h. To the potassium pyrrole solution 18-crown-6 (9 mmol) was added and stirred for 15 min. To the reaction mixture, 1-bromododecane (108 mmol) was added dropwise and the stirring was continued for 18 h. The precipitated inorganic salt was filtered off and the solvents were removed under reduced pressure. The residue was extracted with dichloromethane. The combined organic extracts were washed with brine followed by water and dried over sodium sulfate. The solvents were removed and the crude

product was purified by column chromatography over silica gel using petroleum ether to give the *N*-dodecylpyrrole in 88% yield. Details of the characterization data are given below.

Yield 88%;  $^1\text{H}$  NMR ( $\text{CDCl}_3$ , 300 MHz)  $\delta$  6.64 (m, 2H, aromatic), 6.11 (t, 2H, aromatic), 3.85 (t, 2H,  $\text{NCH}_2$ ), 1.73 (m, 2H,  $\text{CH}_2$ ), 1.25 (m, 18H,  $\text{CH}_2$ ), 0.86 (t, 3H,  $\text{CH}_3$ );  $^{13}\text{C}$  NMR ( $\text{CDCl}_3$ , 75.4 MHz)  $\delta$  120.23, 107.70, 49.46, 31.68, 31.47, 31.10, 29.58, 29.48, 29.41, 29.31, 29.22, 26.60, 22.52, 14.00.

#### 2.5.4. Preparation of *N*-dodecylpyrrole-2-carboxaldehyde (11)

To a solution of dry DMF (35 mmol) and phosphorus oxychloride (9 mmol) at 10-20 °C, *N*-dodecylpyrrole (9 mmol) in dry DMF was added slowly with stirring. The mixture was stirred at 35 °C for 45 min. and then poured into crushed ice. The clear solution formed at 20-30 °C was neutralized with aqueous NaOH. The mixture was boiled for 1 min, cooled to room temperature and extracted with diethyl ether. Removal of the solvent gave a viscous liquid, which was chromatographed on silica gel using petroleum ether-ethyl acetate (9.5:0.5) to give the *N*-dodecylpyrrole-2-carboxaldehyde in 70% yield.

Yield 70%;  $^1\text{H}$  NMR ( $\text{CDCl}_3$ , 300 MHz)  $\delta$  9.5 (s, 1H, aldehyde), 6.8 (m, 2H, aromatic), 6.1 (t, 1H, aromatic), 4.2 (t, 2H,  $\text{NCH}_2$ ), 1.1-1.8 (m, 20H,  $\text{CH}_2$ ), 0.7-0.9 (t, 3H,  $\text{CH}_3$ );  $^{13}\text{C}$  NMR ( $\text{CDCl}_3$ , 75.4 MHz)  $\delta$  179.10, 131.8, 131.0, 124.6, 109.30, 49.0, 31.48, 29.58, 29.41, 29.22, 23.60, 22.90, 14.49.

### 2.5.5. Preparation of 1,4-bis(bromomethyl) benzene (13)

To a solution of 4,4'-dimethyl benzene (10 mmol) in 50 mL of dry carbon tetrachloride was added *N*-bromosuccinimide (20.5 mmol) and AIBN. The reaction mixture was refluxed for 18 h., cooled, filtered and the solvents were removed under reduced pressure to give the crude product which was then purified by recrystallization from CCl<sub>4</sub>.

Yield 92%; <sup>1</sup>H NMR (CDCl<sub>3</sub>, 300 MHz) δ 7.14 (s, 4H, aromatic), 4.52 (s, 4H, CH<sub>2</sub>Br); <sup>13</sup>C NMR (CDCl<sub>3</sub>, 75.4 MHz) δ 137.70, 133.98, 29.98

### 2.5.6. Preparation of 4,4'-bis(bromomethyl) biphenyl (16)

Compound **16** was prepared using the same procedure as that of compound **13**.

Yield 88%; mp. 139 °C; <sup>1</sup>H NMR (CDCl<sub>3</sub>, 300 MHz) δ 7.38 (m, 4H, aromatic), 7.28 (m, 4H, aromatic), 4.53 (s, 4H, CH<sub>2</sub>Br); <sup>13</sup>C NMR (CDCl<sub>3</sub>, 75.4 MHz) δ 142.26, 137.50, 130.43, 128.61, 29.56.

### 2.5.7. Preparation of 2,5-bis(methoxy)-1,4-bis(bromomethyl)benzene (19) and 4,8-didodecyloxy-1,5-bis(bromomethyl)naphthalene (25)

To a suspension of the appropriate hydroquinone dialkyl ether (10 mmol) in glacial acetic acid (35 mL), paraformaldehyde (30.25 mmol) was added and sonicated for 10 min. To this mixture, 33% of HBr in acetic acid (31.12 mmol) was added and sonicated for 3 h. After a further addition of 5 mL acetic acid followed by sonication for 30 min, the reaction mixture was poured into cold water. The precipitated product was filtered and dried to give the appropriate derivatives in high yields.

**2,5-Bis(methoxy)-1,4-bis(bromomethyl)benzene (19)**

Yield 92%; mp 203-204 °C;  $^1\text{H}$  NMR ( $\text{CDCl}_3$ , 300 MHz)  $\delta$  6.81 (s, 2H, aromatic), 4.60 (s, 4H,  $\text{CH}_2\text{Br}$ ), 3.80 (s, 6H,  $\text{OCH}_3$ );  $^{13}\text{C}$  NMR ( $\text{CDCl}_3$ , 75.4 MHz)  $\delta$  150.72, 127.51, 114.62, 56.20, 29.65.

**4,8-Didodecyloxy-1,5-bis(bromomethyl)naphthalene (25)**

Yield 65%;  $^1\text{H}$  NMR ( $\text{CDCl}_3$ , 90 MHz)  $\delta$  7.37 (d, 2H, aromatic), 6.83 (d, 2H, aromatic), 5.31 (s, 4H,  $\text{CH}_2\text{Br}$ ), 4.12 (t, 4H,  $\text{OCH}_2$ ), 2.04 (m, 4H,  $\text{CH}_2$ ), 1.27 (m, 36H,  $\text{CH}_2$ ) 0.88 (t, 6H,  $\text{CH}_3$ );  $^{13}\text{C}$  NMR ( $\text{CDCl}_3$ , 75.4 MHz)  $\delta$  157.14, 131.34, 126.50, 125.72, 106.91, 69.19, 39.07, 31.90, 29.64, 29.59, 29.56, 29.50, 29.42, 29.34, 29.19, 28.98, 26.43, 26.20, 22.68, 14.10.

**2.5.8. Preparation of tetraethyl[arylbis(methylene)]bisphosphonates**

The bisphosphonates **14**, **17**, **20**, **22** and **26** were prepared by the reaction of the corresponding bisbromomethyl derivatives **13**, **16**, **19**, **21** and **25** (10 mmol) respectively with 5 mL of triethyl phosphite at 80 °C for 10 h followed by the removal of the unreacted triethyl phosphite under reduced pressure. The product was used as such for further reaction.

**Tetraethyl[1,4-phenylenebis(methylene)]bisphosphonate (14)**

Yield 95%;  $^1\text{H}$  NMR ( $\text{CDCl}_3$ , 300 MHz)  $\delta$  7.39 (s, 4H, aromatic), 4.01 (m, 8H,  $\text{OCH}_2$ ), 3.13 (d, 4H,  $\text{CH}_2\text{P}$ ), 1.20 (m, 12H,  $\text{CH}_3$ );  $^{13}\text{C}$  NMR ( $\text{CDCl}_3$ , 75.4 MHz)  $\delta$  130.01, 129.72, 61.86, 34.26, 15.97.

**Tetraethyl[4,4'-biphenylbis(methylene)]bisphosphonate (17)**

Yield 94%;  $^1\text{H}$  NMR ( $\text{CDCl}_3$ , 300 MHz)  $\delta$  7.56 (m, 4H, aromatic), 7.22 (m, 4H, aromatic), 4.12 (m, 8H,  $\text{OCH}_2$ ), 3.22 (d, 4H,  $\text{CH}_2\text{P}$ ), 1.12 (m, 12H,  $\text{CH}_3$ ).  $^{13}\text{C}$  NMR ( $\text{CDCl}_3$ , 75.4 MHz)  $\delta$  141.23, 131.29, 129.83, 127.56, 62.45, 36.12, 15.99.

**Tetraethyl[2,5-bis(methoxy)-1,4-phenylenebis(methylene)]bisphosphonate (20)**

Yield 95%;  $^1\text{H}$  NMR ( $\text{CDCl}_3$ , 300 MHz)  $\delta$  6.92 (s, 2H, aromatic), 4.02 (m, 8H,  $\text{OCH}_2$ ), 3.92 (s, 6H,  $\text{OCH}_3$ ), 3.21 (d, 4H,  $\text{OCH}_2\text{P}$ ), 1.20 (m, 12H,  $\text{CH}_3$ );  $^{13}\text{C}$  NMR ( $\text{CDCl}_3$ , 75.4 MHz)  $\delta$  151.39, 119.40, 114.48, 56.41, 61.90, 31.23, 16.20.

**Tetraethyl[9,10-anthrylbis(methylene)]bisphosphonate (22)**

Yield: 80%.  $^1\text{H}$  NMR ( $\text{CDCl}_3$ , 300 MHz):  $\delta$  8.35 (dd, 4H, aromatic), 7.55 (d, 4H, aromatic), 4.2 (d, 4H,  $\text{OCH}_2\text{P}$ ), 3.7-3.9 (m, 8H,  $\text{OCH}_2$ ), 1.05 (t, 12H,  $\text{CH}_3$ );  $^{13}\text{C}$  NMR ( $\text{CDCl}_3$ , 75.4 MHz):  $\delta$  130.08, 125.53, 125.35, 124.00, 61.99, 28.04, 16.06.

**Tetraethyl[1,5-bis(dodecyloxy)-4,8-naphthylbis(methylene)]bisphosphonate (26)**

Yield: 90%.  $^1\text{H}$  NMR ( $\text{CDCl}_3$ , 300 MHz):  $\delta$  7.26 (m, 2H, aromatic), 6.81 (d, 2H, aromatic), 4.13 (d, 4H,  $\text{OCH}_2\text{P}$ ), 4.06 (t, 4H,  $\text{OCH}_2$ ), 3.78-3.91 (m, 8H,  $\text{OCH}_2$ ), 2.00 (m, 4H,  $\text{CH}_2$ ), 1.26 (m, 36H,  $\text{CH}_2$ ), 1.10 (t, 12H,  $\text{CH}_3$ ), 0.89 (t, 6H,  $\text{CH}_3$ ).  $^{13}\text{C}$  NMR ( $\text{CDCl}_3$ , 75.4 MHz):  $\delta$  156.14, 130.35, 126.79, 119.94, 106.36, 68.62, 61.60, 35.82, 33.99, 31.05, 29.26, 26.28, 22.64, 16.40, 13.97.

**2.5.9. General method for the preparation of bispyrroles (1a-c)**

A suspension of sodium hydride (30 mmol) in THF was added slowly to a solution of the corresponding bisphosphonate (5 mmol) and the respective *N*-alkylpyrrole-2-carboxaldehyde (10 mmol) in THF. After refluxing for 10 h the reaction mixture was cooled and THF was removed under reduced pressure to give a pasty residue. The residue was suspended in water and extracted with dichloromethane. The organic layer was washed with brine, dried over Na<sub>2</sub>SO<sub>4</sub> and concentrated to give the crude product. Further purification was done either by precipitation using methanol from a dichloromethane solution or by column chromatography over silica gel using 5% ethyl acetate-petroleum ether mixture.

**(*E,E*)-1,4-Bis[2-(1-dodecylpyrrol-2-yl)vinyl] benzene (1a)**

Yield 55%; mp 90 °C; IR (KBr)  $\nu_{\max}$  2921, 2849, 1695, 1649, 1541, 1506, 1472, 1074, 950, 689 cm<sup>-1</sup>; <sup>1</sup>H NMR (CDCl<sub>3</sub>, 300 MHz)  $\delta$  7.4 (s, 2H, aromatic), 6.85 (d, 2H, vinylic, *J* = 16.0 Hz), 6.93 (d, 2H, vinylic, *J* = 16.0 Hz), 6.67 (s, 2H, aromatic), 6.49 (s, 4H, aromatic), 6.15 (s, 2H, aromatic), 3.95 (t, 4H, NCH<sub>2</sub>), 1.2-1.7 (m, 40H, CH<sub>2</sub>), 0.86 (t, 6H, CH<sub>3</sub>); <sup>13</sup>C NMR (CDCl<sub>3</sub>, 75.4 MHz)  $\delta$  136.78, 131.42, 126.27, 125.62, 122.68, 116.74, 108.34, 106.59, 47.14, 31.99, 31.67, 29.7, 29.6, 29.41, 29.3, 26.9, 22.76, 14.1. HRMS (FAB): calcd for C<sub>42</sub>H<sub>64</sub>N<sub>2</sub> (M<sup>+</sup>): 596.5070; found 596.5089.

**(*E, E*)-4,4'-Bis[2-(1-dodecylpyrrol-2-yl) vinyl] biphenyl (1b)**

Yield 42%; mp. 94 °C; IR (KBr)  $\nu_{\max}$  2912, 2846, 1699, 1467, 1281, 1076, 956, 857, 698  $\text{cm}^{-1}$ ;  $^1\text{H}$  NMR ( $\text{CDCl}_3$ , 300 MHz)  $\delta$  7.59 (d, 4H, aromatic); 7.51 (d, 4H, aromatic), 6.99 (d, 2H, vinylic,  $J = 16.02$  Hz), 6.90 (d, 2H, vinylic,  $J = 16.02$  Hz), 6.68 (s, 2H, aromatic), 6.52 (m, 2H, aromatic), 6.15 (t, 2H, aromatic), 3.97 (m, 12H,  $\text{NCH}_2$ ), 1.76 (m, 4H,  $\text{CH}_2$ ), 1.24 (m, 40H,  $\text{CH}_2$ ), 0.87 (m, 6H,  $\text{CH}_3$ );  $^{13}\text{C}$  NMR ( $\text{CDCl}_3$ , 75.4 MHz)  $\delta$  139.09, 137.03, 131.25, 126.95, 126.35, 125.29, 122.65, 117.16, 108.26, 106.32, 47.05, 31.90, 31.58, 29.62, 29.58, 29.50, 29.33, 29.21, 26.80, 22.67, 14.09; HRMS calcd for  $\text{C}_{48}\text{H}_{68}\text{N}_2$  ( $M^+$ ): 672.5382; found 672.5379.

**(*E, E*)-1,4-Bis[2-(1-dodecylpyrrol-2-yl)vinyl]-2,5-dimethoxybenzene (1c)**

Yield 70%; mp 85-86 °C; IR (KBr)  $\nu_{\max}$  2927, 2857, 1543, 1496, 1461, 1336, 1288, 1206, 1046, 955  $\text{cm}^{-1}$ ;  $^1\text{H}$  NMR ( $\text{CDCl}_3$ , 300 MHz)  $\delta$  7.03 (d, 2H, vinylic,  $J = 16.12$  Hz), 6.91 (d, 2H, vinylic,  $J = 16.3$  Hz), 6.89 (s, 2H, aromatic), 6.56 (s, 2H, aromatic), 6.40 (m, 2H, aromatic), 6.05 (t, 2H, aromatic), 3.88 (t, 4H,  $\text{NCH}_2$ ), 3.80 (s, 6H,  $\text{OCH}_3$ ), 1.69 (t, 4H,  $\text{CH}_2$ ), 1.17-1.25 (m, 36H,  $\text{CH}_2$ ), 0.80 (t, 6H,  $\text{CH}_3$ );  $^{13}\text{C}$  NMR ( $\text{CDCl}_3$ , 75.4 MHz)  $\delta$  151.40, 131.85, 126.53, 122.40, 120.79, 117.71, 109.56, 108.26, 106.82, 56.34, 47.08, 31.91, 31.59, 29.62, 29.37, 29.31, 26.91, 22.74, 14.12; HRMS Calcd for  $\text{C}_{44}\text{H}_{68}\text{N}_2\text{O}_2$  ( $M^+$ ): 656.5281; found 656.5256.

**(*E,E*)-9,10-Bis[2-(1-dodecylpyrrol-2-yl)vinyl]anthracene (1d)**

Yield 68% ; mp 126-127 °C; IR (KBr)  $\nu_{\max}$  2925, 2852, 1697, 1642, 1537, 1505, 1455, 1396, 1067, 958, 752  $\text{cm}^{-1}$ ;  $^1\text{H}$  NMR ( $\text{CDCl}_3$ , 300 MHz)  $\delta$  8.42 (dd, 4H, aromatic), 7.68 (d, 2H, vinylic,  $J = 16.20$  Hz), 7.45 (dd, 4H, aromatic), 6.78 (d, 2H, vinylic,  $J = 15.95$  Hz), 6.76 (m, 4H, aromatic), 6.27 (t, 2H, aromatic), 3.91 (t, 4H,  $\text{NCH}_2$ ), 1.72 (m, 4H,  $\text{CH}_2$ ), 1.20-1.24 (m, 36H,  $\text{CH}_2$ ), 0.86 (t, 6H,  $\text{CH}_3$ );  $^{13}\text{C}$  NMR ( $\text{CDCl}_3$ , 75.4 MHz)  $\delta$  132.81, 129.67, 126.51, 126.11, 125.04, 121.91, 108.25, 106.43, 47.20, 31.87, 31.84, 29.56, 29.46, 29.29, 29.24, 26.80, 22.65, 14.09; HRMS (FAB): calcd for  $\text{C}_{50}\text{H}_{68}\text{N}_2(\text{M}^+)$ , 696.5383; found, 696.5377.

**(*E,E*)-1,5-Bis[2-(1-dodecylpyrrol-2-yl)vinyl]-4,8-didodecyloxynaphthalene (1e)**

Yield 48% ; mp 71 °C ; IR (KBr)  $\nu_{\max}$  2921, 2854, 1728, 1587, 1519, 1465, 1378, 1276, 1067, 950, 710  $\text{cm}^{-1}$ ;  $^1\text{H}$  NMR ( $\text{CDCl}_3$ , 300 MHz)  $\delta$  8.0 (d, 2H, vinylic,  $J = 15.55$  Hz), 7.37 (d, 2H, aromatic), 6.84 (d, 2H, aromatic), 6.62 (s, 2H, aromatic), 6.45 (d, 2H, vinylic,  $J = 15.74$  Hz), 6.42 (s, 2H, aromatic), 6.13 (s, 2H, aromatic), 4.03 (t, 4H,  $\text{NCH}_2$ ), 3.93 (t, 4H,  $\text{OCH}_2$ ), 1.75-1.87 (m, 8H,  $\text{CH}_2$ ), 1.25 (m, 72H,  $\text{CH}_2$ ), 0.87 (m, 12H,  $\text{CH}_3$ );  $^{13}\text{C}$  NMR ( $\text{CDCl}_3$ , 75.4 MHz)  $\delta$  156.44, 132.34, 131.80, 129.47, 126.15, 125.67, 121.18, 115.17, 107.75, 107.30, 105.04, 69.22, 46.90, 31.93, 31.91, 31.69, 29.7, 29.65, 29.58, 29.47, 29.34, 29.28, 26.85, 26.51, 22.69, 14.11, 13.15. HRMS (FAB): calcd for  $\text{C}_{70}\text{H}_{114}\text{N}_2\text{O}_2(\text{M}^+)$ , 1014.888; found, 1014.9021.

**2.5.10. General procedure for the synthesis of the polysquaraines (2a-c)**

The bispyrroles **1a-e** (0.15 mmol) and squaric acid (0.15 mmol) in butanol/benzene (1:3, 50 mL) were refluxed for 16-22 h under azeotropic removal of water. The reaction mixture was cooled, filtered and the filtrate was concentrated under reduced pressure. The products were further washed several times with *n*-butanol and methanol to remove the unreacted squaric acid followed by washing with toluene. The resultant dark green residue was dissolved in dichloromethane and the product was precipitated with light petroleum ether. The product was redissolved in dichloromethane and reprecipitated with petroleum ether and washed several times with petroleum ether followed by drying.

**2a:** Yield 57%; IR (KBr)  $\nu_{\max}$  2921, 2854, 1613, 1485, 1431, 1344, 1270, 1094, 939  $\text{cm}^{-1}$ ; Anal. Calcd for  $(\text{C}_{46}\text{H}_{62}\text{N}_2\text{O}_4 \cdot \text{H}_2\text{O})_n$ : C, 79.72; H, 9.31; N, 4.04. Found: C, 80.12; H, 9.28; N, 4.11.

**2b:** Yield 36%; IR (KBr),  $\nu_{\max}$  2921, 2858, 1615, 1480, 1428, 1354, 1271, 1092, 941  $\text{cm}^{-1}$ ; Anal. Calcd for  $(\text{C}_{52}\text{H}_{66}\text{N}_2\text{O}_4 \cdot \text{H}_2\text{O})_n$ : C, 81.21; H, 8.91; N, 3.64. Found: C, 81.43; H, 8.89; N, 3.57.

**2c:** Yield 70%; IR (KBr)  $\nu_{\max}$  2923, 2860, 1621, 1486, 1359, 1291, 1088, 950  $\text{cm}^{-1}$ ; Anal. Calcd for  $(\text{C}_{48}\text{H}_{66}\text{N}_2\text{O}_4 \cdot \text{H}_2\text{O})_n$ : C, 76.55; H, 9.21; N, 3.72. Found: C, 76.40; H, 9.37; N, 3.66.

**2d:** Yield 43%; IR (KBr)  $\nu_{\max}$  2926, 2856, 2363, 1626, 1504, 1388, 1301, 1115  $\text{cm}^{-1}$ ; Anal. Calcd for  $(\text{C}_{54}\text{H}_{66}\text{N}_2\text{O}_4 \cdot \text{H}_2\text{O})_n$ : C, 81.77; H, 8.64; N, 3.53. Found: C, 81.48; H, 8.73; N, 3.51.

**2e:** Yield 63%; IR (KBr)  $\nu_{\max}$  2921, 2854, 1587, 1519, 1465, 1378, 1276, 1067, 953  $\text{cm}^{-1}$ ;  $^1\text{H}$  NMR ( $\text{CDCl}_3$ , 300 MHz)  $\delta$  8.5 (m, broad, vinylic), 7.88 (m, broad, aromatic), 7.51 (d, broad, aromatic), 6.67-6.91 (m, vinylic + aromatic), 4.84 (s, broad,  $\text{NCH}_2$ ), 4.01 (m, broad,  $\text{NCH}_2 + \text{OCH}_2$ ), 1.75-1.87 (m, 8H,  $\text{CH}_2 + \text{CH}$ ), 1.25 (m,  $\text{CH}_2$ ), 0.85 (m,  $\text{CH}_3$ ). Anal. Calcd for  $(\text{C}_{74}\text{H}_{112}\text{N}_2\text{O}_4 \cdot \text{H}_2\text{O})_n$ : C, 79.95; H, 10.34; N, 2.52. Found: C, 80.51; H, 10.37; N, 2.67.

#### 2.5.11. Preparation of the $\pi$ -extended dyes (3a-d)

The model dyes **3a-d** were prepared under high dilution as follows. The corresponding bispyrrole (0.4 mmol) and squaric acid (0.2 mmol) were dissolved in butanol/benzene (1:3, 80 mL) and the reaction mixture was refluxed under azeotropic conditions. The reaction was monitored by recording the absorption spectrum at different intervals. The reaction was stopped when the absorption bands corresponding to the higher homologues started appearing. The reaction mixture was cooled, filtered and the benzene was removed under reduced pressure to give a viscous solution. The product was precipitated by adding methanol. The crude product was dissolved in chloroform and reprecipitated by adding light petroleum ether. The unreacted bispyrrole monomers were removed using repeated washings with petroleum ether and diethyl ether. The product was further

purified by column chromatography over silica gel using 50% petroleum ether-ethyl acetate mixture to yield dyes in 10-40% yields.

**3a:** Yield 29 %; IR (KBr)  $\nu_{\max}$  2921, 2851, 1619, 1509, 1465, 1360, 1299, 1109, 1074, 1047, 952, 814, 759  $\text{cm}^{-1}$ ;  $^1\text{H}$  NMR ( $\text{CDCl}_3$ , 300 MHz)  $\delta$  7.84 (s, 2H, aromatic), 7.47 (m, 8H, aromatic+vinylic), 7.20 (m, 4H, vinylic) 6.98-6.84 (m, 6H, aromatic+vinylic), 6.70 (m, 2H, aromatic), 6.53 (m, 2H, aromatic), 6.17 (s, 2H, aromatic), 4.83 (t, 4H,  $^+\text{NCH}_2$ ), 3.97 (t, 4H,  $\text{NCH}_2$ ), 1.58 (m, 20H,  $\text{CH}_2$ ), 1.25 (m, 60H,  $\text{CH}_2$ ), 0.85 (m, 12H,  $\text{CH}_3$ ); HRMS calcd for  $\text{C}_{88}\text{H}_{126}\text{N}_4\text{O}_2(\text{M}^+)$ : 1270.9881; found: 1270.86; Anal. calcd for  $\text{C}_{88}\text{H}_{126}\text{N}_4\text{O}_2 \cdot \text{H}_2\text{O}$ : C, 81.93; H, 10.0; N, 4.34. Found: C, 81.85; H, 9.96; N, 4.37.

**3b:** Yield 10 %; IR (KBr)  $\nu_{\max}$  2922, 2850, 1619, 1510, 1496, 1379, 1263, 1105, 1074, 1018, 956, 855, 804  $\text{cm}^{-1}$ ; Anal. calcd for  $\text{C}_{100}\text{H}_{134}\text{N}_4\text{O}_2 \cdot \text{H}_2\text{O}$ : C, 83.28; H, 9.51; N, 3.88. Found: C, 83.66; H, 9.48; N, 3.94.

**3c:** Yield 34%; IR (KBr)  $\nu_{\max}$  2924, 2853, 1621, 1505, 1440, 1370, 1298, 1213, 1102, 956  $\text{cm}^{-1}$ ;  $^1\text{H}$  NMR ( $\text{CDCl}_3$ , 300 MHz)  $\delta$  7.85 (s, 2H, aromatic), 7.55 (d, 2H, vinylic  $J = 15.40$  Hz), 7.17 (d, 2H, vinylic,  $J = 15.41$  Hz), 7.06 (m, 4H, vinylic), 6.96 (m, 4H, aromatic), 6.70 (m, 4H, aromatic+vinylic), 6.53 (m, 2H, aromatic), 6.15 (s, 2H, aromatic), 4.79 (s, 4H,  $\text{NCH}_2$ ), 3.91 (m, 16H,  $\text{OCH}_3 + \text{NCH}_2$ ), 1.71 (m, 8H,  $\text{CH}_2$ ), 1.51 (m, 40H,  $\text{CH}_2$ ), 1.29 (m, 32H,  $\text{CH}_2$ ), 0.88 (m, 12H,  $\text{CH}_3$ );  $^{13}\text{C}$  NMR (75.4 MHz,  $\text{CDCl}_3$ ),  $\delta$  166.48, 152.49, 131.64, 132.03, 129.46, 129.17, 124.44, 123.96, 119.42, 119.26, 115.64, 114.45, 113.67, 111.01, 109.81, 108.95,

108.25, 107.53, 56.12, 50.96, 41.96, 33.09, 31.95, 29.65, 29.45, 29.67, 29.34, 26.23, 26.26, 22.58, 14.09.; HRMS calcd for  $C_{92}H_{134}N_4O_6$  ( $M^+$ ): 1392.0303, found 1391.1593; Anal.calcd for  $C_{92}H_{134}N_4O_6 \cdot H_2O$ : C, 78.36; H, 9.72; N, 3.97. Found: C, 78.03; H, 9.88; N, 3.95.

**3d**: Yield 19%; IR (KBr)  $\nu_{max}$  2921, 2851, 1619, 1509, 1465, 1360, 1299, 1109, 1074, 1047, 952, 814, 759  $cm^{-1}$ ;  $^1H$  NMR ( $CDCl_3$ , 300 MHz)  $\delta$  8.41 (dd, 8H, aromatic), 8.18 (d, 2H, vinylic,  $J = 15.82$  Hz), 7.93 (m, 2H, aromatic), 7.63 (d, 2H, vinylic,  $J = 16.17$  Hz), 7.44 (m, 8H, aromatic), 7.15 (d, 2H, vinylic,  $J = 14.40$  Hz), 7.12 (m, 2H, aromatic), 6.95 (d, 2H, vinylic,  $J = 16.12$  Hz), 6.77 (m, 2H, aromatic), 6.69 (m, 2H, aromatic), 6.21 (s, 2H, aromatic), 4.74 (t, 4H,  $N^+CH_2$ ), 3.88 (t, 4H,  $NCH_2$ ), 1.54 (m, 20H,  $CH_2$ ), 1.18 (m, 60H,  $CH_2$ ), 0.80 (m, 12H,  $CH_3$ );  $^{13}C$  NMR ( $CDCl_3$ , 75.4 MHz)  $\delta$  131.10, 130.50, 129.71, 129.61, 126.93, 126.65, 126.00, 125.68, 125.31, 121.36, 113.83, 110.78, 109.26, 108.41, 106.79, 106.65, 96.71, 59.42, 47.23, 38.15, 32.56, 31.89, 31.23, 29.68, 29.60, 29.58, 28.53, 29.31, 29.25, 26.82, 26.58, 22.74, 22.67, 14.09; HRMS calcd for  $C_{104}H_{134}N_4O_2$  ( $M^+$ ): 1472.20; Found 1472.19.

## 2.6. References

1. Saxena, V.; Malhotra, B. D. *Curr. Appl. Phys.* **2003**, *3*, 293-305.
2. Roncali, J. *Chem. Rev.* **1997**, *97*, 173-205.
3. van Mullekom, H. A. M.; Vekeman, J. A. J. M.; Havinga, E. E.; Meijer E. W. *Mater. Sci. Eng.* **2001**, *32*, 1-40.

4. Burroughes, J. H.; Bradley, D. D. C.; Brown, A. R.; Marks, R. N.; Mackay, K.; Friend, R. H.; Burns, P. L.; Holmes, A. B. *Nature* **1990**, *347*, 539.
5. Gustafsson, G.; Cao, Y.; Treacy, G. M.; Klavetter, F.; Colaneri, N.; Heeger, A. J. *Nature* **1993**, *365*, 629.
6. Garnier, F.; Yassar, A.; Hajlaoui, R.; Horowitz, G.; Deloffre, F.; Servet, B.; Ries, S.; Alnot, P. J. *Am. Chem. Soc.* **1993**, *115*, 8716.
7. Lous, E. J.; de Leeuw, D. M. *Synth. Met.* **1994**, *65*, 45.
8. Hagler, T. W.; Pakbaz, K.; Voss, K. F.; Heeger, A. J. *Phys. Rev. B* **1991**, *44*, 8652.
9. Brocks, G.; Tol, A. *J. Phys. Chem.*, **1996**, *100*, 1838.
10. Schmidt, A. H. *Synthesis* **1980**, 961 and references cited therein.
11. Law, K.-Y. *Chem. Rev.*, **1993**, *93*, 449.
12. Treibs A.; Jacob, K. *Angew. Chem., Int. Ed. Engl.* **1965**, *4*, 694.
13. Chen, Y.-Y.; Hall, Jr., H. K. *Polym. Bull.*, **1986**, *16*, 419.
14. Havinga, E. E.; ten Hoeve, W.; Wynberg, H. *Polym. Bull.*, **1992**, *29*, 119.
15. Havinga, E. E.; ten Hoeve, W.; Wynberg, H., *Synth. Met.*, **1993**, *55–57*, 299.
16. Lynch, D. E.; Geissler, U.; Kwiatowski, J.; Whittaker, A. K. *Polym. Bull.*, **1997**, *38*, 493.
17. Lynch, D. E.; Geissler, U.; Peterson, I. R.; Floersheimer, M.; Terbrack, R.; Chi, L. F.; Fuchs, H.; Calos, N. J.; Wood, B.; Kennard C. H. L.; Langley, G. J. *J. Chem. Soc., Perkin Trans. 2*, **1997**, 827.
18. Lynch, D. E.; Peterson, I. R.; Floersheimer, M.; Essing, D.; Chi, L. F.; Fuchs, H.; Calos, N. J.; Wood, B.; Kennard, C. H. L.; Langley, G. J. *J. Chem. Soc., Perkin Trans. 2*, **1998**, 779.
19. Ajayaghosh, A.; Chenthamarakshan, C. R.; Das, S.; George, M. V. *Chem. Mater.*, **1997**, *9*, 644.
20. Chenthamarakshan, C. R.; Ajayaghosh, A. *Chem. Mater.*, **1998**, *10*, 1657.

21. Chenthamarakshan, C. R.; Eldo, J.; Ajayaghosh, A. *Macromolecules*, **1999**, *32*, 251.
22. Chenthamarakshan, C. R.; Ajayaghosh, A. *Tetrahedron Lett.*, **1998**, *39*, 1795.
23. Chenthamarakshan, C. R.; Eldo, J.; Ajayaghosh, A. *Macromolecules*, **1999**, *32*, 5846.
24. Ajayaghosh, A.; Eldo, J. *Org. Lett.*, **2001**, *3*, 2595.
25. Eldo, J.; Ajayaghosh, A. *Chem. Mater.*, **2002**, *14*, 410.
26. Eldo, J.; Arunkumar, E.; Ajayaghosh, A. *Tetrahedron Lett.* **2000**, *41*, 6241.
27. Bunz, U. H. F. *Chem. Rev.* **2000**, *100*, 1605.
28. Halkyard, C. E.; Rampey, M. E.; Kloppenburg, L.; Studer-Martinez, S. L.; Bunz, U. H. F. *Macromolecules* **1998**, *31*, 8655.
29. McCullough, R. D.; Lowe, R. D.; Jayaraman, M.; Anderson, D. L. *J. Org. Chem.* **1993**, *58*, 904.
30. McCullough, R. D.; Tristram-Nagle, S.; Williams, S.P.; Lowe, R. D.; Jayaraman, M. *J. Am. Chem. Soc.* **1993**, *115*, 4910.
31. Chen, T. -A. ; Wu, X.; Rieke, R. D. *J. Am. Chem. Soc.* **1995**, *117*, 233.
32. Eldo, J. Ph.D thesis, 2001 and references cited therein.

## Chapter 3

### Control of Optical and Aggregation Properties of a few Bispyrrole Derived Squaraine Dyes: Effect of Alkoxy Chains of the Aromatic Bridging Moiety

---

#### 3.1. Abstract

*In this chapter, synthesis, characterization and aggregation properties of a few  $\pi$ -extended squaraine dyes **2a-c** derived from dialkoxydivinylbenzene bridged bispyrroles **1a-c**, are described. In solution, these squaraine dyes exhibit intense absorption in the wavelength range of 600-850 nm and hence belong to the class of near-IR dyes. In the solid-state, the absorption spectra are broad and shifted towards long wavelength region. The optical properties of these dyes showed considerable dependence on the length and the nature of the alkyl side chains attached to the benzene ring. Aggregation of these dyes in solution and solid-state could be controlled by the alkyl chain substituents on the benzene moiety. Steric effects of longer and branched side chains favored the formation of J-aggregates both in solution and in the solid-state. The dye **2a** with butyl side chains on the benzene preferentially forms H-aggregates in DMSO-water and THF-water solvent mixtures. The presence of long alkyl side chains on **2b** accelerates the aggregation in the DMSO-water solvent mixture containing very small amount of water. The dye **2c** with branched chain showed tendency to form J-aggregates in*

addition to H-aggregates. Below 18% water in DMSO, the dye **2c** showed temperature dependent interconversion between the H- and J-aggregates whereas above 18% water in DMSO, the H-aggregates transform into J-aggregates upon heating. In THF-water mixtures, the dye **2a** forms H-aggregates. On the other hand the dyes **2b** and **2c** form both H- and J-aggregates in THF-water.

### 3.2. Introduction

Squaraine dyes form a class of organic photoconducting materials that have been extensively studied for a variety of technological applications<sup>1</sup> including organic solar cells,<sup>2</sup> optical recording media<sup>3</sup> and xerographic photoreceptors.<sup>4,5</sup> They exhibit strong absorption in the visible to the near infrared region. Aggregation of squaraine dyes makes considerable changes to their optical properties, the most important being in the electronic absorption spectra. The spectral features of these dye aggregates can be correlated to their structures by the exciton theory of Kasha, Hochstrasser, Kuhn and coworkers.<sup>6-9</sup> According to the exciton theory,<sup>10</sup> the excited state energy level of the monomeric dye splits into two upon aggregation, one level being lower and the other higher in energy than the monomer excited state. The allowed and forbidden transitions are then governed by the tilt angle ' $\alpha$ ' of the transition moments with respect the line of centers (Figure 3.1). When ' $\alpha$ ' is less than approximately 54°, the allowed transition is to the lowest excited level resulting in a red-shifted absorption relative to that of the monomer. Such aggregates are known as J-type aggregates (head-to-

tail arrangement). When ' $\alpha$ ' is greater than  $54^\circ$ , the allowed transition is to the highest excited level, resulting in a blue shifted absorption, typical of H-type aggregates (card-pack arrangement).

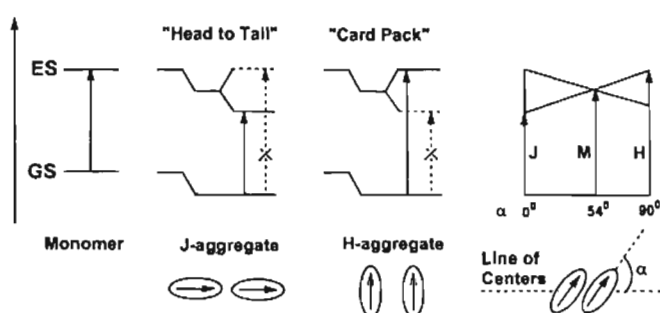


**Figure 3.1.** Schematic representation of splitting of the excited state of an organic dye during aggregation.

Studies have shown that squaraines can exist as different kinds of aggregates with the prominent limiting structures of J- and H-type that are commonly occurring. The aggregation properties are influenced by a number of factors including the structure of the chromophore, solvents used, presence of foreign materials, temperature etc. In recent years, a variety of squaraine dyes have been subjected to aggregation studies. For example, Das *et al.* have reported the formation of aggregates of bis(2,4-dihydroxyphenyl)squaraine (**3a**) and bis(2,4,6-trihydroxyphenyl)squaraine (**3b**) in acetonitrile (Chart 3.1).<sup>11</sup> The appearance of the sharp band at 665 nm at higher concentration of the dye was due to the aggregated species. Intermolecular hydrogen bonding between the monomer molecules was responsible for the aggregation. The aggregation of **3b** in ethanol and tetrahydrofuran has been reported by Li and coworkers, which reveals the role

of hydrogen bonding in the aggregation process.<sup>12</sup> The halogenated derivatives **4a** and **4b** form H-aggregates in methanol–buffer solutions.<sup>13</sup> The intramolecular hydrogen bonding interactions between the electronegative atoms of one squaraine units and the hydroxyl groups of the others rendered stability to the aggregates.

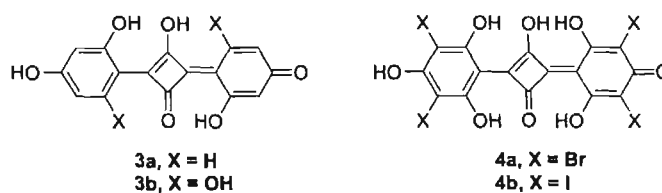


**Chart 3.1**

Law and coworkers have reported the aggregation of a series surfactant squaraines (Chart 3.2).<sup>14-17</sup> Aggregation of **5a** was studied in a variety of media including organic solvents, aqueous cyclodextrin solutions, vesicles, monolayers, Langmuir-Blodgett films and in the solid films. In all the cases blue shifted absorption was observed for the aggregates. It has been concluded that the dye adopts either a transition layer or a glide layer structure in these aggregates. Squaraines **5b** and **5c** exhibited multiple aggregation behavior in LB films and in DMSO-water binary solvent system. The blue shifted H-aggregates in LB films are shown to rearrange to J-aggregates with increase in temperature. The reversal of the process could be achieved by treating the J- or the red-shifted aggregates using steam at 65 °C. By comparing the cross sectional area of the squaraine chromophores and the limiting area of a hydrocarbon chain, it has been concluded that multiple aggregation is a 'free area effect'. The aggregation study in DMSO-

water mixtures suggests that hydrophobic and charge transfer interactions play the key role in these phenomena.

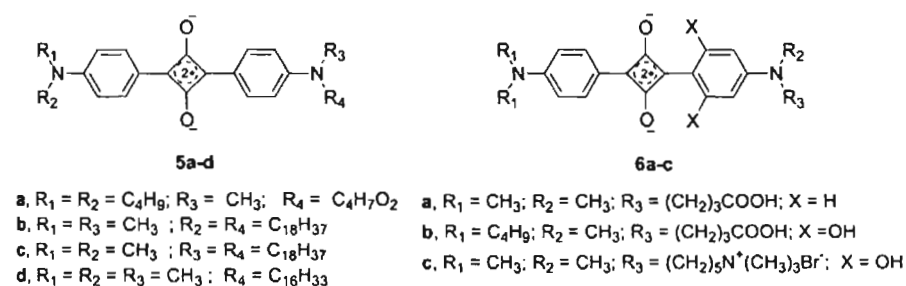
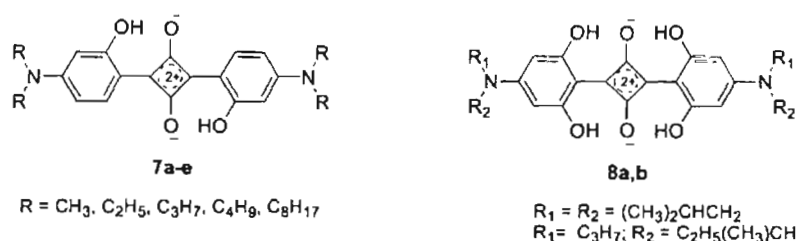


Chart 3.2

Amphiphilic squaraines **6a-c** resulted in blue shifted chiral aggregates in aqueous and in mixed aqueous-organic solutions and in micro heterogeneous media<sup>17</sup> (bilayer vesicles). In the monomer to aggregate conversion, presence of intermediate dimer could be detected in some of the cases. The aggregation number in this case was found to be 4. A chiral pinwheel structure was assigned for the tetramer. The tendency for aggregation was found to increase with increase in length of the alkyl side chain on the nitrogen.

The squaraine dye **7** (Chart 3.3) forms two types of aggregates preferentially in different DMSO-water compositions. A dynamic conversion between the aggregates is observed in specific DMSO-water composition.<sup>18,19</sup> In pure DMSO and in DMSO-water mixtures containing more than 70% DMSO, **7d** exists in the monomeric form, which has a sharp absorption centered around 600 nm. In 70% DMSO, it exists as stable aggregates that has blue shifted absorption

band ( $\lambda_{\max} = 530$  nm). In 20-50% DMSO, a second type of aggregate with a broad absorption band in the region of 550-700 nm was observed. This species undergoes a time dependent change to the aggregated species in DMSO rich solvent mixtures. Similar observations were made in the aggregation of bis(4-alkylamino-2-hydroxyphenyl)squaraines in DMSO-water mixtures.



**Chart 3.3**

Tian *et al.* have noticed that **8a** and **8b** with branched *N*-alkyl groups such as *sec*-butyl and *iso*-butyl with large limiting areas form J-aggregates in monolayers whereas molecules with shorter *N*-alkyl side chains form H-aggregates.<sup>20</sup> This behavior is attributed to the steric hindrance of the branched alkyl groups. The intramolecular H-bonding between the aromatic hydroxyl groups favors the formation of H-aggregates at air-water interface. It has been found that branching of *N*-alkyl side chains greatly enhances the sublimation ability of the squaraine dyes.

Recently, Dimitriev and coworkers have reported enhanced aggregation of squaraine dyes in solution capillary layers.<sup>21,22</sup> Spectral differences in the capillary and bulk solution were dependent on chemical structure of the dye and the solvent

used. The enhanced adsorption of squaraine dye molecules and the liquid crystalline state of the solution near the liquid-solid interface was pointed out as the driving force for this unusual behavior. Aggregation of squaraines in zeolites<sup>23</sup> and on semiconductor surfaces<sup>24,25</sup> were also studied. Recent studies reveal the potential use of squaraine dye aggregates in the optoelectronic field. Ultra fast non-linear optical response has been observed in J-aggregates of *N,N*-dialkyl squaraines.<sup>26,27</sup> Considerable work in this area has been carried out independently by the groups of Nakazumi<sup>28-30</sup> and Meier.<sup>31-34</sup> Petermann *et al.* have reported the formation of J-aggregates in the spin cast films of dialkylamino extended bis(dialkylamino)phenyl squaraines.<sup>35</sup> For near-IR absorbing squarylium dye containing a hydroperimidine moiety, the conversion between blue shifted aggregate and monomer was observed by changing the percentage of DMSO in DMSO-water mixtures.<sup>36</sup>

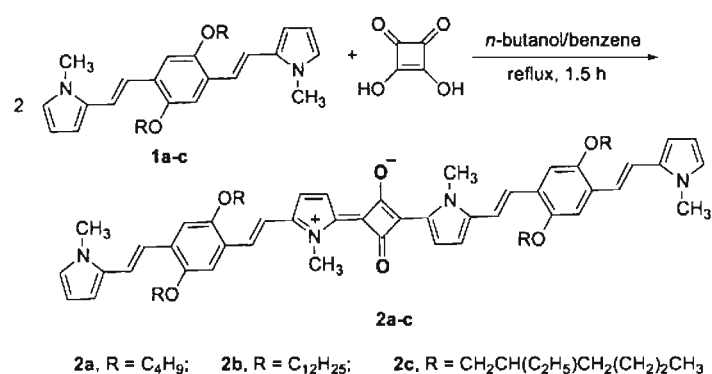
A detailed survey of the literature pertaining to the aggregation of squaraine dyes reveals that majority of the studies are based on *N,N*-dialkyl aniline derived squaraine dyes. Due to the fast growing importance of near-IR absorbing squaraine dyes, detailed studies on the factors controlling the aggregation behavior of such dyes have great significance. This is particularly true of pyrrole derived  $\pi$ -extended squaraine dyes. In the present study, a few  $\pi$ -extended squaraine dyes of dialkoxydivinylbenzene bridged bispyrroles were prepared and characterized. The alkyl group at the pyrrole nitrogen is kept the same (-CH<sub>3</sub>) and those on the benzene ring are changed. The aggregation of these dyes in solution and in solid-

state have been studied. These studies reveal that the nature of the alkyl side chains on the benzene ring play a crucial role and hence can be utilized in controlling the aggregation behavior of bispyrrole derived squaraine dyes.

### 3.3. Results and Discussion

#### 3.3.1. Synthesis and Characterization

Squaraine dyes **2a-c** (Scheme 3.1) were synthesized following the standard procedures described in the previous chapter. For this purpose, the required bispyrroles **1a-c** were prepared and characterized as reported previously.<sup>37</sup> Reaction of squaric acid with two equivalents of bispyrroles under azeotropic removal of water resulted in the formation of the dyes **2a-c** in 23 - 36% yields. Significant amounts of polymeric dyes were also formed which were removed by precipitation and column chromatography.



Scheme 3.1

The newly synthesized dyes were characterized using IR,  $^1\text{H}$  NMR,  $^{13}\text{C}$  NMR, HRMS and elemental analyses. All the dyes showed strong peak between 1625-1620  $\text{cm}^{-1}$  region which corresponds to the C-O stretching frequency of the cyclobutenediylum-1,3-diolate moiety.  $^1\text{H}$  NMR spectra of the dyes showed strong *trans* coupling for the vinylic linkages, which was in agreement with the structure assigned to the dyes. The *N*-methyl protons were observed as two singlets of equal intensity around  $\delta$  4.25 ppm and 3.7 ppm indicating the strong resonance stabilization in the dyes. The *O*-CH<sub>2</sub> protons gave characteristic multiplet at  $\delta$  3.95 ppm. The -CH<sub>2</sub> protons of the alkyl chains appeared as broad multiplet around  $\delta$  1.82-1.25 ppm. Methyl protons of the alkyl side chains were observed as multiplet at  $\delta$  1.0-0.88 ppm. Thermogravimetric analysis in air and in nitrogen atmosphere showed a decomposition temperature above 250 °C indicating that the dyes are stable up to 250 °C (Figure 3.2).

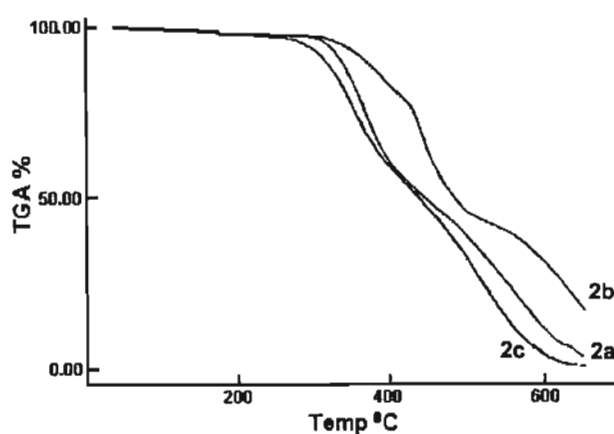
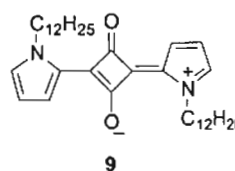


Figure 3.2. Thermogravimetric analysis (TGA) of the squaraine dyes 2a-c.

### 3.3.2. Electronic Absorption Spectra of the $\pi$ -Extended Squaraine Dyes 2a-c

The dyes **2a-c** showed intense absorption around 760 nm ( $\epsilon > 1.3250 \times 10^5$ ) and a shoulder band around 670 nm. This shoulder is common to many squaraine dyes and could be attributed to excitonic interaction. A red-shift of the 213 nm is observed for **2a-c** when compared to the absorption spectrum of the reported squaraine dye **9** obtained from *N*-alkylpyrrole

( $\lambda_{\text{max}} = 547$  nm in toluene). This is in agreement with the reports that optical properties of squaraines are tunable by extending the conjugation length or by introducing



electron donating moieties. The emission spectra of the dyes were recorded in toluene which showed weak emission in the range 750-850 nm with maximum centered around 800 nm.

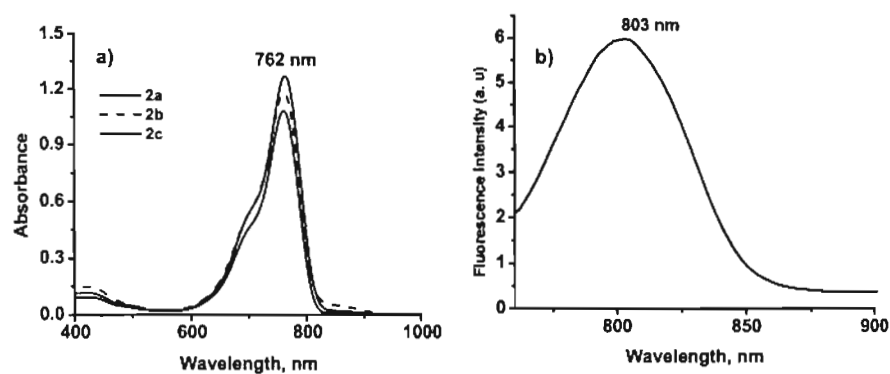


**Figure 3.3.** (a) Absorption spectra of **2a-c** and (b) emission spectrum of **2a** in toluene (Excitation wavelength = 760 nm; [dye] =  $5.61 \times 10^{-6}$  M).

### 3.3.3. Aggregation

#### 3.3.3.1. Aggregation Behavior of Dyes 2a-c in DMSO-water

In mixed solvent systems such as DMSO-water, THF-water and chloroform-methanol, the dyes **2a-c** exhibited significant changes in the absorption spectra. These changes in the absorption spectra could be attributed to the aggregation of the dyes in solvent mixtures. For example, the absorption spectra of **2a** in DMSO-water mixtures of different composition are shown in Figure 3.4.

In pure DMSO, the dye exhibited a strong absorption maximum at 779 nm. Upon increasing the percentage of water, the intensity of the monomer absorption at 779 nm is decreased gradually till 20% (v/v) water is added. In 20% (v/v) water, the intensity of the monomer band is decreased drastically and a blue shifted band at 640 nm is formed. This observation with the change in the solvent composition is typical of the H-type aggregation of squaraine dyes. Thus, in 20% (v/v) water, **2a** exists as a mixture of monomers and aggregates. In DMSO-water mixtures containing water content beyond 20%, the dye was mainly present in the H-aggregate form, as evident from the nearly complete shift of the absorption maximum from 779 nm to 640 nm (Figure 3.4). For example, at 60 - 90% water in DMSO, the spectra showed an absorption maximum at 640 nm.

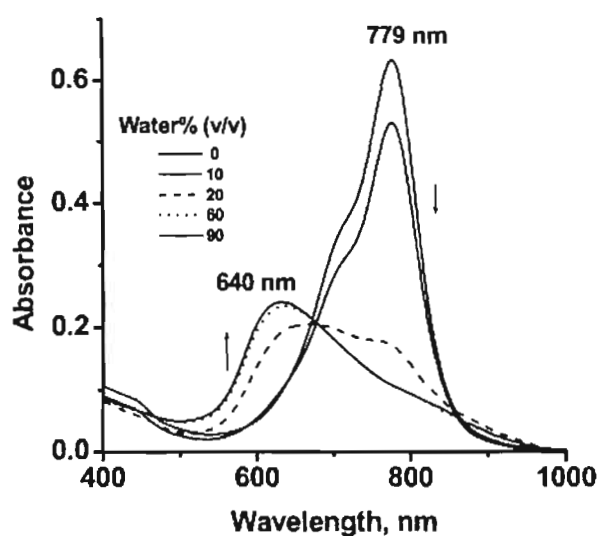


**Figure 3.4.** Absorption spectra of **2a** in DMSO-water solvent mixture of different composition ( $[\text{dye}] = 6.46 \times 10^{-6} \text{ M}$ ).

A concentration dependent change in the absorption spectrum of **2a** in DMSO-water (80%) is shown in Figure 3.5. At very low concentration, the dye exists mainly as monomers in DMSO-water mixture containing 80% water as indicated by the absorption maximum at 779 nm. As the concentration is increased, the intensity of the aggregate band at 650 nm gradually increased. At higher concentrations, the dye exists predominantly as the aggregates. The aggregation number of dye **2a** was determined by plotting  $\log [\text{aggregate}]$  against  $\log [\text{monomer}]$  (Figure 3.6). A straight line with a slope of 2 indicates that the aggregate exists mainly as dimers.

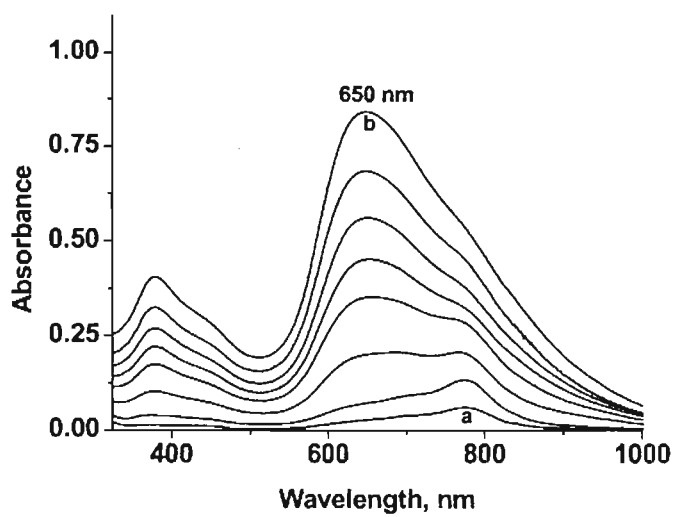


**Figure 3.5.** UV-vis absorption spectra of squaraine dye **2a** at different concentrations in 80% DMSO-water mixture. Spectrum 'a' is for 1.1  $\mu\text{M}$ , and spectrum 'b' is for 20.5  $\mu\text{M}$  of the dye.

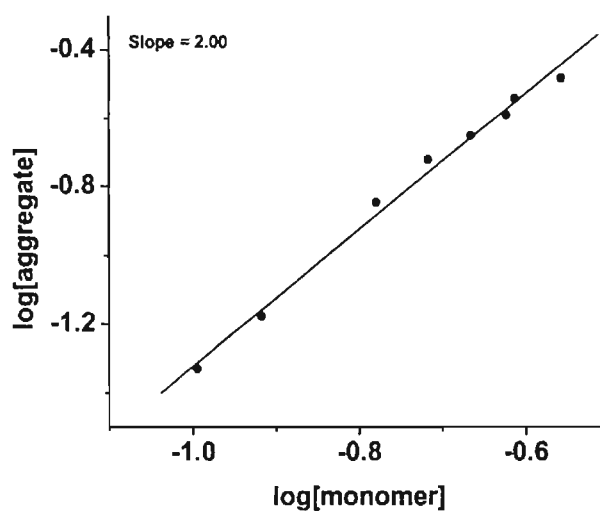


**Figure 3.6.** Plot of log [aggregate] vs log [monomer] of **2a** in 80% DMSO-water mixture.

Temperature dependent change in the absorption spectrum of **2a** in DMSO-water (80%) mixture is shown in Figure 3.7. In this composition at 25 °C, a major portion of **2a** exists as the aggregates. Upon increasing the temperature, the aggregate absorption at 656 nm gradually decreases with the concomitant growth of the monomer band at 764 nm. At 65 °C, even though the intensity of the aggregate band is significantly decreased, a complete shift of the aggregate to the monomer could not be achieved. This observation indicates that in 80% DMSO-water, the aggregates do not break completely. This means that the temperature dependent interconversion of the aggregates to the monomer was strongly influenced by the composition of the solvent. The aggregates are very stable above 50% water in DMSO and hence the rate of conversion of the aggregates to the monomer is very slow at higher water compositions.

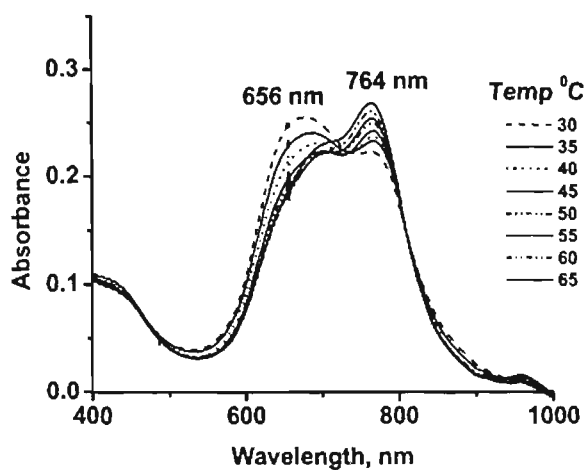


**Figure 3.7.** Temperature dependent absorption changes of **2a** in 80% DMSO-water ( $[\text{dye}] = 6.46 \times 10^{-6} \text{ M}$ ).

In pure DMSO, at a concentration of  $3.76 \times 10^{-6}$  M, **2b** initially exhibited an absorption maximum at 776 nm. An interesting observation in the case of the dye **2b** in DMSO is that, the intensity of the 776 nm band decreases with time and the absorption maximum is shifted to 682 nm. It must be noted that dye **2a** did not exhibit such a time dependent change in the absorption maximum. Dye **2b** existed in the form of aggregates even in pure DMSO. Addition of water to the solvent in this case further facilitated the formation of aggregates with 4% of water content in DMSO. Further increase in water content resulted in the precipitation of the dye from the solution.

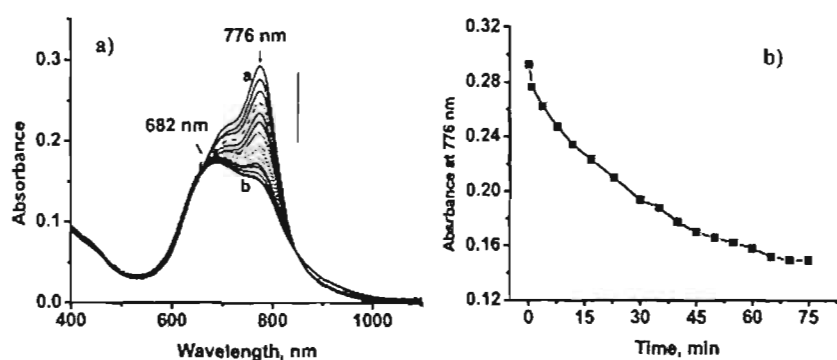


**Figure 3.8.** a) Time dependent absorption changes of the dye **2b** in DMSO. Spectrum 'a' is recorded immediately after the addition of the dye to DMSO and spectrum 'b' is after 75 min. b) Plot of absorbance at 776 nm against time for dye **2b** in DMSO ( $[\text{dye}] = 3.76 \times 10^{-6}$  M).

Spectrum 'a' corresponds to the initial spectrum of the dye **2b** in DMSO and spectrum 'b' is that of the same solution recorded after 75 minutes. Figure 3.8b shows the plot of intensity of the monomer absorption at 776 nm against time which indicates the gradual decrease of the absorbance at 776 nm. The change in

the absorption spectrum of **2b** with temperature in DMSO-water (3%) mixture is shown in Figure 3.9. Increase in temperature resulted in a decrease in the intensity of the 640 nm band characteristic of the H-aggregates and a concomitant increase in the intensity of the band at 769 nm, characteristic to the monomer. In this case, the nearly complete shift of the aggregate absorption to the monomer absorption indicates complete breaking of the aggregates. The concentration dependent absorption spectra of **2b** in DMSO showed the formation of blue shifted aggregates at higher concentration of the dye (Figure 3.10). The aggregation number was found to be 1.80, which indicates that aggregates are dimeric in nature.

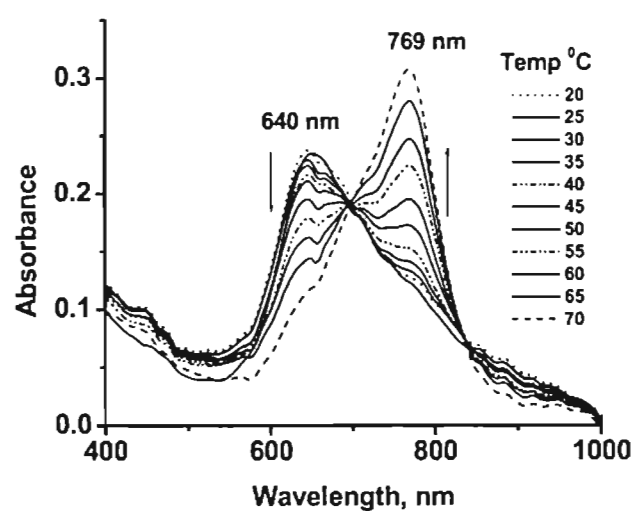


**Figure 3.9.** Temperature dependent absorption changes of dye **2b** in 97% DMSO-water ( $[\text{dye}] = 3.76 \times 10^{-6} \text{ M}$ ).

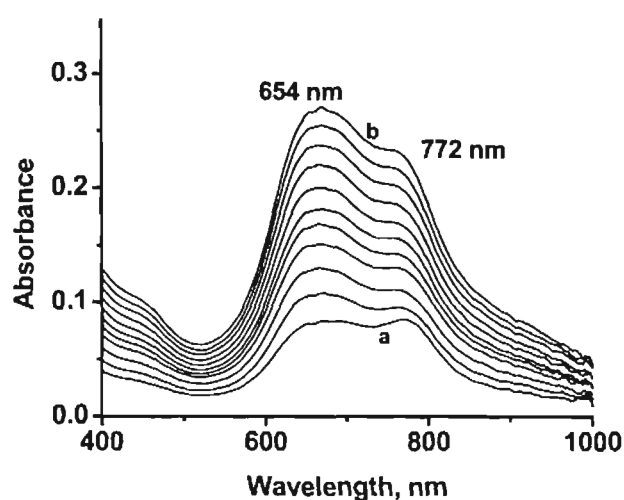


**Figure 3.10.** a) UV-vis absorption spectra of squaraine dye **2b** at different concentrations. Spectrum 'a' is for 2.1  $\mu\text{M}$  and spectrum 'b' is for 21.5  $\mu\text{M}$  of the dye in 97% DMSO-water mixture.

Changes observed in the absorption spectra of dye **2c** in DMSO-water mixtures are shown in Figure 3.11. In this case also, the dye tends to aggregate even with low percentage of water in DMSO. At very low percentage of water, **2c** exists as monomer which absorbs at 780 nm. Intensity of this band was decreased as the percentage of water in DMSO-water mixtures is increased. A drastic decrease in the intensity of the 780 nm band was observed in 10% (v/v) water. With further increase in water content, the spectral pattern changed completely with the formation of a blue shifted band with maximum centered around 650 nm and another red-shifted band centered around 885 nm. These observations in the case of **2c** are different from the behavior of the dyes **2a** and **2b** which showed only the blue shifted aggregate bands. In the case of **2c**, a red-shifted band at 885

nm was observed in addition to the blue shifted band at 650 nm. This observation indicates the formation of both the H- and J-type aggregates of **2c** in DMSO-water.

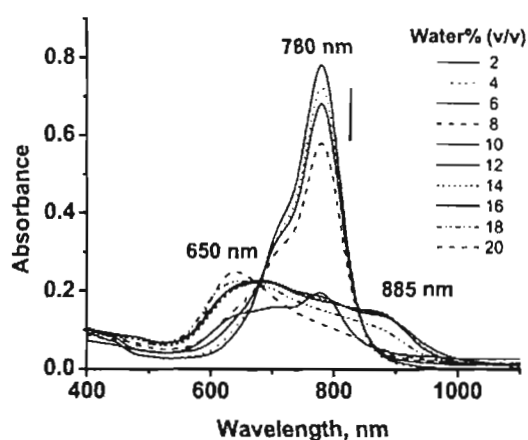


**Figure 3.11.** Absorption spectra of **2c** in DMSO-water solvent mixture of different composition ( $[\text{dye}] = 4.44 \times 10^{-6} \text{ M}$ ).

In DMSO-water mixtures with water content more than 8%, the dye **2c** exhibited a time dependent change in the absorption spectrum. For example, on keeping, a gradual decrease in the intensity of the monomer band is observed with evolution of a red-shifted peak around 900 nm. This observation indicates that both H- and J-aggregates are formed in this case. Figure 3.12 shows the absorption spectra of **2c** in 12% v/v water-DMSO with time. Change in the absorbance at 640 nm, 780 nm and 900 nm with time ( $[\text{dye}] = 4.44 \times 10^{-6} \text{ M}$ ) in 12% v/v water-DMSO is shown in Figure 3.13. It can be noted that at the initial time scales, the monomer band at 780 nm exhibited significant decrease in the intensity with significant broadening of the spectrum. While the 900 nm band showed a slow and

continuous growth, the 640 nm band showed an initial slow growth followed by a slow decrease in the intensity. This observation indicates that the H-aggregates may have a tendency to slowly reorganize to form the thermodynamically more stable J-aggregates. This is further confirmed by the temperature dependent spectral changes at various DMSO-water compositions.

Effect of temperature on the absorption spectra of **2c** in different DMSO-water compositions is shown in Figure 3.14. At 8% (v/v) water-DMSO, a complete dissociation of the aggregates to the monomers was observed upon heating (Figure 3.14a). Dye **2c** exists mainly as a mixture of monomer and H-aggregate in 10% (v/v) water-DMSO solvent composition.

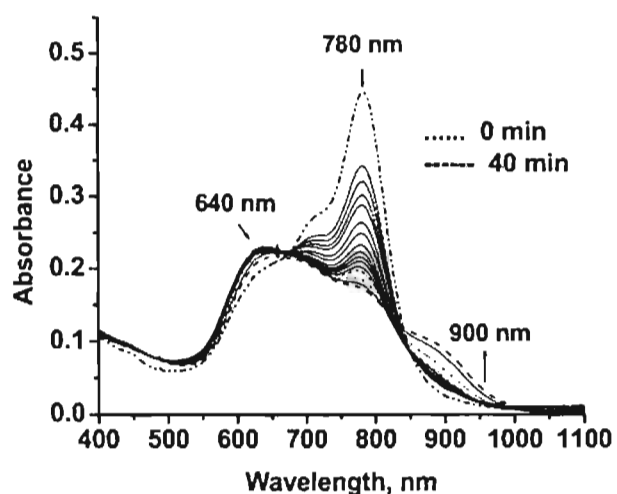


**Figure 3.12.** Time dependent changes in the absorption spectrum of **2c** in 12% v/v water-DMSO ( $[\text{dye}] = 4.44 \times 10^{-6} \text{ M}$ ).

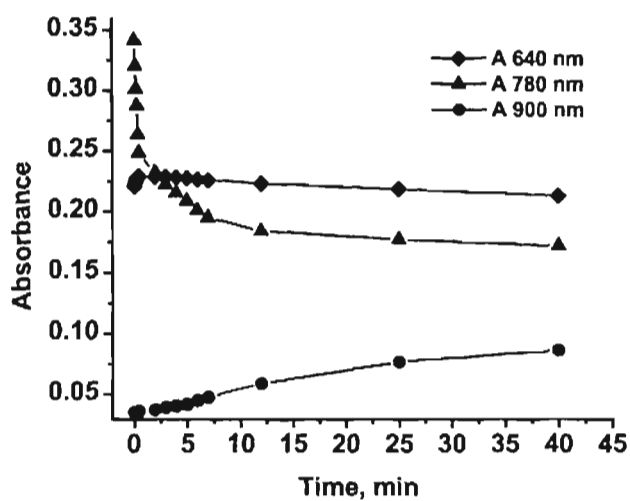


**Figure 3.13.** Plots of absorbance at 640 nm, 780 nm and 900 nm with time for 2c in 12% v/v water-DMSO.

Upon heating, the intensity of the band at 656 nm is reduced and the monomer band at 764 nm is regained (Figure 3.14b). Cooling the solution to room temperature regenerated the absorption corresponding to the aggregate, indicating that in this solvent composition aggregation is a reversible process (Figure 3.14c). In 12% (v/v) water-DMSO, H-aggregates, J-aggregates and monomers coexist (Figure 3.14d). Upon heating, the intensity of both H- and J-aggregate bands is marginally decreased to form the monomer peak. Thus above 10% of water in DMSO, the dye exists as a mixture of H- and J-aggregates along with the monomer.

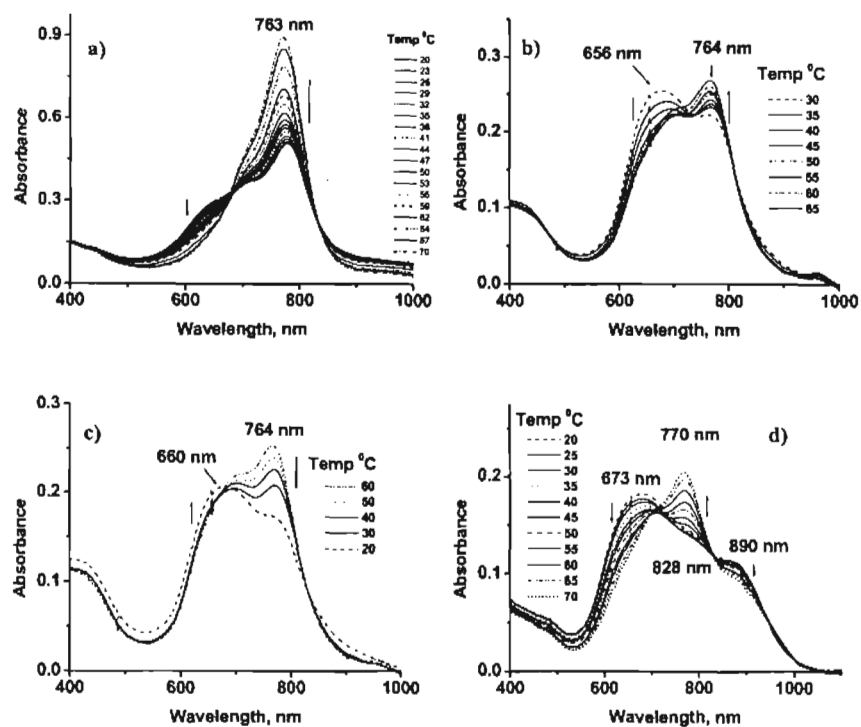


**Figure 3.14.** Temperature dependent absorption spectra of **2c** in a) 8% (v/v) water-DMSO, b) 10% (v/v) water-DMSO while heating, c) 10% (v/v) water-DMSO cooling cycle and d) 12% (v/v) water-DMSO ( $[\text{dye}] = 4.44 \times 10^{-6} \text{ M}$ ).

In a mixture of 20% (v/v) water-DMSO, the dye **2c** existed mainly as H-aggregates (Figure 3.15). Surprisingly, upon increasing the temperature from 25 °C – 70 °C, a red-shifted peak ( $\lambda_{\text{max}}$  at 880 nm) was formed without significant increase in the monomeric absorption. On cooling the mixture, the spectral features are retained with a small shift of the 880 nm peak to 900 nm (Figure 3.15b). These observations indicate that the H-aggregates rearrange to J-aggregates upon heating which do not reverse back to H-aggregates upon cooling.

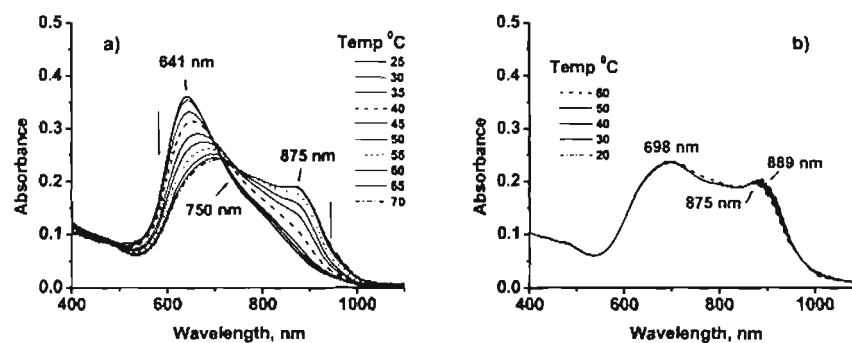


**Figure 3.15.** Temperature dependent absorption spectra of **2c** in 20% (v/v) water-DMSO (a) heating cycle (b) cooling cycle ( $[\text{dye}] = 4.44 \times 10^{-6} \text{ M}$ ).

Thus, temperature dependent studies in DMSO-water below 20% water content shows that the H- and J-aggregates can be interconverted by heating and cooling. However with DMSO-water mixture having >20% of water, such a change is not observed. Therefore, the processes involved in the aggregation behavior of **2c** in DMSO-water mixtures can be represented as shown below.



### 3.3.3.2. Aggregation behavior of Dyes **2a-c** in THF-water

The dyes **2a-c** are soluble in THF and showed intense absorption between 600-800 nm having maxima at 766, 769 and 770 nm, respectively with a shoulder band around 700 nm. However, in THF-water mixtures, these dyes exhibited significant changes in their absorption spectra. The change in the absorption

spectrum of the dye **2a** ( $5.4 \times 10^{-6}$  M) in THF-water mixtures of different composition is shown in Figure 3.16. With increase in the amount of water content, the intensity of the absorption maximum of the dye is gradually decreased. At higher amount of water, a blue shifted band at 639 nm is formed. This observation is similar to that seen in DMSO-water mixtures and is characteristic of the formation of the H-aggregates.

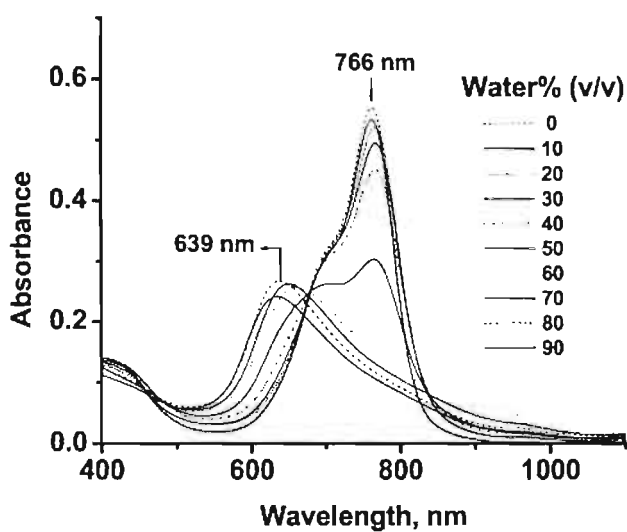


**Figure 3.16.** Absorption spectra of **2a** in THF-water solvent mixtures ( $[\text{dye}] = 5.4 \times 10^{-6}$  M).

Temperature dependent changes of **2a** were studied in THF-water with 50% v/v of water. Upon increasing the temperature, the aggregate absorption at 650 nm is decreased with a growth of the monomer band at 757 nm through an isosbestic point at 685 nm. Cooling the solution to room temperature regenerated the

aggregated form (Figure 3.17). However, a complete reversal of the aggregates to the monomer was not observed in this case.

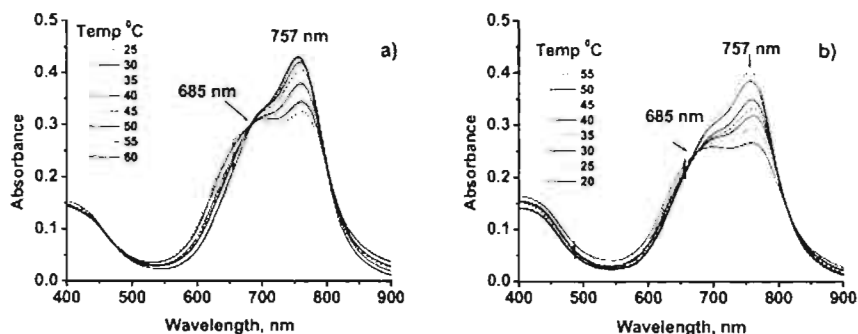


**Figure 3.17.** Temperature-dependent absorption spectra of **2a** in 50 % (v/v) THF-water mixture a) heating cycle and b) cooling cycle ( $[\text{dye}] = 5.4 \times 10^{-6} \text{ M}$ ).

The UV-vis spectral changes of the dyes **2b** and **2c** in THF-water mixture of different compositions are shown in Figures 3.18 and Figure 3.19, respectively. In these cases, upon increasing the water content, the intensity of the monomer bands is decreased and broad spectra with blue and red-shifted peaks are formed at 50% of water. This observation indicates that both H- and J-aggregates are formed in these cases. It is observed that above 50% of water in THF, the intensity of the band at 902 nm is decreased. In 90% water-THF mixture, the spectrum of **2c** mainly showed the 673 nm band indicating the predominant formation of the H-aggregates.

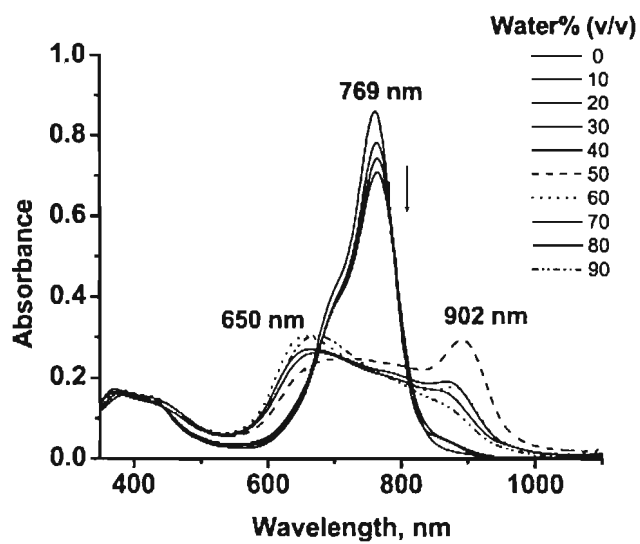


Figure 3.18. Absorption spectra of 2b in THF-water solvent mixtures ( $[\text{dye}] = 5.08 \times 10^{-6} \text{ M}$ ).

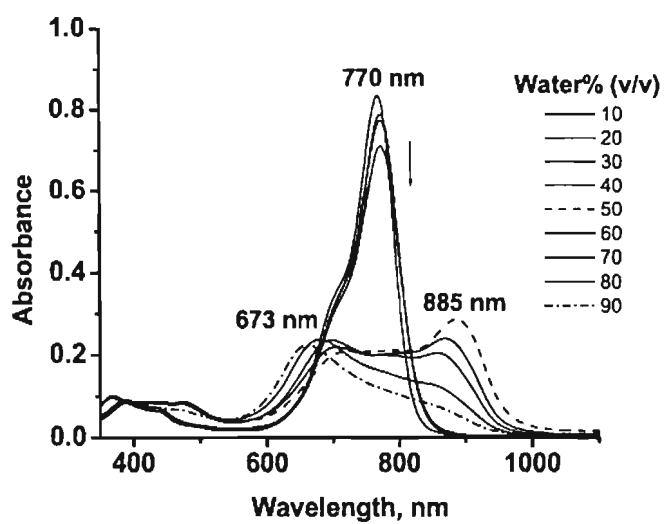
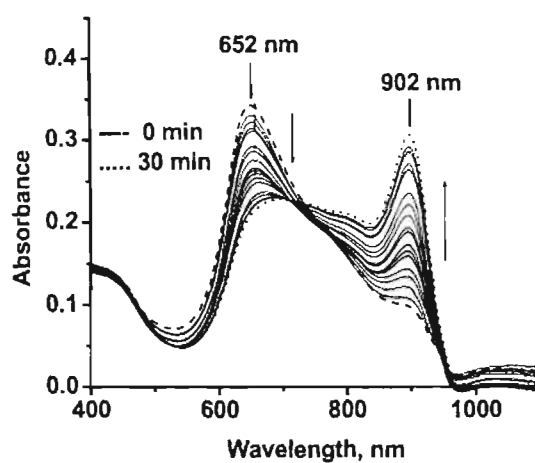
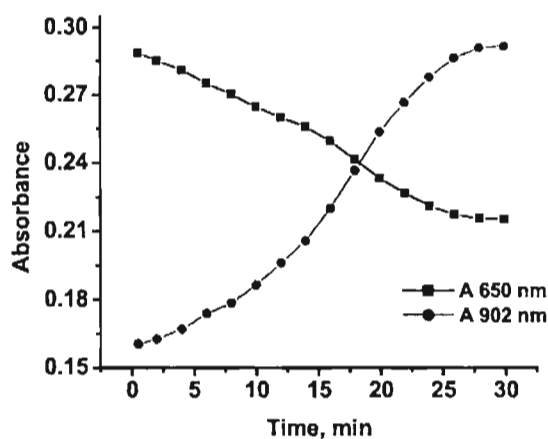


Figure 3.19. Absorption spectra of 2c in THF-water solvent mixtures ( $[\text{dye}] = 6.03 \times 10^{-6} \text{ M}$ ).

Time dependent studies of dyes **2b** and **2c** in 50% (v/v) THF-water showed a decrease in the intensity of the H-aggregate band with the simultaneous increase in the J-aggregate band. For example, addition of the dye **2b** to a solution of 50% (v/v) water in THF resulted in a broad spectrum with a blue shifted band at 652 nm and red-shifted weak band at 902 nm. With time, the intensity of the band at 652 nm is decreased with the growth of a peak at 902 nm (Figure 3.20). This is clear from the plots of the absorbance at 650 nm and 902 nm with time (Figure 3.21). This observation indicates time dependent rearrangement of the initially formed H-aggregates to J-aggregates in 50% water-THF solvent mixture. However, at higher water content (> 50%), the rate of conversion of the 673 nm band to 885 nm becomes slow. In this case, the H-aggregates may be kinetically trapped and may not rearrange to the J-aggregates. This could be the reason for the low intensity of the 885 nm band at 90% water-THF mixture.



**Figure 3.20.** Time dependent absorption changes of **2b** in 50% (v/v) THF-water mixture ( $[\text{dye}] = 5.08 \times 10^{-6} \text{ M}$ ).



**Figure 3.21.** Plots of intensities of H-aggregate (652 nm) and J-aggregate (902 nm) bands of **2b** against time in 50% (v/v) THF-water.

The temperature dependent change of **2b** was studied in 56% (v/v) THF. In this composition, significant amount of J-aggregates are formed. Upon increasing the temperature, the aggregate absorption at 915 nm is gradually decreased with the concomitant growth of the monomer band at 757 nm through an isosbestic point at 805 nm (Figure 3.22a). The change in the absorbance at 915 nm with temperature is shown in the inset of the Figure 3.22a. Cooling of the solution regenerated the aggregated species, indicating the reversibility of the process (Figure 3.22b).

Concentration dependent absorption changes of the dye **2c** in 56% (v/v) THF-water mixture are shown in Figure 3.23. In 50% (v/v) THF-water mixture, considerable amount of J-aggregate was formed with increase in concentration of

the dye. The aggregation number was found to be 1.98, which indicates the dimeric nature of the aggregates (Figure 3.24).

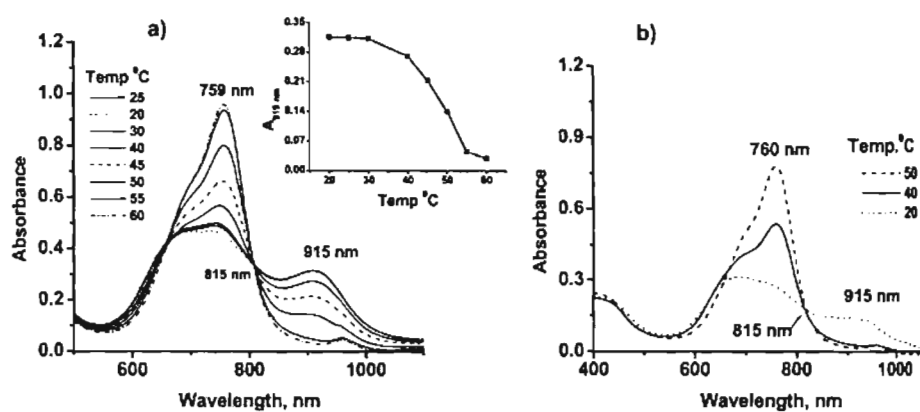


**Figure 3.22.** Temperature-dependent absorption spectra of **2b** in 56% (v/v) THF-water mixture a) heating cycle and b) cooling cycle. Inset of Figure a is the plot of absorbance at 915 nm with temperature in the heating cycle.

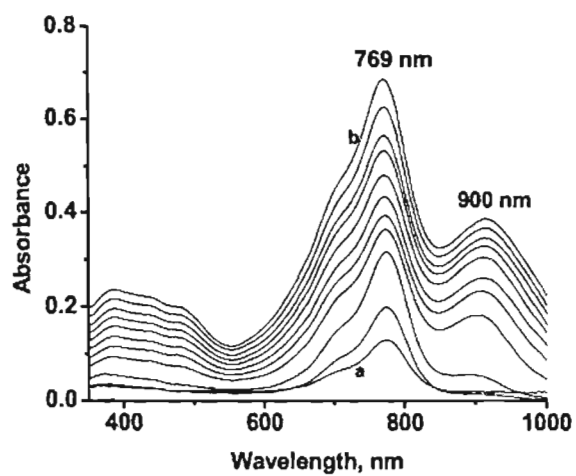


**Figure 3.23.** UV-vis absorption spectra of the squaraine dye **2c** at different concentrations. Spectrum 'a' is for 2.0  $\mu\text{M}$  and spectrum 'b' for is 20  $\mu\text{M}$  of the dye in 56% THF-water mixture.

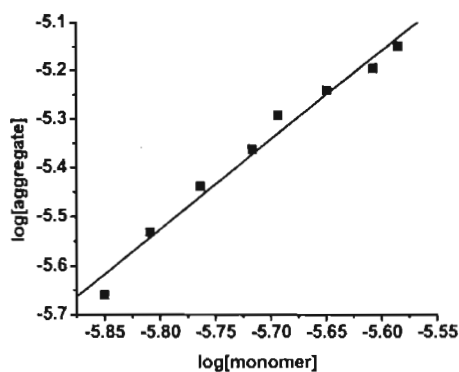


Figure 3.24. Plot of log [aggregate] against log [monomer] of **2c** in 44% THF-water mixture.

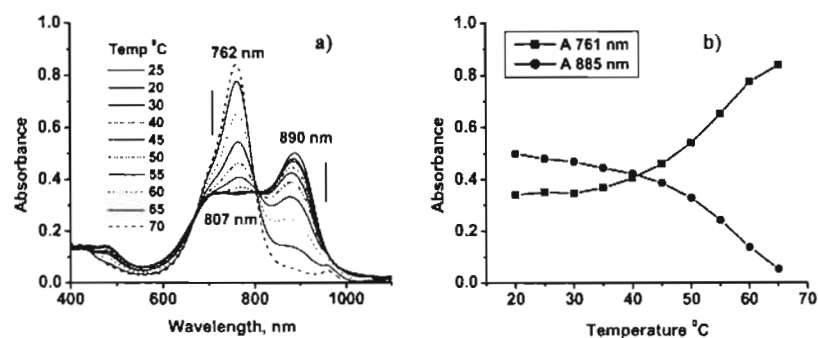


Figure 3.25. (a) Temperature dependent absorption spectra of **2c** and (b) Plots of the intensity of the absorption at 761 nm and 885 nm of **2c** in 50% (v/v) THF against temperature.

The temperature dependent conversion of J-aggregates of **2c** in 50% (v/v) THF-water to the corresponding monomer is shown in Figure 3.25a. In 50% (v/v) THF, **2c** exists mainly as J-aggregates. The intensity of the monomer band at 761 nm gradually increased with increase in temperature. At 70 °C the aggregate band at 885 nm almost vanished with complete recovery of the monomer band. Plots of

the intensities of the absorption of the monomer at 761 nm and the J-aggregate at 885 nm against temperature are shown as Figure 3.25b.

The absorption spectral changes of **2a-c** in different solvent mixtures indicate the role of *O*-alkyl side chains of the phenyl group on the aggregation behavior. Dye **2a** with the shortest side chain (*O*-butyl) formed only H-aggregates in both the solvent systems. The shorter side chains favored a card pack array of the transition dipoles and remained unaffected by the percentage of water content in the systems. However, for the dye **2b** with *O*-dodecyl side chains and the dye **2c** with the branched side chains, the mode of aggregation was found to be dependent on the percentage of water content in the solvent mixtures. Dye **2b** tends to form aggregates even in pure DMSO and the aggregation process is facilitated with <5% of water in DMSO. Aggregation of **2b** in THF-water and **2c** in DMSO-water and THF-water followed a similar pattern. For **2c**, the branched side chain preferred the less strained slipped stack assembly than a sterically strained card pack assembly at lower water content. With increased water content, hydrophobicity of the side chains prevented the extended packing which resulted in the formation of the head-to-head packed blue shifted H-aggregates.

#### 3.3.4. Solid-State Absorption Properties

The solid-state absorption spectra of the dyes were quite different from the corresponding solution state spectra. In the solid-state, broadening of the spectra is observed with the formation of new absorption bands, which are blue and red-

shifted with respect to the absorption maximum in solution. It is well known that in the solid-state, the absorption of many of the squaraine dyes becomes broad and red-shifted to the near-IR region. This broadening of the absorption is due to the strong intermolecular interaction and aggregation, the type of which is determined by the structure of the dye. In most of the cases, squaraine dyes show similar trend of aggregation in solid-state as observed in solvent systems.

In the solid-state, the dye **2a** with *O*-butyl side chains exhibited a blue shift in the absorption maximum ( $\lambda_{\text{max}} = 670 \text{ nm}$ ) relative to that in chloroform ( $\lambda_{\text{max}} = 762 \text{ nm}$ ). A red shifted shoulder band is also formed around 850 nm the intensity of which is relatively weak when compared to that of the blue shifted band. Comparison of the solution and solid-state absorption spectra of the dye is shown in Figure 3.26.

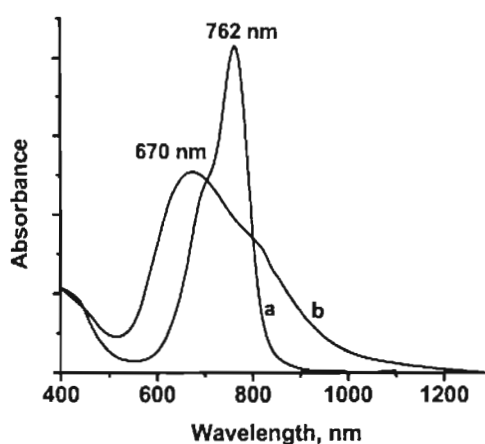


**Figure 3.26.** Absorption spectra of dye **2a**, a) in chloroform and b) in the solid-state (film).

The dye **2b** with *N*-methyl and *O*-dodecyl side chains showed a broad spectrum when compared to that of dye **2a** (Figure 3.27), which indicates the formation of both H- and J-aggregates in almost equal intensity.

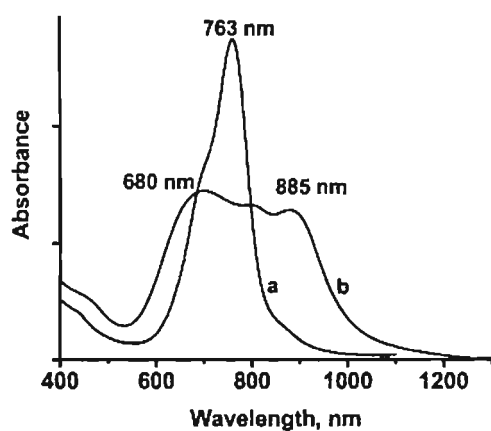


Figure 3.27. Absorption spectra of dye **2b**, a) in chloroform and b) in the solid-state (film).

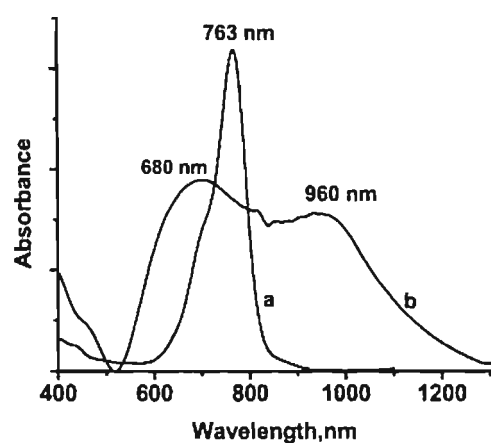


Figure 3.28. Absorption spectra of dye **2c**, a) in chloroform and b) in the solid-state (film).

A comparison of the solid-state absorption spectrum of the dye **2c** having ethylhexyl side chains with the corresponding solution state spectrum is shown in Figure 3.28. In this case, the solid-state spectrum is relatively broader than that of **2b**. While the H-aggregates of **2b** and **2c** absorb at 680 nm, the J-aggregates of **2c** in the solid-state showed the maximum red-shift towards 960 nm which is 75 nm more than that of **2b**.

These studies indicate that the dye **2a** with short side chains prefers to form H-aggregates both in the solvent mixtures as well as in the solid-state. However, the dyes with long alkyl side chains and branched side chains form both H- and J-type aggregates in the solvent mixtures and in the solid-state. The shift towards the near-IR region is found to be maximum for the dye **2c** with 2-ethylhexyl side chains in the solid-state. This observation reveals that the branched side chains on the phenyl bridge prefer to form the slipped aggregates with minimum tilt angle.

### 3.3.5. X-ray Diffraction Studies

Insight into the molecular packing of **2a-c** in the solid state was obtained from their X-ray diffraction patterns. The peaks in the XRD pattern could be correlated with the aggregation pattern of the dyes in the solid state. Squaraine dyes which form J-aggregates in the solid-state gave sharp XRD signals. Elongation and branching of the hydrocarbon side chains have significant influence on the molecular packing as evident from the comparison of the XRD data of **2a-c** (Figure 3.29). The calculated wingspan of the dyes **2b** and **2c** are

33.37 Å and 19.83 Å respectively. The XRD peaks are observed at 20.47 Å for **2b** and at 13.17 Å for **2c**. These *d*-spacing indicate more closely packed interdigitated assembly of the aggregates in the solid-state. A possible molecular packing diagram of the squaraine dye **2c** is shown in Figure 3.30. The wide-angle region remained broad revealing weak  $\pi$ -interactions between the dyes and hence the absence of strong long range orders in the solid-state. These observations imply that the *O*-alkyl chains have significant influence on the inter-chain packing of the molecules.

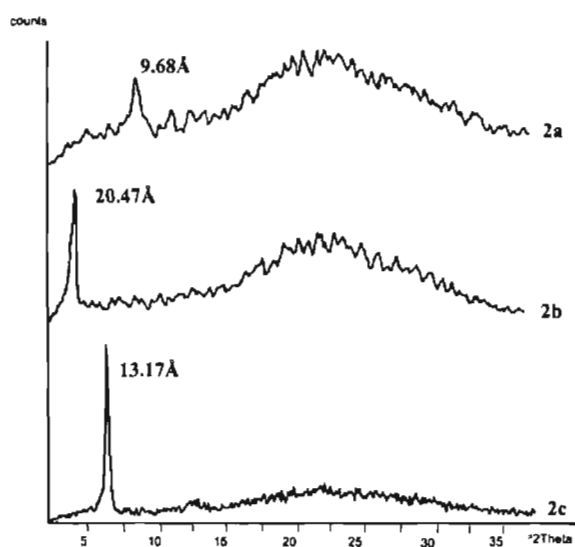


Figure 3.29. X-ray diffraction patterns of the squaraine dyes **2a-c**.

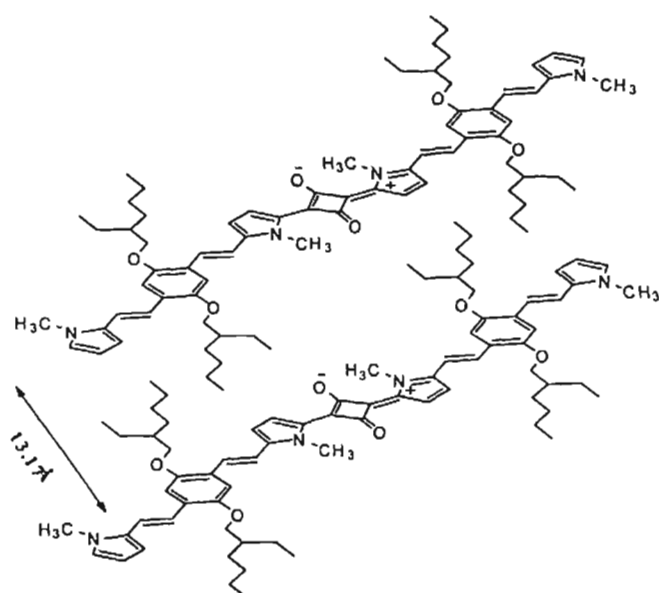


Figure 3.30. A possible molecular packing diagram of the squaraine dye 2c.

### 3.4. Conclusions

The present study reveals the crucial role of side chain substituents in controlling the electronic absorption and aggregation properties of the  $\pi$ -extended squaraine dyes 2a-c. These dyes form aggregates in solution as well as in solid-state. The hydrophobic interactions and the steric effects of the hydrocarbons chains play a major role in the aggregation process. Aggregates formed in DMSO-water and THF-water solvent mixtures bear resemblance to those in their solid-state. X-ray diffraction patterns showed interdigitated packing of the dyes in the solid state.

## 3.5. Experimental

### 3.5.1. General methods

The general experimental methods used are described in Chapter 2 of the thesis.

### 3.5.2. Preparation of bispyrroles (1a-c)

Bispyrroles **1a-c** were synthesized according to the procedures given in Chapter 2.

**1a:** Yield 63%; mp 141 °C; IR (KBr)  $\nu_{\max}$  2949, 2868, 1462, 1417, 1327, 1197, 1039, 1012, 954, 707  $\text{cm}^{-1}$ ;  $^1\text{H}$  NMR (300 MHz,  $\text{CDCl}_3$ )  $\delta$  7.08 (d, 2H, vinylic  $J=16.26$  Hz), 7.00 (d, 2H, vinylic,  $J=16.30$  Hz), 6.91 (s, 2H, aromatic), 6.56 (s, 2H, aromatic), 6.42 (m, 2H, aromatic), 6.09 (t, 2H, aromatic), 3.96 (t, 4H,  $\text{OCH}_2$ ), 3.63 (s, 6H,  $\text{NCH}_3$ ), 1.74 (t, 4H,  $\text{CH}_2$ ), 1.50 (m, 4H,  $\text{CH}_2$ ), 0.94 (t, 6H,  $\text{CH}_3$ );  $^{13}\text{C}$  NMR (75.4 MHz,  $\text{CDCl}_3$ )  $\delta$  150.93, 132.87, 126.56, 123.44, 121.46, 117.56, 110.95, 108.23, 106.63, 69.12, 34.15, 31.66, 19.47, 13.91; HRMS calcd for  $\text{C}_{28}\text{H}_{36}\text{N}_2\text{O}_2$  ( $\text{M}^+$ ): 432.2777, found 432.2770.

**1b:** Yield 48%; mp 80 °C; IR (KBr)  $\nu_{\max}$  2921, 2851, 1543, 1496, 1463, 1310, 1227, 1206, 1046, 960  $\text{cm}^{-1}$ ;  $^1\text{H}$  NMR (300 MHz,  $\text{CDCl}_3$ )  $\delta$  7.14 (d, 2H, vinylic  $J=16.28$  Hz), 7.05 (d, 2H, vinylic,  $J=16.34$  Hz), 6.97 (s, 2H, aromatic), 6.63 (s, 2H, aromatic), 6.48 (m, 2H, aromatic), 6.15 (m, 2H, aromatic), 4.01 (t, 4H,  $\text{OCH}_2$ ), 3.69 (s, 6H,  $\text{NCH}_3$ ), 1.84 (m, 4H,  $\text{CH}_2$ ), 1.51 (m, 4H,  $\text{CH}_2$ ), 1.26 (m, 32H,

CH<sub>2</sub>) 0.86 (t, 6H, CH<sub>3</sub>); <sup>13</sup>C NMR (75.4 MHz, CDCl<sub>3</sub>), δ 150.95, 132.87, 126.60, 123.44, 121.44, 117.53, 110.96, 108.24, 106.68, 69.52, 34.19, 31.90, 29.63, 29.49, 29.34, 26.30, 22.67, 14.10. HRMS calcd for C<sub>44</sub>H<sub>68</sub>N<sub>2</sub>O<sub>2</sub> (M<sup>+</sup>): 656.5281, found 656.5263.

**1c**: Yield 74%; mp 110 °C; IR (KBr) ν<sub>max</sub> 2934, 2857, 1543, 1491, 1424, 1325, 1288, 1196, 1046, 953 cm<sup>-1</sup>; <sup>1</sup>H NMR (300 MHz, CDCl<sub>3</sub>) δ 7.16 (d, 2H, vinylic, J=16.30 Hz), 7.03 (d, 2H, vinylic, J=16.23 Hz), 6.99 (s, 2H, aromatic), 6.62 (s, 2H, aromatic), 6.47 (m, 2H, aromatic), 6.15 (m, 2H, aromatic), 3.92 (d, 4H, OCH<sub>2</sub>), 3.70 (s, 6H, CH<sub>3</sub>), 1.78 (m, 2H, CH), 1.37 (m, 16H, CH<sub>2</sub>), 0.88-0.99 (m, 12H, CH<sub>3</sub>); <sup>13</sup>C NMR (75.4 MHz, CDCl<sub>3</sub>), δ 150.98, 132.94, 126.52, 123.52, 121.40, 117.36, 110.31, 108.27, 106.78, 71.55, 39.85, 34.35, 30.85, 29.25, 24.17, 23.12, 14.15, 11.32; Anal. calcd for C<sub>36</sub>H<sub>52</sub>N<sub>2</sub>O<sub>2</sub>(M<sup>+</sup>): C, 79.36; H, 9.62; N, 5.14. Found: C, 78.96; H, 9.83; N, 5.14.

### 3.5.3. Preparation of π-extended squaraine dyes (2a-c)

The π-extended squaraine dyes **2a-c** were synthesized according to the procedure given in the previous chapter.

**2a**: Yield 36%; IR (KBr) ν<sub>max</sub> 2930, 1620, 1440, 1352, 1283, 1096, 939 cm<sup>-1</sup>; <sup>1</sup>H NMR (300 MHz, CDCl<sub>3</sub>) δ 7.77 (s, 2H, aromatic), 7.4 (m, 2H, vinylic, J = 15.61 Hz), 7.17-7.10 (m, 6H, vinylic+aromatic), 6.92 (m, 6H, vinylic+aromatic), 6.63 (s, 2H, aromatic), 6.51 (s, 2H, aromatic), 6.16 (s, 2H, aromatic), 4.22 (s, 6H, NCH<sub>3</sub>), 4.04 (s, 6H, NCH<sub>3</sub>), 3.48-3.67 (m, 8H, OCH<sub>2</sub>), 1.85 (m, 8H, CH<sub>2</sub>), 1.63 (m, 8H,

CH<sub>2</sub>), 1.03 (m, 12H, CH<sub>3</sub>); <sup>13</sup>C NMR (75.4 MHz, CDCl<sub>3</sub>), δ 168.52, 152.45, 131.65, 130.96, 130.22, 129.18, 120.84, 118.94, 115.49, 115.06, 113.64, 113.29, 113.15, 110.43, 109.88, 109.06, 108.47, 107.35, 69.45, 69.19, 34.19, 33.09, 31.95, 22.68, 13.98; HRMS calcd for C<sub>60</sub>H<sub>70</sub>N<sub>4</sub>O<sub>6</sub> (M<sup>+</sup>): 942.5295, found 942.5321. Anal. calcd for C<sub>60</sub>H<sub>70</sub>N<sub>4</sub>O<sub>6</sub>·H<sub>2</sub>O: C, 74.96; H, 7.55; N, 5.82. Found: C, 74.97; H, 7.96; N, 6.07.

**2b**: Yield 23%; IR (KBr) ν<sub>max</sub> 2924, 1625, 1491, 1434, 1351, 1284, 1206, 1093, 865 cm<sup>-1</sup>; <sup>1</sup>H NMR (300 MHz, CDCl<sub>3</sub>) δ 7.80 (s, 2H, aromatic), 7.47 (d, 2H, vinylic *J* = 15.67 Hz), 7.19 (d, 2H, vinylic, *J* = 15.41 Hz), 7.14 (m, 4H, vinylic), 6.96 (m, 4H, aromatic), 6.90 (s, 2H, aromatic), 6.63 (s, 2H, aromatic), 6.52 (m, 2H, aromatic), 6.15 (s, 2H, aromatic), 4.20 (s, 6H, NCH<sub>3</sub>), 4.04 (m, 8H, OCH<sub>2</sub>), 3.68 (s, 6H, NCH<sub>3</sub>), 1.88 (m, 8H, CH<sub>2</sub>), 1.59 (m, 32H, CH<sub>2</sub>), 1.26 (m, 40H, CH<sub>2</sub>), 0.88 (m, 12H, CH<sub>3</sub>); <sup>13</sup>C NMR (75.4 MHz, CDCl<sub>3</sub>), δ 169.79, 152.13, 132.65, 124.01, 120.84, 118.94, 115.49, 115.06, 113.64, 113.29, 113.15, 110.43, 109.88, 109.06, 108.47, 107.35, 106.1, 105.12, 69.45, 69.19, 34.19, 33.09, 31.95, 29.65, 29.52, 29.43, 29.34, 26.33, 26.26, 22.68, 14.09; MALDI TOF: calcd for C<sub>92</sub>H<sub>134</sub>N<sub>4</sub>O<sub>6</sub> (M<sup>+</sup>): 1392.0303, found 1392.06; Anal. calcd for C<sub>92</sub>H<sub>134</sub>N<sub>4</sub>O<sub>6</sub>·H<sub>2</sub>O: C, 78.36; H, 9.72; N, 3.97. Found: C, 77.93; H, 10.05; N, 3.92.

**2c**: Yield 25%; IR (KBr) ν<sub>max</sub> 2924, 1620, 1506, 1439, 1356, 1289, 1206, 1087, 948 cm<sup>-1</sup>; <sup>1</sup>H NMR (300 MHz, CDCl<sub>3</sub>) δ 7.82 (d, 2H, aromatic), 7.51 (d, 2H, vinylic *J* = 16.10 Hz), 7.21 (d, 2H, vinylic, *J* = 16.23 Hz), 7.18 (m, 2H, vinylic),

7.10 (d, 2H, vinylic,  $J = 16.39$  Hz), 7.01 (m, 2H, aromatic), 6.98 (m, 2H, aromatic), 6.89 (d, 2H, aromatic), 6.65 (s, 2H, aromatic), 6.51 (m, 2H, aromatic) 6.17 (m, 2H, aromatic), 4.30 (s, 6H, NCH<sub>3</sub>), 3.97 (m, 8H, OCH<sub>2</sub>), 3.72 (s, 6H, NCH<sub>3</sub>), 1.82 (m, 4H, CH), 1.51 (m, 8H, CH<sub>2</sub>), 1.25 (m, 24H, CH<sub>2</sub>), 0.89-0.99 (m, 24H, CH<sub>3</sub>); <sup>13</sup>C NMR (75.4 MHz, CDCl<sub>3</sub>),  $\delta$  166.48, 152.22, 150.96, 132.66, 131.22, 130.96, 129.29, 124.41, 124.08, 120.72, 118.78, 114.90, 114.46, 113.69, 111.40, 109.97, 108.49, 107.53, 71.54, 39.81, 34.35, 34.07, 30.84, 29.24, 24.24, 23.08, 14.11, 11.30. MALDI TOF: calcd for C<sub>76</sub>H<sub>102</sub>N<sub>4</sub>O<sub>6</sub> (M<sup>+</sup>) 1167.6464, found 1167.68; Anal. calcd for C<sub>76</sub>H<sub>102</sub>N<sub>4</sub>O<sub>6</sub>·H<sub>2</sub>O: C, 76.99; H, 8.84; N, 4.73. Found: C, 75.64; H, 8.99; N, 4.74.

### 3.6. References

1. Law, K. -Y. *Chem. Rev.* **1993**, *93*, 449.
2. Law, K. -Y. *J. Phys. Chem.* **1988**, *92*, 4226.
3. Emmelius, M.; Pawlowski, G.; Vollmann, H. W. *Angew. Chem. Int. Ed. Engl.* **1989**, *28*, 1445.
4. Tam, A. C. *Appl. Phys. Lett.* **1980**, *37*, 978.
5. Law, K.-Y. In *Handbook of Organic Conductive Molecules and Polymers*; Nalwa, H. S. Eds.; John Wiley and sons: Chichester, 1997, p 487.
6. Kasha, M.; El-Bayoumi, M.A.; Rhodes, W. J. *Chem. Phys.* **1961**, *58*, 916.
7. Hochstrasser, R. M.; Kasha, M. *Photochem. Photobiol.* **1964**, *3*, 317.
8. Czikkely, V.; Fosterling, H. D.; Kuhn, H. *Chem. Phys. Lett.* **1970**, *6*, 207.
9. Czikkely, V.; Fosterling, H. D.; Kuhn, H. *Chem. Phys. Lett.* **1970**, *6*, 11.
10. McRae, f. G.; Kasha, M. In *Physical Processes in Radiation Biology*, Augenstein, I.; Rosenberg, B.; Mason, S. F. Eds; Academic: New York, 1963, p 23.

11. Das, S.; Thanulingam, L. T.; Thomas, K. G.; Kamat, P. V.; George, M. V. *J. Phys. Chem.* **1993**, *97*, 13620.
12. Li, X. -H.; Zhang, B. -W.; Cao, Y. *Dyes Pigm.* **2000**, *45*, 209.
13. Arun, K. T.; Epe, B.; Ramaiah, D. *J. Phys. Chem. B* **2002**, *106*, 11622.
14. Law, K. -Y.; Chen, C. C. *J. Phys. Chem.* **1989**, *93*, 2533.
15. Chen, H.; Herkstroeter, W. G.; Perlstein, J.; Law, K. -Y.; Whitten, D. G. *J. Phys. Chem.* **1994**, *98*, 5138.
16. Liang, K.; Law, K. -Y.; Whitten, D. G. *J. Phys. Chem.* **1994**, *98*, 13379.
17. Chen, H.; Farahat, M. S.; Law, K. -Y.; Whitten, D. G. *J. Am. Chem. Soc.* **1996**, *118*, 2584.
18. Buncel, E.; McKerrow, A. J.; Kazmaier, P. M. *J. Chem. Soc. Chem. Commun.* **1992**, 1242.
19. McKerrow, A. J.; Buncel, E.; Kazmaier, P. M. *Can. J. Chem.* **1995**, *73*, 1605.
20. Tian, M.; Furuki, M.; Iwasa, I.; Sato, Y.; Pu, L. Y.; Tatsuura, S. *J. Phys. Chem. B* **2002**, *106*, 4370.
21. Dimitriev, O. P. *J. Mol. Liq.* **2005**, *120*, 131.
22. Dimitriev, O. P.; Dimitriyeva, A. P.; Tolmachev, A. I.; Kurdyukov, V. V. *J. Phys. Chem. B* **2005**, *109*, 4561.
23. Cano, M. L.; Cozens, F. L.; Esteves, M. A.; Márquez, F.; Gareia, H. *J. Org. Chem.* **1997**, *62*, 7121.
24. Kim, Y. -S.; Liang, K.; Law, K. -Y.; Whitten, D. G. *J. Phys. Chem.* **1994**, *98*, 984.
25. Hotchandani, S.; Das, S.; Thomas, K. G.; George, M. V.; Kamat, P. V. *Res. Chem. Intermed.* **1994**, *20*, 927.
26. Furuki, M.; Pu, L. S.; Sasaki, F.; Kobayashi, S.; Tani, T. *Appl. Phys. Lett.* **1998**, *72*, 2648. Tatsuura, S.; Wada, O.; Tian, M.; Furuki, M.; Sato, Y.; Iwasa, I.; Pu, L. S.; Kawashima, H. *Appl. Phys. Lett.* **2001**, *79*, 2517
27. Tatsuura, S.; Wada, O.; Tian, M.; Furuki, M.; Sato, Y.; Iwasa, I.; Pu, L. S.; Kawashima, H. *Appl. Phys. Lett.* **2001**, *79*, 2517.

28. Yagi, S.; Hyodo, Y.; Matsumoto, S.; Takahashi, N.; Kono, H.; Nakazumi, H. *J. Chem. Soc., Perkin Trans. I* **2000**, *4*, 599.
29. Hyodo, Y.; Nakazumi, H.; Yagi, S.; Nakai, K. *J. Chem. Soc., Perkin Trans. I* **2001**, 2823.
30. Yagi, S.; Murayama, S.; Hyodo, Y.; Fujie, Y.; Hirose, M.; Nakazumi, H. *J. Chem. Soc., Perkin Trans. I* **2002**, 1417.
31. Meier, H.; Dullweber, U. *Tetrahedron Lett.* **1996**, *37*, 1191.
32. Meier, H.; Dullweber, U. *J. Org. Chem.* **1997**, *62*, 4821.
33. Gerold, J.; Holzenkamp, U.; Meier, H. *Eur. J. Org. Chem.* **2001**, 2757.
34. Meier, H.; Petermann, R. *Helv. Chim. Acta* **2004**, *87*, 1109.
35. Petermann, R.; Tian, M.; Tatsuura, S.; Furuki, M. *Dyes Pigm.* **2003**, *57*, 43.
36. Kim, S.-H.; Kim, J.-H.; Cui, J.-Z.; Gal, Y.-S.; Jin, S.-H.; Koh, K. *Dyes Pigm.* **2002**, *55*, 1.
37. Eldo, J.; Arunkumar, E.; Ajayaghosh, A. *Tetrahedron Lett.* **2000**, *41*, 6241.

## Chapter 4

### 2,2'-Bipyridine Bridged Bispyrroles: New Ratiometric Fluorescence Probes for the Selective Sensing of Zn<sup>2+</sup>

---

#### 4.1. Abstract

Selective detection of ions is important in various fields of chemistry and biology. In this chapter, synthesis, characterization and cation binding studies of a few 2,2'-bipyridine linked bispyrroles **1a-d** are described. These molecules are found to be selective fluorescent sensors, for the detection of Zn<sup>2+</sup>. For example, while the absorption spectra of **1a-d** showed similar changes with a variety of cations, the emission spectral changes with Zn<sup>2+</sup> were significantly different from other cations. The emission of **1a-d** at 537 nm was significantly quenched by Cu<sup>2+</sup>, Ni<sup>2+</sup>, Hg<sup>2+</sup>, Co<sup>2+</sup>, and Mn<sup>2+</sup> whereas the titration of Zn<sup>2+</sup> resulted in a strong orange-red emission at 635 nm ( $\Delta E_{em} = 97$  nm) through an isoemissive point at 601 nm. Alkali and alkaline earth metal ions could not effect any noticeable change to the fluorescence. The Job plot and the ratiometric plot revealed a 1:1 complexation between the fluorophore and the metal ion. The Benesi-Hildebrand plot gave a binding constant of  $1.23 \times 10^5$  for Zn<sup>2+</sup>. Addition of Zn<sup>2+</sup> into the non-emissive **1a-Cu<sup>2+</sup>** resulted in the strong orange-red emission of **1a-Zn<sup>2+</sup>** complex thereby unambiguously proving the selectivity of **1a** to the sensing of Zn<sup>2+</sup>. Bispyrrole **1d** with a polyether side chain allowed the detection of Zn<sup>2+</sup> under aqueous physiological conditions. The maximum change in the fluorescence

*intensity was observed in the pH window of 6.8-7.4 which is suited for the detection of  $Zn^{2+}$  in biological system.*

#### **4.2. Introduction**

Zinc is the second most abundant transition metal ion in the human body, where it has multiple roles in both intra and extra cellular functions.<sup>1-3</sup> A large number of proteins and enzymes were identified to contain  $Zn^{2+}$ . Zinc is found to be associated with membrane lipids, DNA and RNA and plays important roles in the central nervous system (CNS). Zinc has been identified to be associated with severe neurological disorders such as Alzheimer's disease, lateral sclerosis, Parkinsons disease and Epilepsy.<sup>4</sup> Intense exposure to  $Zn^{2+}$  can be neurotoxic, killing cortical neurons after several minutes. The World Health Organization estimates that more than 40% of children in Africa and Asia have stunted growth associated with limited dietary zinc.<sup>5</sup> The extent to which zinc deficiency conditions persist today is difficult to estimate because of the lack of suitable biochemical markers for zinc ions. Besides growth, numerous body functions are affected, including immune, endocrine and gastro-enterological systems. Thus, the scope for the exploration of the diverse physiological roles of biological zinc demands sensitive and non-invasive technique for the real time local imaging of  $Zn^{2+}$  concentration. While the total concentration of the  $Zn^{2+}$  in a cell is relatively high, the concentration of the free zinc, which is not strongly bound to proteins, is extremely low and highly controlled. The estimation of the free zinc has been

proved to be difficult using classical methods. Since  $Zn^{2+}$  is silent to most of the analytical techniques, fluorescent techniques stand out as a method of choice.

Based on the ion sequestering pathways, fluorescent sensors are classified into three groups namely 'fluorogenic chelating agents', 'fluoroionophores' with separate fluorophore and ionophore linked with or without a spacer and 'fluorescent sensors' based on resonance energy transfer.<sup>6</sup> 'Fluoroionophores' with an appropriate combination of the fluorophore and ionophores are the most widely used strategy in probe design. Ionophores, specific for  $Zn^{2+}$  are limited to certain groups such as quinolines, bis(2-pyridylmethyl) amine ( or di-2-picoyl amine, DPA), linear and cyclic polyamines and some bioligands such as zinc-finger domains.

Quinolines and their derivatives are the traditional fluorogenic sensors for  $Zn^{2+}$  and many other metal ions.<sup>7</sup> A milestone development in the history of zinc sensors happened in 1987 when a sulphonamido derivative of quinoline, namely 6-methoxy-8-*p*-toluenesulphonamido-quinoline (**2**, TSQ), was used for the *in vitro* imaging of  $Zn^{2+}$  ions.<sup>8</sup> The fluorescence of the apo-ligand is too weak to be observed, while its  $Zn^{2+}$  complex emits strong fluorescence, with emission maximum at 495 nm. Compound **2** is being used as a pH independent, non-toxic fluorescent probe for the selective detection of  $Zn^{2+}$ . However, this has several limitations, the foremost being poor water solubility followed by the requirement for UV excitation, which may cause damage to the living cells. Water soluble derivatives of **2** were obtained by introducing carboxylic acid or ester group

instead of methoxy group (3, Zinquin).<sup>9,10</sup> Another attempt to improve the solubility of TSQ was to replace the methyl group on the benzene rings with a carboxylic acid group (4, TLF-Zn).<sup>11</sup> This probe was only sparingly soluble in water in neutral medium and was not widely adopted in bioassays (Chart 4.1).

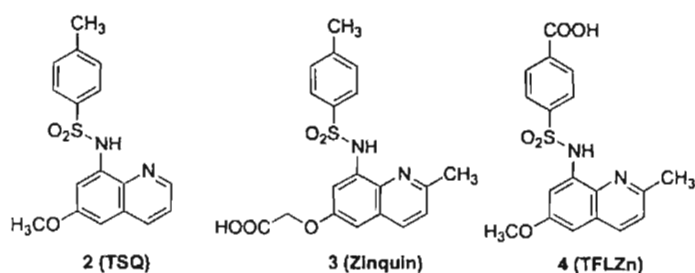


**Chart 4.1**

Ward *et al.* reported a series of zinquin homologues, several of them have higher fluorescent sensitivity and selectivity than TSQ.<sup>12,13</sup> Fluorescence of quinoline probes is independent of pH and the intensity of the emission increases 100 fold by addition of  $Zn^{2+}$  owing to metal coordination to the quinoline *N*-atom, which inhibits a quenching pathway. Despite their ability to image intracellular zinc, quinoline probes generate uncertainty in the measurement of free  $Zn^{2+}$  due to their ability to form mixed complexes with partially coordinated zinc in cells. Imperiali and coworkers have synthesized fluorescent ligands based on oxine for selective detection of zinc ions.<sup>14</sup>

Many fluorescent sensors utilize the principle of photoinduced electron transfer (PET) for the signaling of the binding process. Metal coordination to the

receptor unit makes it a less efficient electron donor to an attached fluorophore. Thus the native fluorescence of the fluorophore is restored. This signaling is highly selective for the analyte. Sensors operating according to this principle are known as CHEF (chelation-enhanced fluorescence) type sensors (Figure 4.1).

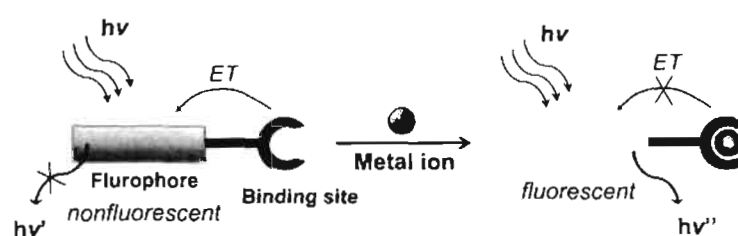


**Figure 4.1.** Schematic representation of CHEF-type fluorescent sensor for metal ions.

The amino nitrogen of di-2-phenylpicolylamine (DPA) ligand is a good electron donor in PET process. DPA based sensor **5** is a typical PET sensor for protons and post transition metal ions like zinc (Chart 4.2).<sup>15</sup> Upon binding of the metal ion, the quenching process is interrupted and the fluorescence quantum yield is increased. In order to shift the excitation wavelength to the visible region, fluorescein and its derivatives were used as fluorophores. Only the anionic form of the fluorescein emits strongly, which means that the pKa values are an important factor for the pH dependent performance. Attachment of electron withdrawing groups renders better performance in a much broader pH range. When the fluorophores are connected to DPA, the electron transfer from the DPA facilitates quenching of the fluorescence. This process is interrupted when the amino nitrogen coordinates  $Zn^{2+}$ . Newport Green DCF (**6**) and Newport Green DPX (**7**)

are DPA based sensors that shows fluorescence enhancement upon binding to zinc.<sup>16</sup>

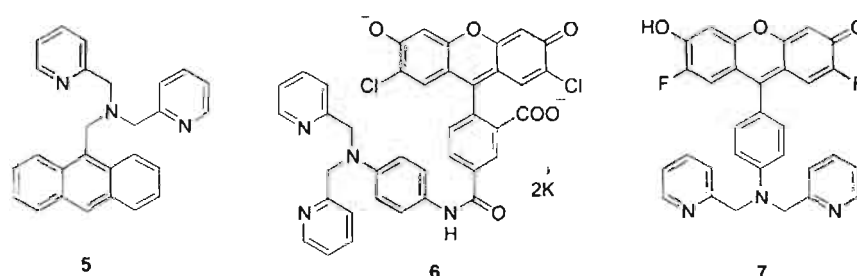


Chart 4.2

Lippard and coworkers have prepared a series of DPA based fluorescent sensors for Zn<sup>2+</sup> detection. The first generation probes **8a** (ZP1) and **8b** (ZP2) exhibit ~3-6 fold fluorescence enhancement upon addition of one equivalent of zinc.<sup>17,18</sup> They have high background fluorescence and can form dinuclear complexes owing to the presence of two DPA moieties on the xanthone ring. The second-generation sensors **9a-d** contains an aniline-derived DPA-derivatized ligand linked to an unsymmetrically functionalized fluorescein platform. They exhibit low background fluorescence than the first generation probes due to a lowering of the pK<sub>a</sub> values of the nitrogen atoms, responsible for PET quenching of the free ZP dyes.<sup>19-21</sup> Fluorescent sensors **10**, **11** and **12** (Zinspy family) that contains pyridyl-amine-thioether derivatized ligand are water soluble and generally display ~1.4-4.5-fold fluorescence enhancement upon Zn<sup>2+</sup> coordination.<sup>22</sup> The Zinspy sensors exhibit improved selectivity for Zn<sup>2+</sup> when compared to the di-(2-picolyl)amine-based Zinpyr family (Chart 4.3).

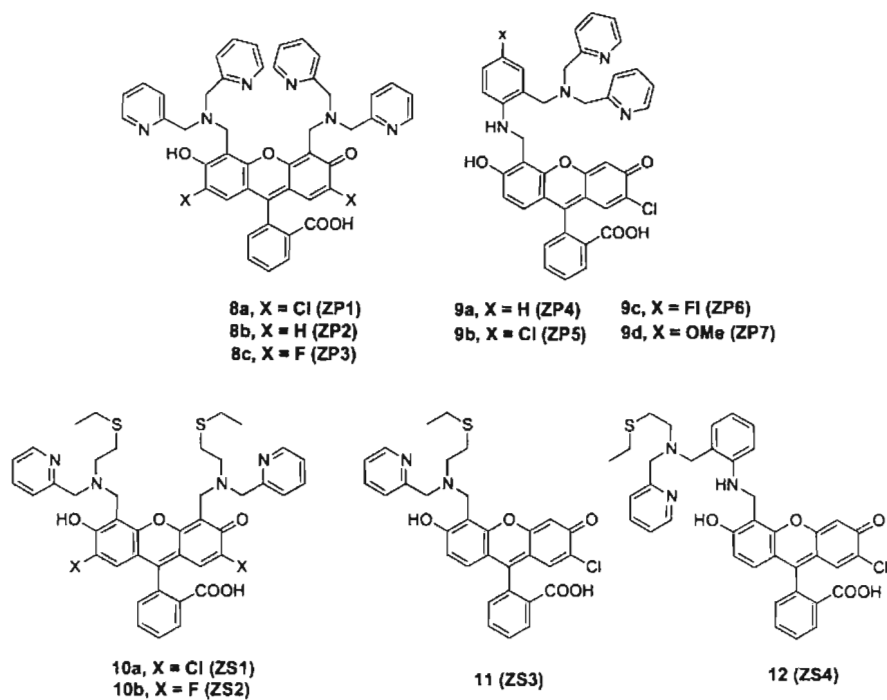


Chart 4.3

Another family of zinc sensors (ZnAF) was obtained by combining DPA with 5- or 6-aminofluorescein (Chart 4.4).<sup>23,24</sup> These compounds have an additional coordination from the amino nitrogen of the fluorescein derivative. The secondary amino nitrogen atom is a strong electron transfer quencher. As a result substantial fluorescence enhancement is observed upon binding of  $\text{Zn}^{2+}$ . The fluorescence of the  $\text{Zn}^{2+}$  complexes decreases below pH 7 in aqueous solutions. The difluoro derivatives **13b** and **14b** have lower  $\text{pK}_a$  values (4.9) and behave better under neutral or slightly acidic conditions.



almost 120-fold larger fluorescence intensity than that of the free ligand **18** ( $n = 2$ ) at pH 12.

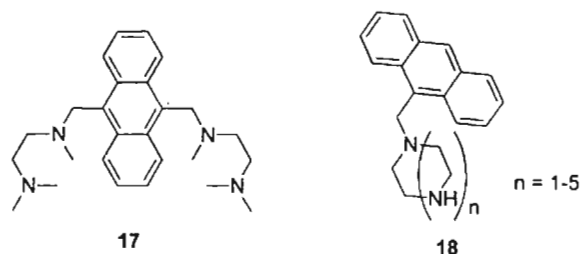


Chart 4.6

Kimura *et al.* have reported a dansyl group attached aminoethylcyclen (**19**) which upon coordination with  $Zn^{2+}$  results in a distorted square-pyramidal geometry.<sup>31,32</sup> The application of cyclen as a receptor for  $Zn^{2+}$  in a sensor design was extended to a pair of probes utilizing xanthene chromophores as the responding units. The sensors **20** and **21** have excitation and emission wavelengths  $\lambda_{ex}/\lambda_{em}$  as 495/515 and 505/525 respectively, which are ideal for intracellular studies. On saturation with  $Zn^{2+}$ , the intensity of **20** is increased by 14 fold and that of **21** by 26 fold. Although, these sensors have exceptional optical properties, they have low affinity and require intricate multistep synthesis with low overall yields.<sup>33</sup> Owing to steric hindrance, these are kinetically very slow in metal binding, making them unsuitable for real time imaging. A hybrid of fluorescein and rhodamine as fluorophore and pyridine appended cyclen as the receptor could give only moderate enhancement in fluorescence.<sup>34</sup> The methyl coumarin

derivative **22** has been used in  $Zn^{2+}$  imaging of live rat pituitary tumor cells.<sup>35</sup> The binding was very slow with a half-life longer than 60 min.

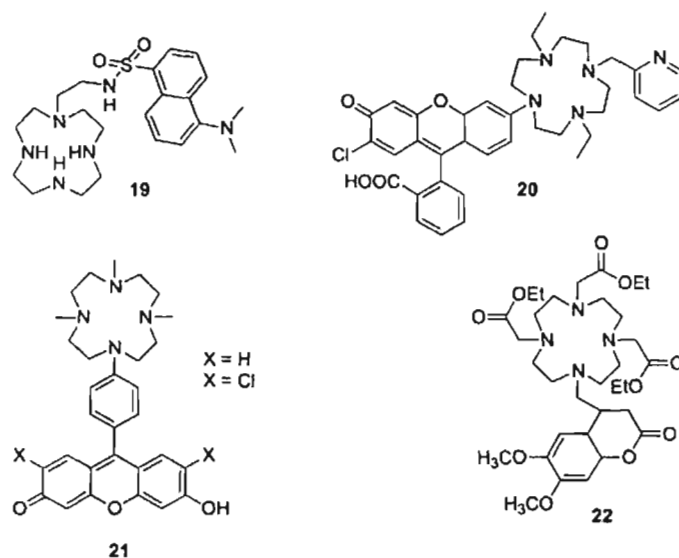


Chart 4.7

The current interest in  $Zn^{2+}$  specific sensors is based on ratiometric sensing. Ratiometric sensing behavior can be expected when the analyte binding changes the electronic properties of the chromophore resulting in absorption or emission at a different wavelength. Thus, a fluorescent ratiometric sensor responds upon binding to an analyte by a shift in its emission maximum which may or may not be concomitant with an increase in emission. This shift in the emission wavelengths should be enough to distinguish the  $\lambda_{max}$  of the co-existing  $Zn^{2+}$ -free and  $Zn^{2+}$ -bound species, allowing the determination of the ratio of emission maxima of the two species. Together with the known binding constant of the sensor, the unknown

zinc concentration can be determined.<sup>36</sup> A ratiometric signal is internally calibrated and neither the light source nor the photobleaching affect the signal ratio of the bound to unbound sensor.

Ratiometric probes **23** (ZnAF-R1) and **24** (ZnAF-R2) were reported for  $\text{Zn}^{2+}$ , which utilizes the internal charge transfer in the fluorophore containing the electron donating DPA, conjugated to electron withdrawing benzofuran derivative (Chart 4.8).<sup>37</sup> When these molecules form complexes with  $\text{Zn}^{2+}$ , the wavelengths of the excitation maxima were blue-shifted, while the emission maxima remained unchanged. Sensor **24** is more soluble and has a better fluorescence quantum yield than **23** in water making it useful for biological applications. Lim and Brückner have reported a coumarin derived sensor **25** for the ratiometric detection of zinc.<sup>38</sup>

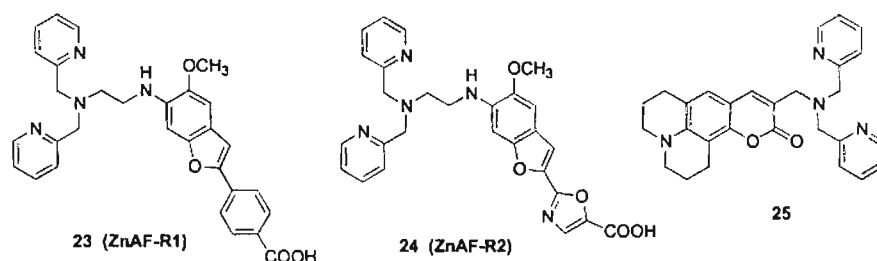
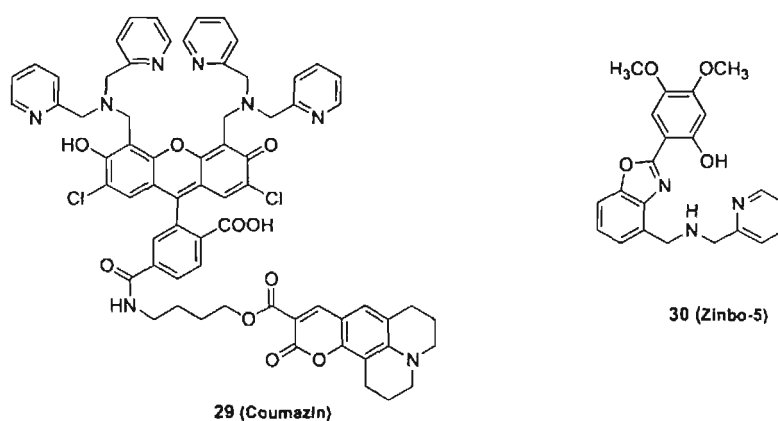


Chart 4.8

The group of Lippard accomplished the realization of a ratiometric sensor based on the  $\text{Zn}^{2+}$  induced shift of the phenoxynaphthoquinone-naphthoxyquinone tautomeric equilibrium.<sup>39</sup> Coordination of  $\text{Zn}^{2+}$  to **28** increases the overall intensity of the sensor and shifts the spectrum to one dominant peak indicative of the phenoxynaphthoquinone tautomer. The diacetate derivative of **28** has been used to



that of DPA, indicating that the phenolate oxygen and benzoxazole nitrogen are likely chelating the metal as the third and fourth ligands. The utility of **30** in two photon excitation fluorescent (TPE) microscopy of mammalian cells is also demonstrated.



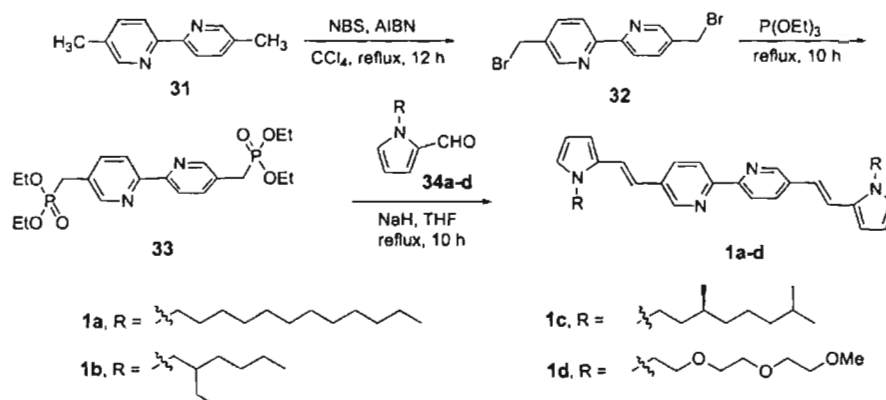
**Chart 4.9**

Thus, a survey of the current literature reveals a variety of  $\text{Zn}^{2+}$  sensors, most of which involve multistep complex synthetic steps. The present work describes the synthesis and metal ion binding properties of a few fluorescent bispyrroles having 2,2'-bipyridine as the cation binding unit. The synthesis of these molecules are relatively simple, they are highly fluorescent and are amenable for further functional group modifications.

### 4.3. Results and Discussion

#### 4.3.1. Synthesis

The bispyrroles **1a-d** were prepared through a 3-step reaction as shown in Scheme 4.2. Bromination of 5,5'-dimethyl-2,2'-bipyridine was carried out with *N*-bromosuccinimide. The bisbromomethyl derivative **32** was converted to the corresponding bisphosphonate ester by Michaelis-Arbuzov reaction in 70-80% yield. The Wittig-Horner-Emmons olefination reaction of the bisphosphonate ester **33** with *N*-alkylpyrrole-2-carboxaldehydes **34a-d** provided the bispyrroles **1a-d**. The all *trans* configuration of the bispyrroles were confirmed from the coupling constants ( $J = 16-17$  Hz) obtained from their  $^1\text{H}$  NMR spectra.



Scheme 4.2

#### 4.3.2. Optical Properties

The absorption and emission spectra of **1a-d**, recorded in toluene, dichloromethane and acetonitrile showed intense absorption in the range 370-450

nm due to  $\pi$ - $\pi^*$  transition. In these solvents, these molecules exhibited broad absorption without noticeable difference in spectral shape from each other. The absorption maxima showed minor shift with polarity of the solvent. For example, in toluene, **1a** showed absorption maximum at 412 nm. Changing the solvent from toluene to acetonitrile resulted in a mere blue shift of 5 nm with absorption maximum around 407 nm (Figure 4.2a).

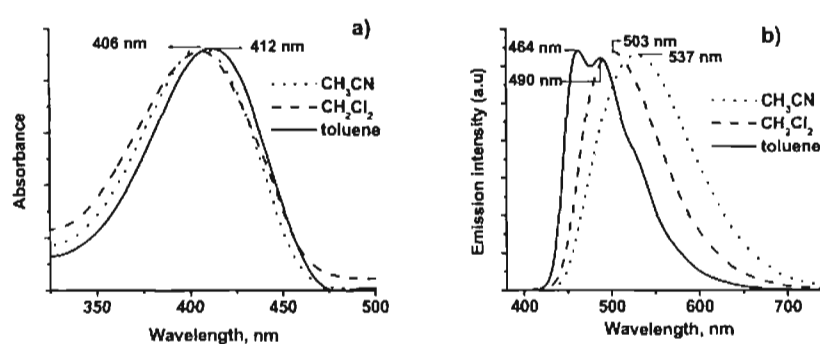


**Figure 4.2.** (a) Normalized absorption and (b) emission spectra of **1a** in different solvents.

The fluorescence emission spectra of the bispyrroles **1a-d** showed intense emission with high fluorescence quantum yields. As the solvent is changed from toluene to acetonitrile, the emission became broad with a red-shift. For example, in toluene, **1a** showed a structured emission with two maxima at 463 nm and 490 nm. In dichloromethane the absorption is red shifted and a new maximum at 503 nm is observed. When the solvent is changed to acetonitrile, the emission is red-shifted to 537 nm (Figure 4.2b). The fluorescence quantum yields ( $\Phi_f$ ) of the bispyrroles in toluene, dichloromethane and in acetonitrile were determined using

quinine sulfate as the standard. The  $\Phi_f$  values in toluene are found to be higher than that in dichloromethane and acetonitrile. All the bispyrroles under study showed quantum yields above 0.5 in toluene. The fluorescence lifetime measurements in toluene showed monoexponential decay in all cases. The optical characteristics of bispyrroles **1a-d** are listed in Table 4.1.

**Table 4.1.** Optical properties of bispyrroles **1a-d**.

Bispyrrole	Toluene			Acetonitrile		
	$\lambda_{\max}(\text{nm})^a$	$\lambda_{\max}(\text{nm})^b$	$\Phi_f$	$\lambda_{\max}(\text{nm})^a$	$\lambda_{\max}(\text{nm})^b$	$\Phi_f$
<b>1a</b>	412	463,490	0.68	407	537	0.48
<b>1b</b>	412	463,490	0.71	407	537	0.47
<b>1c</b>	411	463,490	0.67	407	537	0.47
<b>1d</b>	410	463,489	0.61	407	535	0.45

<sup>a</sup> absorption, <sup>b</sup> emission

#### 4.3.3. Cation Binding Properties of **1a-d**

Photophysical properties of the bispyrrole **1a-d** are highly sensitive to the presence of different transition metal ions. The responses of **1a-d** for a series of metal ions were studied in acetonitrile. The absorption spectral changes for the binding of different metal ions followed a similar pattern. Alkali and alkaline earth metal ions were not able to produce any noticeable changes in the optical properties of **1a-d** except for  $\text{Mg}^{2+}$ . Figure 4.3 shows the absorption and the emission spectra of **1a** in acetonitrile upon addition of  $\text{Ca}^{2+}$  ions.

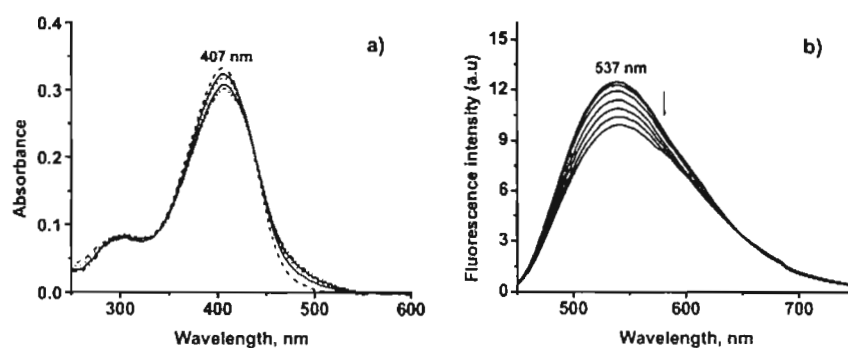


**Figure 4.3.** Changes in (a) the absorption spectrum and (b) the emission spectrum of **1a** ( $6 \mu\text{M}$  in acetonitrile) upon addition of  $\text{Ca}(\text{ClO}_4)_2$ ; ( $[\text{Ca}^{2+}] = 0\text{-}7 \mu\text{M}$ ).

Figure 4.4 shows the response of **1a** towards  $\text{Mg}^{2+}$  ions. Upon addition of  $\text{Mg}^{2+}$ , the absorption maximum at 405 nm was red-shifted to 422 nm and the color of the solution changed to pale yellow. Fluorescence maximum was shifted to 601 nm through an isoemissive point at 578 nm.

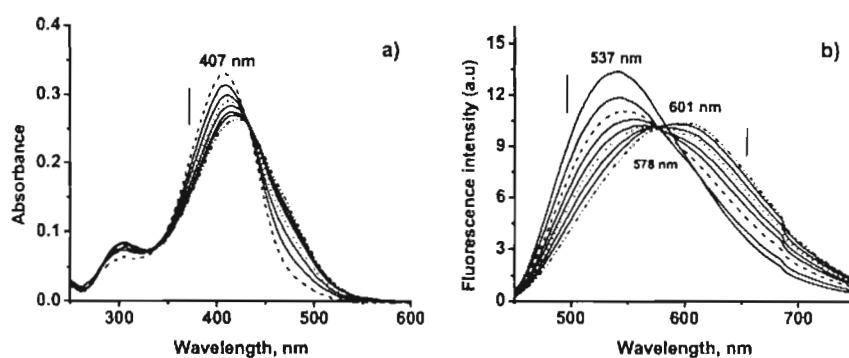


**Figure 4.4.** Changes in (a) the absorption spectrum and (b) the emission spectrum of **1a** ( $6 \mu\text{M}$  in acetonitrile) upon addition of  $\text{Mg}(\text{ClO}_4)_2$ ; ( $[\text{Mg}^{2+}] = 0\text{-}7 \mu\text{M}$ ).

Addition of divalent metal ions of the first row transition series such as  $\text{Cu}^{2+}$ ,  $\text{Ni}^{2+}$ ,  $\text{Hg}^{2+}$ ,  $\text{Co}^{2+}$ ,  $\text{Mn}^{2+}$ , and  $\text{Zn}^{2+}$  showed significant decrease in the absorption band around 407 nm with the concomitant formation of a new red-

shifted absorption band through two isosbestic points at 340 and 457 nm (Figure 4.5). Since all these cations showed changes in the absorption spectrum, it was not possible to distinguish a specific cation by change in the UV-vis spectral properties. Therefore, we focused the studies on the fluorescence properties of the probes with these cations.

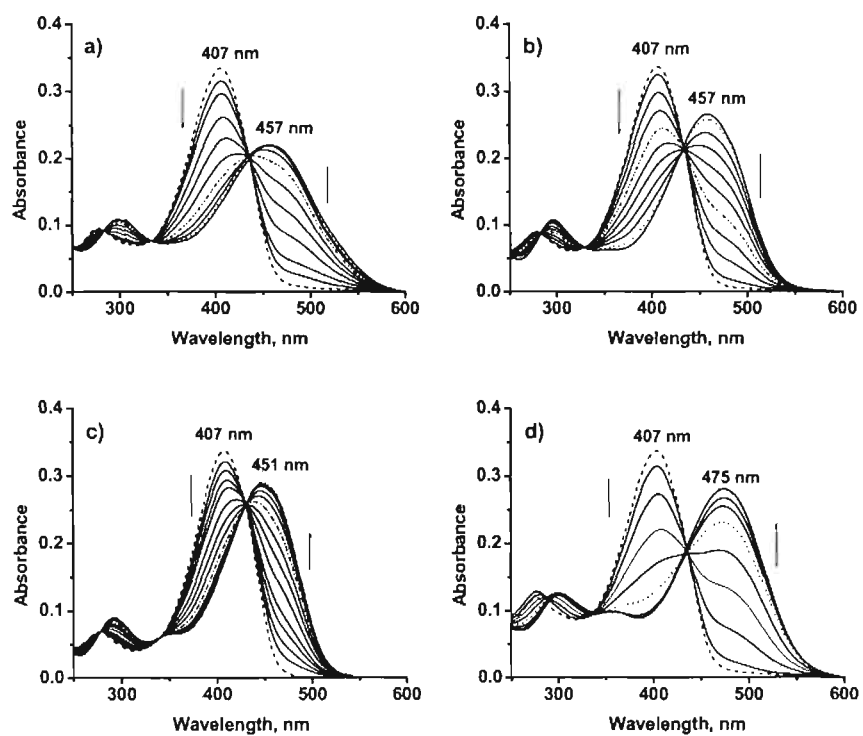


**Figure 4.5.** Changes in the absorption spectrum of **1a** (6 μM in acetonitrile) upon addition of (a) Co<sup>2+</sup>, (b) Ni<sup>2+</sup> (c) Mn<sup>2+</sup> and (d) Hg<sup>2+</sup> ([M<sup>2+</sup>] in μM).

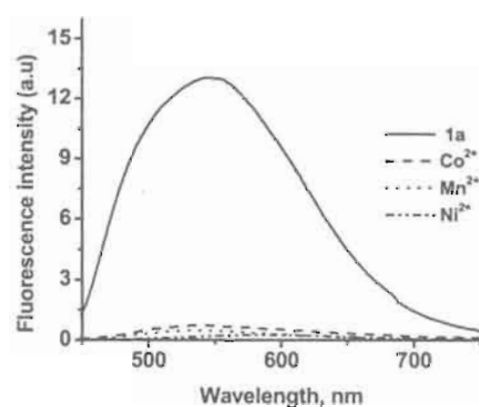


**Figure 4.6.** Emission spectra of **1a** ( $6 \mu\text{M}$  in acetonitrile) with different divalent transition metal ions. Solid line indicates **1a** in the absence of metal ions.

Interestingly, the emission of **1a-d** at 537 nm was significantly quenched by  $\text{Cu}^{2+}$ ,  $\text{Ni}^{2+}$ ,  $\text{Hg}^{2+}$ ,  $\text{Co}^{2+}$ , and  $\text{Mn}^{2+}$  except for  $\text{Zn}^{2+}$ . The fluorescence response of **1a** towards  $\text{Mn}^{2+}$ ,  $\text{Co}^{2+}$ ,  $\text{Ni}^{2+}$ , and  $\text{Hg}^{2+}$  are shown in Figure 4.6. The titration of  $\text{Zn}^{2+}$  resulted in a strong orange-red emission at 635 nm ( $\Delta E_{em} = 97 \text{ nm}$ ) through an isoemissive point at 601 nm (Figure 4.7).

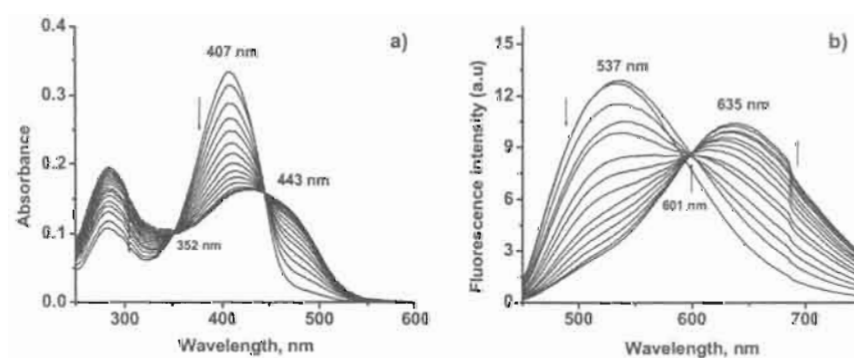


**Figure 4.7.** Changes in (a) the absorption spectrum and (b) the emission spectrum of **1a** ( $6 \mu\text{M}$  in acetonitrile) upon addition of  $\text{Zn}(\text{ClO}_4)_2$ ; ( $[\text{Zn}^{2+}] = 0-6 \mu\text{M}$ ).

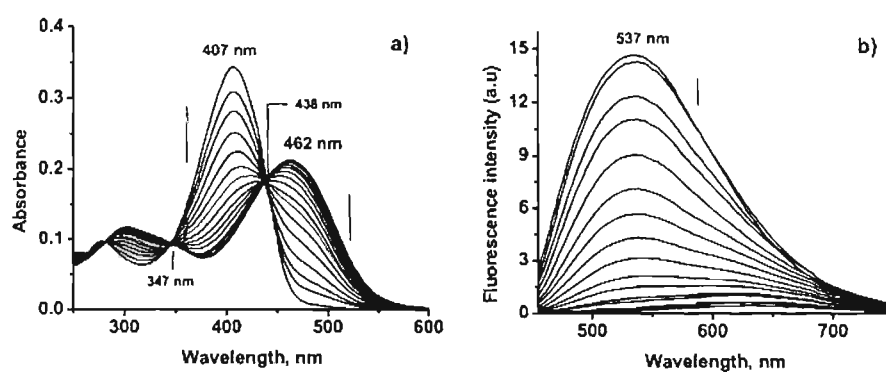


**Figure 4.8.** Changes in (a) the absorption spectrum and (b) the emission spectrum of **1a** ( $6\mu\text{M}$  in acetonitrile) upon addition of  $\text{Cu}(\text{ClO}_4)_2$ ; ( $[\text{Cu}^{2+}] = 0\text{-}6\mu\text{M}$ ).

Figure 4.8 shows the response of **1a** towards  $\text{Cu}^{2+}$ . In all these cases, except  $\text{Zn}^{2+}$ , other cations significantly quenched the emission of the probe. Therefore, **1a** is useful as a fluorogenic probe for the specific detection of  $\text{Zn}^{2+}$ . Besides transition metal ions, inner transition metal ions such as  $\text{Ce}^{3+}$ ,  $\text{Pr}^{3+}$ ,  $\text{Pm}^{3+}$ ,  $\text{Nd}^{3+}$  and  $\text{Eu}^{3+}$  are also found to influence the optical properties of **1a-d**. Partial quenching of the fluorescence is observed for most of the inner transition elements. A representative case of  $\text{Pr}^{3+}$  is shown in Figure 4.9.

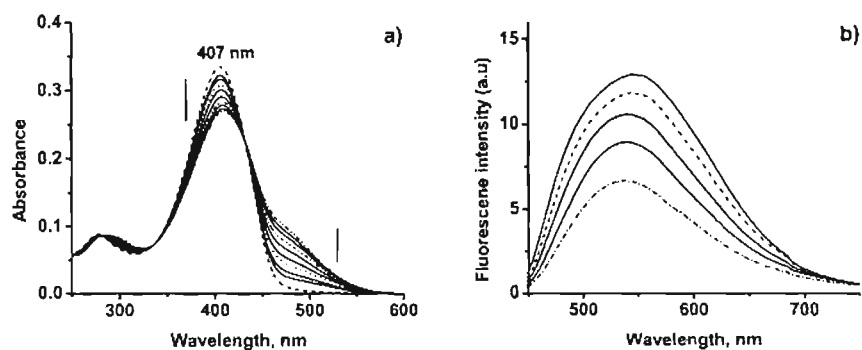


**Figure 4.9.** Changes in the (a) absorption spectrum and (b) emission spectrum of **1a** ( $6\mu\text{M}$  in acetonitrile) upon addition of  $\text{Pr}^{3+}$  ions; ( $[\text{Pr}^{3+}] = 0\text{-}6\mu\text{M}$ ).

In order to have an understanding on the mode of binding of the bispyrroles to the metal ions, binding of  $\text{Cu}^{2+}$  and  $\text{Zn}^{2+}$  were studied in detail. The Job plot and Benesi-Hildebrand plots of **1a** upon addition of  $\text{Zn}^{2+}$  and  $\text{Cu}^{2+}$  are shown in Figure 4.10 and 4.11, respectively.

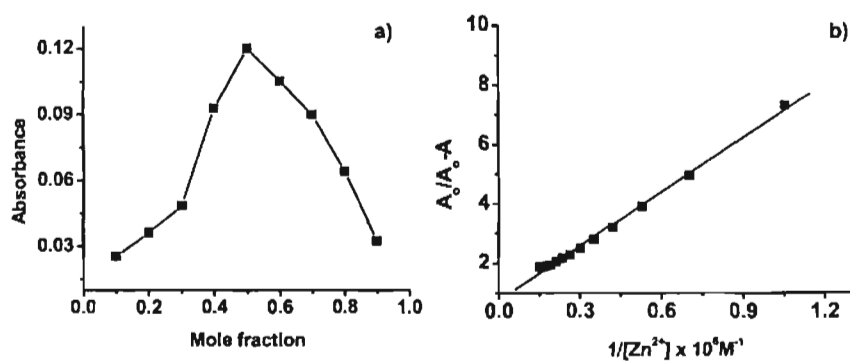


Figure 4.10. (a) Job plot and b) Benesi-Hildebrand plots obtained for the titration of **1a** with  $\text{Zn}^{2+}$ .

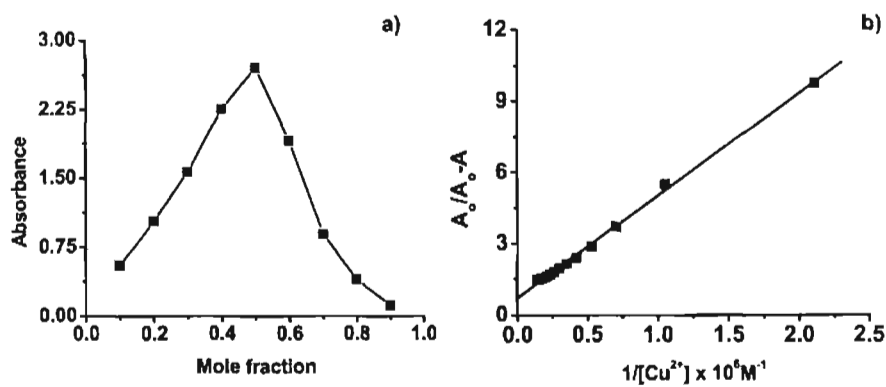
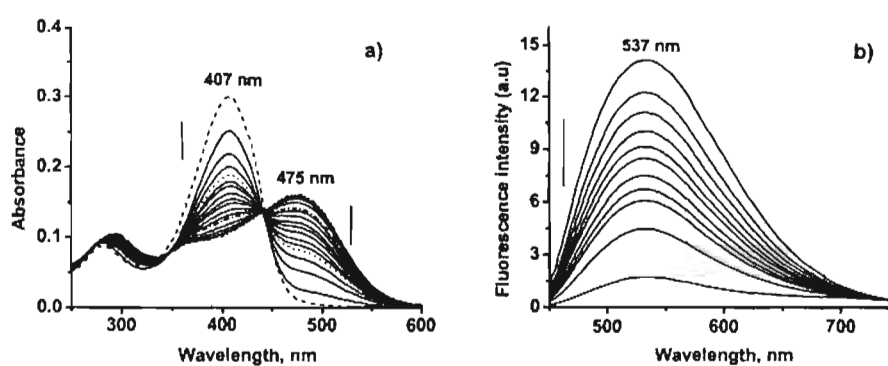


Figure 4.11. (a) Job plot and b) Benesi-Hildebrand plot obtained for the titration of **1a** with  $\text{Cu}^{2+}$ .

The Job plot and the Benesi-Hildebrand plots revealed a 1:1 complexation between the fluorophore and the metal ion. The Benesi-Hildebrand plot gave a

binding constant of  $1.23 \times 10^5$  for  $\text{Zn}^{2+}$  in acetonitrile. The binding constants obtained were comparable to the reported values for zinc-bipyridine systems.

Bispyrroles **1a-d** upon titration with trifluoroacetic acid showed similar changes in the absorption and emission spectra as in the case of cation binding. A new peak at 475 nm was observed in the absorption spectrum while the fluorescence spectrum showed a quenching of the original fluorescence as shown in the case of **1a** (Figure 4.12).



**Figure 4.12.** Changes in (a) the absorption spectrum and (b) the emission spectrum of **1a** ( $6 \mu\text{M}$  in acetonitrile) upon addition of trifluoroacetic acid.

Ion responsive studies were carried out in HEPES buffer (50 mM HEPES, 100 mM NaCl) at varying pH of 6.4-7.4. Upon changing the solvent to water, the emission maximum of the bispyrrole was shifted to 600 nm and the  $\text{Zn}^{2+}$ -bound species emitted at 623 nm (Figure 4.13).

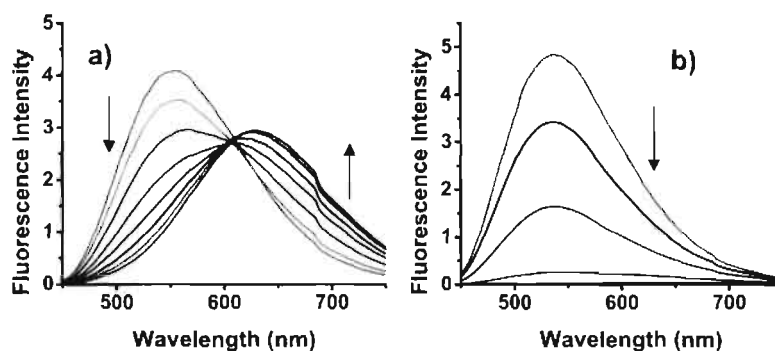


**Figure 4.13.** Changes in the emission spectrum of **1d** (6 μM in acetonitrile-water, 9:1 v/v) upon addition of a) Zn(ClO<sub>4</sub>)<sub>2</sub> and b) Cu(ClO<sub>4</sub>)<sub>2</sub>.

#### 4.3.4. Cation Binding Properties of **1d**: A Selective Sensor for Zn<sup>2+</sup> under Aqueous Conditions

The bispyrrole **1d** with oxyethylene side chains has better solubility in acetonitrile and aqueous acetonitrile. Figure 4.14 shows the changes in the absorption and the emission spectra of **1d** in 8:2 (v/v) water-acetonitrile mixture upon addition of Zn(ClO<sub>4</sub>)<sub>2</sub> solution.

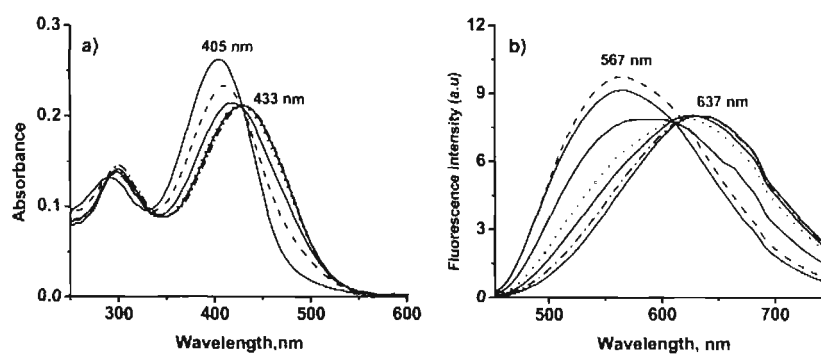


**Figure 4.14.** Changes in the (a) absorption and (b) emission spectra of **1d** (6 μM) in 8:2 (v/v) water-acetonitrile mixture upon addition of Zn(ClO<sub>4</sub>)<sub>2</sub> (0-6 μM).

Addition of  $\text{Zn}(\text{ClO}_4)_2$  induced a red-shift of the absorption maximum (403 nm) to 450 nm through an isosbestic point at 430 nm. The Job plot and the Benesi-Hildebrand plot for the binding of  $\text{Zn}^{2+}$  to **1d** are shown in Figure 4.15. The individual emission response of **1d** against different transition metal ions revealed a remarkable selectivity of  $\text{Zn}^{2+}$  binding (Figure 4.16).

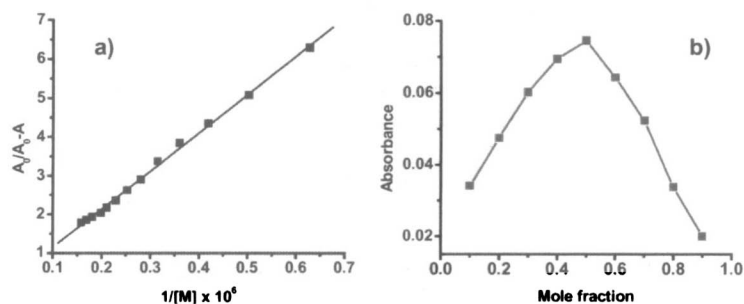


**Figure 4.15.** (a) Benesi-Hildebrand and (b) Job plot showing the 1:1 binding of **1d** to  $\text{Zn}^{2+}$  ions (0-6  $\mu\text{M}$ ) in acetonitrile-water (1:1).

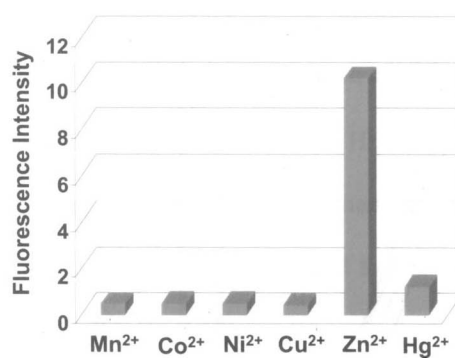


**Figure 4.16.** Plots of fluorescence intensity of **1d** monitored at 650 nm with different metal ions in acetonitrile-water (1:1).

The plot of fluorescence intensity at 530 nm and at 650 nm against the  $Zn^{2+}$  concentration shows the change in fluorescence intensity upon  $Zn^{2+}$  complexation, making the probe a ratiometric sensor (Figure 4.17). An important requirement of a  $Zn^{2+}$  probe for any practical application is the ability for visual sensing by naked eye, which is useful for imaging under physiological conditions. Bispyrrole **1d** satisfies the above requirement as evident from the changes in the emission color with different biologically significant cations as shown in Figure 4.18. Although alkali and alkaline earth metal ions could not considerably change the emission of **1d**,  $Cu^{2+}$  significantly quenched the fluorescence. Only in the case of  $Zn^{2+}$ , a red emission was obtained. Promisingly, in a mixture of alkali, alkaline earth and transition metal cations,  $Zn^{2+}$  showed the red emission with **1d**, revealing the high selectivity of the probe, which is useful for biological imaging of  $Zn^{2+}$ .

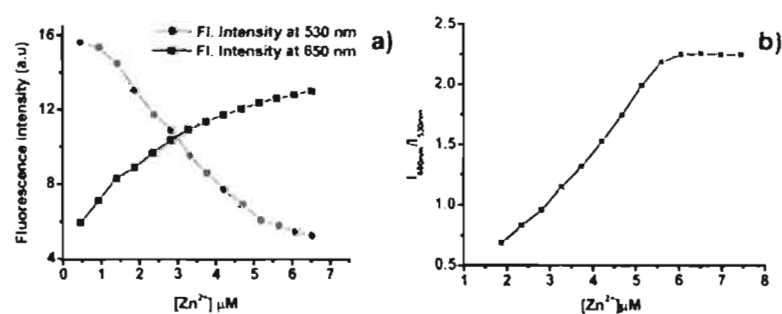


**Figure 4.17.** Spectrofluorimetric titration curves monitored at 530 nm and 650 nm. Fluorescence ratiometric plot constructed from the intensities 650 nm for **1d** (6  $\mu M$ ) upon addition of  $Zn^{2+}$  (0 – 8  $\mu M$ ).

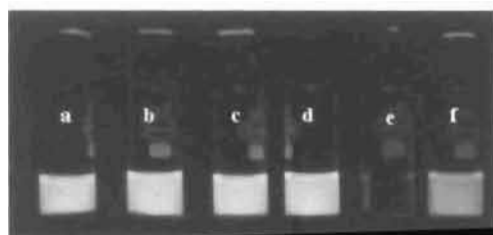


**Figure 4.18.** Emission color changes of **1d** in 20% (v/v) water-acetonitrile mixture with different metal ions. (a) **1d** alone (b) **1d** +  $\text{Na}^+$  (c) **1d** +  $\text{Ca}^{2+}$  (d) **1d** +  $\text{Mg}^{2+}$  (e) **1d** +  $\text{Cu}^{2+}$  and (f) **1d** +  $\text{Zn}^{2+}$ .

The most important criterion for a selective cation probe is the ability to detect a specific cation in the vicinity of other competing ions. This is particularly relevant in the selective detection of a cation in biological systems. In order to clarify this point we have added  $\text{Zn}^{2+}$  into a solution of **1d** containing  $\text{Cu}^{2+}$  in which the original fluorescence of **1d** was completely quenched. Surprisingly, upon addition of  $\text{Zn}^{2+}$ , the strong orange-red emission corresponding to the  $\text{Zn}^{2+}$  complex appeared (Figure 4.19) thereby unambiguously proving the ability of **1d** to compete with other metal ions in the selective sensing of  $\text{Zn}^{2+}$ . Addition of EDTA to this solution regenerates the original fluorescence of **1d** showing the reversible nature of the binding.

For biological applications, it is necessary to establish that metal ion binding occurs under aqueous biological pH. For this purpose detailed studies of the effect of pH (HEPES buffer) on the emission properties were carried out. The response of **1d** towards metal ions in HEPES buffer is shown in Figure 4.20. The fluorescence of **1d** and **1d**- $\text{Zn}^{2+}$  complex was rather insensitive to changes in the

pH of the solution in the range of 6.4 - 7.4, except for the intensity. In acidic pH range ( $< 6.8$ ), the fluorescence intensity of the bispyrrole and the  $Zn^{2+}$ -complex were drastically low. On increasing the pH to 7, fluorescence intensity of the two species also increased and maintained a constant value up to pH 7.4, beyond which it showed a decrease. As evident from Figure 4.21b and 4.22d, within the biological pH window of 6.8-7.4, **1d** did not show considerable emission intensity variation though fluorescence decrease is observed above pH 7.2 and below pH 6.8.

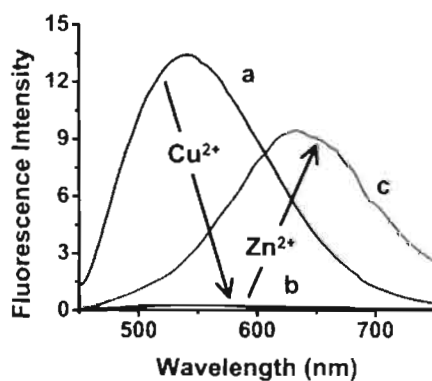


**Figure 4.19.** Changes in the emission spectrum of (a) **1d** alone ( $6 \mu\text{M}$ ) (b) **1d** +  $\text{Cu}^{2+}$  and (c) **1d** +  $\text{Cu}^{2+}$  +  $\text{Zn}^{2+}$  in acetonitrile-water (1:1).

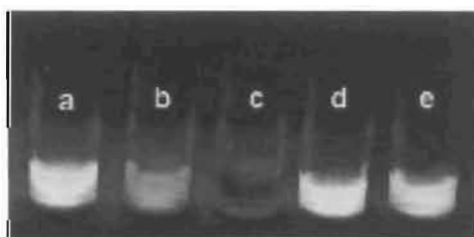


**Figure 4.20.** Emission color changes of **1d** in HEPES buffer with different metal ions. (a) **1d** alone (b) **1d** +  $\text{Zn}^{2+}$  (c) **1d** +  $\text{Cu}^{2+}$  (d) **1d** +  $\text{Na}^+$  and  $\text{K}^+$  and (e) **1d** +  $\text{Ca}^{2+}$  +  $\text{Mg}^{2+}$ .

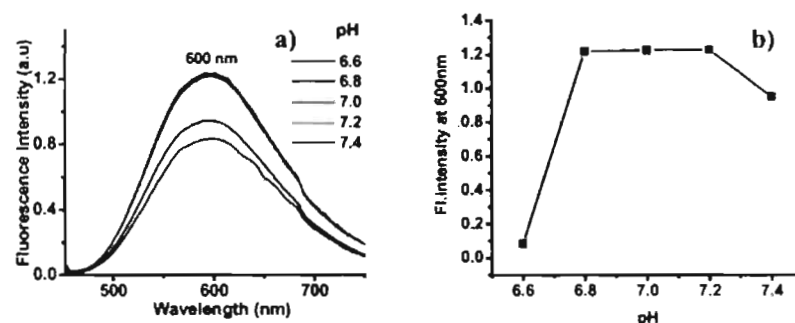


**Figure 4.21.** a) Changes in the emission spectrum of **1d**. (b) Emission intensity variation of **1d** at 600 nm against different pH (HEPES buffer) in water.

From a mechanistic viewpoint, the diamagnetic  $\text{Zn}^{2+}$  with  $d^{10}$  electronic configuration having flexible coordination geometry is advantageous for the specific binding. Molecular modeling of **1d** revealed a torsional angle of  $35.8^\circ$  in the unbound state. Upon binding of  $\text{Zn}^{2+}$ , the absorption and emission of **1d** are red-shifted due to a decrease in the twist angle between the two pyridyl moieties, leading to a near planar conformation of the **1d**- $\text{Zn}^{2+}$  complex. Being a  $d^{10}$  metal ion,  $\text{Zn}^{2+}$  does not have non-radiative decay routes, making the complex an emissive species. In contrast, binding of the paramagnetic  $\text{Cu}^{2+}$  quenches the emission though the absorption spectra are red-shifted to the same extent as that of  $\text{Zn}^{2+}$  complexes. Changes in the optical properties of **1a-d** with different metal ions can be rationalized as shown in Figure 4.23. Upon binding of  $\text{Zn}^{2+}$ , the absorption and emission of **1a-d** are red-shifted, changing the initial fluorescence “ON” state A to the “ON” state B. In contrast, binding of the paramagnetic  $\text{Cu}^{2+}$  quenches the emission to form the fluorescence “OFF” state. Thus the

fluorescence technique becomes an efficient visual tool in distinguishing  $Zn^{2+}$  from other competing cations at an emission wavelength that is compatible for biological samples.

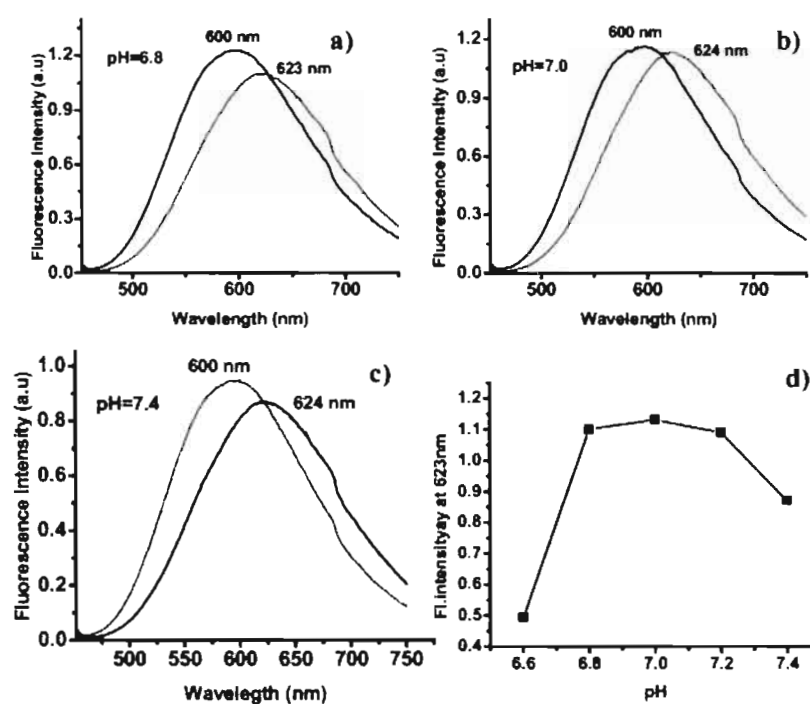


**Figure 4.22.** Changes in the emission spectrum of **1d** ( $6 \mu\text{M}$ ) upon addition of  $Zn^{2+}$  ( $6 \mu\text{M}$ ) at physiological pH range (HEPES buffer) in water: (a) at pH = 6.8; (b) pH = 7.0; (c) pH = 7.4 and (d) emission intensity variation of **1d** after addition of  $Zn^{2+}$ , monitored at 623nm.

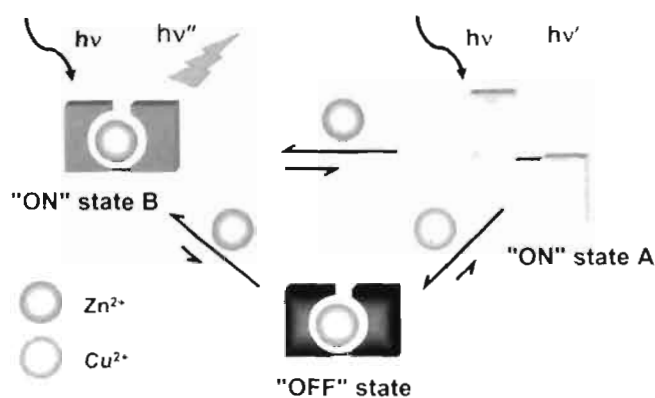


Figure 4.23. Schematic representation of the binding and the signaling events.

#### 4.4. Conclusion

2,2'-Bipyridine bridged bispyrroles are found to be useful probes for the detection of  $Zn^{2+}$ . Even though the bipyridinyl moiety binds to a variety of transition metal cations and induces changes to the absorption spectrum, fluorescence properties showed selective response with  $Zn^{2+}$ . In all other cases except for  $Zn^{2+}$  the fluorescence is quenched. Bispyrrole **1d** with a polyether side chain allowed the detection of  $Zn^{2+}$  in aqueous conditions. Since the fluorescence intensity of **1d** is strong under physiological pH, the molecule is a reliable probe for the detection  $Zn^{2+}$  ions.

#### 4.5. Experimental

##### 4.5.1. General

All solvents were purified and dried by standard methods prior to use. Melting points were determined with a Mel-Temp-II melting point apparatus.

NMR spectra were recorded on a 300 MHz Bruker Avance DPX spectrometer. FT-IR spectra were obtained on a Nicolet Impact 400D infrared spectrophotometer. High-resolution mass spectra were recorded on a JEOL JM 600 Mass Spectrometer and MALDI-TOF mass spectra were obtained on Perspective Biosystems Voyager DE-Pro MALDI-TOF Spectrometer. Electronic absorption spectra were recorded on a Shimadzu UV-3101 PC NIR scanning spectrophotometer and the emission spectra were measured on a SPEX-Fluorolog F112X spectrofluorimeter. Fluorescence quantum yields were determined in spectroscopic grade CH<sub>3</sub>CN using optically matching solutions of Quinine Sulfate ( $\Phi_f = 0.546$  in 0.1N H<sub>2</sub>SO<sub>4</sub>) as standard at an excitation wavelength of 360 nm and the quantum yield is calculated using equation 1.

$$\Phi_f = \Phi_r(A_r F_s / A_s F_r) (\eta_s^2 / \eta_r^2) \quad (1)$$

where,  $A_s$  and  $A_r$  are the absorbance of the sample and reference solutions, respectively at the same excitation wavelength,  $F_s$  and  $F_r$  are the corresponding relative integrated fluorescence intensities and  $\eta$  is the refractive index of the solvent.

#### 4.5.1.1. General procedure for metal ion binding studies

Metal perchlorate solutions were prepared in spectroscopic grade solvents. Bispyrroles were dissolved in acetonitrile or acetonitrile – water mixed solvent system. Metal ion titrations were carried out by adding aliquots (1-5  $\mu$ L) of the metal ion solution to the bispyrrole solution (3 mL) in a quartz cuvette using a

microlitre syringe. After addition of the metal salt solution to the cuvette, the solution was shaken well and kept for 1 min. before recording the absorption and emission of the cation complexed bispyrrole.

For making the Job plot, aliquots of equimolar solutions of the probe (P) and the metal perchlorate (X) were mixed in such a way that total concentration of (P+X) remains constant. The absorbance of each solution is then measured at a suitable wavelength and a graph is made showing the corrected absorbance vs molefraction of X or P. Maximum absorbance is reached at the composition corresponding to the stoichiometry of the predominant complex.

## 4.5.2. Synthesis

### 4.5.2.1. Preparation of 5,5'-bis(bromomethyl)-2,2'-bipyridine (32)

To a solution of 5,5'-dimethyl-2,2'-bipyridine (10 mmol) in 50 mL of dry carbontetrachloride was added *N*-bromosuccinimide (20.5 mmol) and AIBN. The reaction mixture was refluxed for 18 h, cooled, filtered and the solvents were removed under reduced pressure to give the crude product which was further purified by recrystallization from CCl<sub>4</sub>.

Yield 85%; mp. 188 °C; <sup>1</sup>H NMR (CDCl<sub>3</sub>, 300 MHz) δ 8.61 (m, 2H, aromatic), 8.34 (m, 2H, aromatic), 7.79 (m, 2H, aromatic), 4.53 (s, 4H, CH<sub>2</sub>Br); <sup>13</sup>C NMR (CDCl<sub>3</sub>, 75.4 MHz) δ 155.19, 149.27, 137.70, 133.28, 121.25, 29.43.

### 4.5.2.2. Preparation of 5,5'-bis-(diethylphosphonomethyl)-2,2'-bipyridine (33)

Compound 33 was prepared by the reaction of the corresponding bis bromomethyl derivative (32) (2 mmol) with 3 mL of triethyl phosphite at 80 °C

for 10 h followed by the removal of the unreacted triethyl phosphite under reduced pressure. The product was used as such for further reaction.

Yield 94%;  $^1\text{H}$  NMR ( $\text{CDCl}_3$ , 300 MHz)  $\delta$  8.30 (m, 2H, aromatic), 8.01 (m, 2H, aromatic), 7.34 (m, 2H, aromatic), 4.14 (m, 8H,  $\text{OCH}_2$ ), 3.21 (s, 4H,  $\text{CH}_2\text{P}$ ), 1.12 (m, 12H,  $\text{CH}_3$ ).  $^{13}\text{C}$  NMR ( $\text{CDCl}_3$ , 75.4 MHz)  $\delta$  155.21, 150.31, 138.63, 127.64, 119.89, 40.05, 64.12, 15.98.

#### 4.5.2.3. Preparation of Bispyrroles 1a-d

Bispyrroles **1a-d** were synthesized according to standard procedure given in Chapter 2.

##### **(*E, E*)-5,5'-Bis[(1-dodecylpyrrol-2-yl) vinyl]-2,2'-bipyridine (1a)**

Yield 25%; mp. 92-93 °C; FT-IR (KBr)  $\nu_{\text{max}}$  2912, 2846, 1699, 1626, 1460, 1288, 1082, 1016, 850, 704  $\text{cm}^{-1}$ ;  $^1\text{H}$  NMR ( $\text{CDCl}_3$ , 300 MHz)  $\delta$  8.70 (m, 2H, aromatic), 8.30 (d, 2H, aromatic), 7.85 (m, 2H, aromatic), 7.07 (d, 2H, vinylic,  $J = 16.08$  Hz), 6.87 (d, 2H, vinylic,  $J = 16.07$  Hz), 6.71 (s, 2H, aromatic), 6.57 (m, 2H, aromatic), 6.18 (m, 2H, aromatic), 3.98 (t, 4H,  $\text{NCH}_2$ ), 1.95 (m, 4H,  $\text{CH}_2$ ), 1.77 (m, 8H,  $\text{CH}_2$ ), 1.24 (m, 28H,  $\text{CH}_2$ ), 0.86 (t, 6H,  $\text{CH}_3$ );  $^{13}\text{C}$  NMR ( $\text{CDCl}_3$ , 75.4 MHz)  $\delta$  153.97, 147.45, 133.55, 132.68, 130.92, 123.30, 121.46, 120.70, 119.06, 108.56, 107.48, 47.11, 31.89, 31.63, 29.59, 29.54, 29.49, 29.31, 29.19, 26.80, 22.65, 14.07; MALDI-TOF:  $[\text{M}+\text{H}]^+$  Calcd for  $\text{C}_{46}\text{H}_{70}\text{N}_4$ , 678.5600; found 679.1352.

**(*E, E*)-5,5'-Bis{[1-(2-ethyl) hexylpyrrol-2-yl] vinyl}-2,2'-bipyridine (1b)**

Yield: 34%; mp. 85-86 °C; FT-IR (KBr)  $\nu_{\max}$  2925, 2853, 1699, 1626, 1467, 1288, 1069, 950, 850, 711  $\text{cm}^{-1}$ ;  $^1\text{H}$  NMR ( $\text{CDCl}_3$ , 300 MHz)  $\delta$  8.70 (s, 2H, aromatic), 8.34 (d, 2H, aromatic), 7.85 (m, 2H, aromatic), 7.07 (d, 2H, vinylic,  $J = 16.08$  Hz), 6.87 (d, 2H, vinylic,  $J = 16.07$  Hz), 6.67 (s, 2H, aromatic), 6.58 (d, 2H, aromatic), 6.17 (t, 2H, aromatic), 3.93 (m, 4H,  $\text{NCH}_2$ ), 1.76 (m, 2H, CH), 1.28 (m, 16H,  $\text{CH}_2$ ), 0.89 (m, 12H,  $\text{CH}_3$ );  $^{13}\text{C}$  NMR ( $\text{CDCl}_3$ , 75 MHz)  $\delta$  153.87, 147.36, 133.53, 132.58, 130.96, 124.08, 121.20, 120.70, 119.16, 108.37, 107.34, 50.88, 41.27, 30.54, 29.65, 28.56, 23.86, 22.94, 13.98, 10.63. MALDI-TOF:  $[\text{M}+\text{H}]^+$  Calcd for  $\text{C}_{38}\text{H}_{54}\text{N}_4$ , 566.4348; found 566.8965.

**(*E, E*)-5,5'-Bis{[1-(3,7-dimethyl) octylpyrrol-2-yl] vinyl}-2,2'-bipyridine (1c)**

Yield: 43%; mp. 74 °C; FT-IR (KBr)  $\nu_{\max}$  2927, 2857, 1699, 1632, 1469, 1222, 1045, 950, 858, 712  $\text{cm}^{-1}$ ;  $^1\text{H}$  NMR ( $\text{CDCl}_3$ , 300 MHz, TMS)  $\delta$  8.71 (s, 2H, aromatic), 8.37 (d, 2H, aromatic), 7.87 (m, 2H, aromatic), 7.10 (d, 2H, vinylic,  $J = 16.04$  Hz), 6.90 (d, 2H, vinylic,  $J = 16.08$  Hz), 6.72 (s, 2H, aromatic), 6.57 (d, 2H, aromatic), 6.19 (t, 2H, aromatic), 4.02 (m, 4H,  $\text{NCH}_2$ ), 1.76 (m, 4H, CH), 1.25 (m, 12H,  $\text{CH}_2$ ), 0.85 (m, 18H,  $\text{CH}_3$ );  $^{13}\text{C}$  NMR ( $\text{CDCl}_3$ , 75.4 MHz)  $\delta$  154.01, 147.44, 133.52, 132.58, 130.72, 123.15, 121.52, 120.98, 119.34, 108.65, 107.53, 45.29, 39.11, 38.81, 37.04, 31.92, 30.03, 29.70, 29.36, 27.94, 24.61, 22.65, 22.57, 19.60, 14.11, HRMS-FAB:  $[\text{M}]^+$  Calcd for  $\text{C}_{42}\text{H}_{58}\text{N}_4$ : 618.47; Found 618.45.

**(*E,E*)-5,5'-Bis-[[[(Methoxyethoxy)ethoxy]ethyl]pyrrol-2-yl]vinyl]-2,2'-bipyridine (1d)**

Yield 45%; (Pasty solid); <sup>1</sup>H NMR (CDCl<sub>3</sub>, 300 MHz) δ 8.61 (s, 2H, aromatic), 8.29 (d, 2H, aromatic), 7.84 (d, 2H, aromatic), 7.08 (d, 2H, vinylic, *J* = 16.05 Hz), 6.80 (d, 2H, vinylic, *J* = 16.05 Hz), 6.70 (s, 2H, aromatic), 6.51 (m, 2H, aromatic), 6.12 (m, 2H, aromatic), 4.12 (t, 4H, NCH<sub>2</sub>), 3.69 (t, 4H, OCH<sub>2</sub>), 3.49 (m, 12H, OCH<sub>2</sub>), 3.43 (m, 4H, OCH<sub>2</sub>), 3.27 (s, 6H, OCH<sub>3</sub>); <sup>13</sup>C NMR (CDCl<sub>3</sub>, 75.4 MHz) δ 153.93, 147.69, 133.74, 132.84, 131.42, 123.98, 121.68, 120.94, 119.47, 109.13, 107.70, 72.05, 71.29, 71.00, 70.76, 59.16, 47.06; HRMS-FAB: [M]<sup>+</sup> Calcd for C<sub>36</sub>H<sub>46</sub>N<sub>4</sub>O<sub>6</sub>: 630.77; Found 630.76.

**4.6. References**

1. Berg, J. M.; Shi, Y. *Science* **1996**, *271*, 1081.
2. Jiang, P.; Guo, Z. *Coord. Chem. Rev.* **2004**, *248*, 205.
3. Lim, N. C.; Freake, H. C.; Brückner, C. *Chem. Eur. J.* **2005**, *11*, 38.
4. Cuajungco, M. P.; Lees, G. D. *Neurobiol. Dis.* **1997**, *4*, 137.
5. de Onis, M. Frongillo, E. A.; Blossner, M. *Bull. W. H. O.* **2000**, *78*, 1222.
6. Rurack, K. *Specrochim. Acta. A* **2001**, *57*, 2161.
7. Soroka, K.; Vithanga, R. S.; Philips, D. A.; Walker, B.; Dasgupta, P. K. *Anal. Chem.* **1987**, *59*, 629.
8. Frederickson, C. J.; Kasarskis, E. J.; Ringo, D.; Frederickson, R. E. *J. Neurosci. Methods* **1987**, *20*, 91.
9. Zalewski, P. D.; Forbes, I. J.; Betts, W. H. *Biochem. J.* **1993**, *296*, 403.
10. Mahadevan, I. B.; Kimber, M. C.; Lincoln, S. F.; Tiekink, E. R. T.; Ward, A. D.; Betts, W. H.; Forbes, I. J.; Zalewski, P. D. *Aust. J. Chem.* **1996**, *49*, 561.

11. Budde, T.; Minta, A.; White, J. A.; Kay, A. R. *Neuroscience* **1997**, *79*, 347.
12. Kimber, M. C.; Mahadevan, I. B.; Lincoln, S. F.; Ward, A. D.; Tiekink, E. R. T. *J. Org. Chem.* **2000**, *65*, 8204.
13. Kimber, M. C.; Mahadevan, I. B.; Lincoln, S. F.; Ward, A. D.; Betts, W. H. *Aust. J. Chem.* **2001**, *54*, 43.
14. Pearce, D. A.; Jotterand, N.; Carrico, I. S.; Imperiali, B. *J. Am. Chem. Soc.* **2001**, *123*, 5160.
15. De Silva, S. A.; Zavaleta, A.; Baron, d. E.; Allam, O.; Isidor, E. V.; Kashimura, N.; Percarpio, J. M.; *Tetrahedron Lett.* **1997**, *38*, 2237.
16. Haugland, R. P. *Handbook of Fluorescent Probes and Research Products, ninth ed.* Molecular Probes Inc., 2002.
17. Walkup, G. K.; Burdette, S. C.; Lippard, S. J.; Tsien, R. Y. *J. Am. Chem. Soc.* **2000**, *122*, 5644.
18. Burdette, S. C.; Walkup, G. K.; Spingler, B.; Tsien, R. Y.; Lippard, S. J. *J. Am. Chem. Soc.* **2001**, *123*, 7831.
19. Burdette, S. C.; Frederickson, C. J.; Bu, W.; Lippard, S. J. *J. Am. Chem. Soc.* **2003**, *125*, 1778.
20. Chang, C. J.; Nolan, E. M.; Jaworski, J.; Burdette, S. C.; Sheng, M.; Lippard, S. J. *Chem. Biol.* **2004**, *11*, 203.
21. Nolan, E. M.; Burdette, S. C.; Harvey, J. H.; Hilderbrand, S. A.; *Inorg. Chem.* **2004**, *43*, 2624.
22. Nolan, E. M.; Lippard, S. J. *Inorg. Chem.* **2004**, *43*, 8310.
23. Hirano, T.; Kikuchi, K.; Urano, Y.; Nagano, T. *J. Am. Chem. Soc.* **2000**, *122*, 12399.
24. Hirano, T.; Kikuchi, K.; Urano, Y.; Nagano, T. *J. Am. Chem. Soc.* **2002**, *124*, 6555.
25. Fan, J.; Wu, Y.; Peng, X. *Chem. Lett.* **2004**, *33*, 1392.

26. Fan, J.; Peng, X.; Wu, Y.; Lu, E.; Hou, J.; Zhang, H.; Zhang, R.; Fu, X. *J. Luminiscence* **2004**, *33*, 1392.
27. Lim, N. C.; Brückner, C. *Chem. Commun.* **2004**, 1094.
28. Huston, M. H.; Haider, K. W.; Czarnik, A. W. *J. Am. Chem. Soc.* **1988**, *110*, 4460.
29. Akkaya, E. U.; Huston, M. H. Czarnik, A. W. *J. Am. Chem. Soc.* **1990**, *112*, 3590.
30. Czarnik, A. W. *Acc. Chem. Res.* **1994**, *27*, 302.
31. Koike, T.; Watanabe, T.; Aoki, S.; Kimura, E.; Shiro, M. *J. Am. Chem. Soc.* **1996**, *118*, 12696.
32. Kimura, E.; Koike, T. *Chem. Soc. Rev.* **1998**, *27*, 179.
33. Hirano, T.; Kikuchi, K.; Urano, Y.; Higuchi, T.; Nagano, T. *Angew. Chem. Int. Ed.* **2000**, *39*, 1052.
34. Burdette, S. C.; Lippard, S. J. *Inorg. Chem.* **2002**, *41*, 6816.
35. Lim, N. C.; Yao, L.; Freake, H. C.; Brückner, C. *Bioorg. Med. Chem. Lett.* **2003**, *13*, 2251.
36. Lakowicz, J. R. *Principles of Fluorescence Spectroscopy*, 2<sup>nd</sup> ed. Kluwer Academic/Plenum: New York, 1999.
37. Maruyama, S.; Kikuchi, K.; Hirano, T.; Urano, Y.; Nagano, T. *J. Am. Chem. Soc.* **2002**, *124*, 10650.
38. Lim, N. C.; Schuster, J. V.; Porto, M. C.; Tanudra, M. A.; Yao, L.; Freake, H. C.; Brückner, C. *Inorg. Chem.* **2005**, *44*, 2018.
39. Chang, C. J.; Jaworski, J.; Nolan, E. M.; Sheng, M.; Lippard, S. J. *Proc. Natl. Acad. Sci. USA.* **2004**, *101*, 1129.
40. Woodroffe, C. C.; Lippard, S. J. *J. Am. Chem. Soc.* **2003**, *125*, 11458.
41. Taki, M.; Wolford, J. L.; O'Halloran, T. V. *J. Am. Chem. Soc.* **2004**, *126*, 712.

---

**LIST OF PUBLICATIONS**

1. A Ratiometric Fluorescence Probe for Selective Visual Sensing of Zn<sup>2+</sup>  
Ajayaghosh, A.; Carol, P.; Sreejith, S.  
*J. Am. Chem. Soc.* **2005**, *127*, 14962.
2. Ratiometric and Near-Infrared Molecular Probes for the Detection and Imaging of Zinc Ions  
Carol, P.; Sreejith, S, Ajayaghosh, A.  
*Chem. Asian J.* **2007**, *2*, 338.
3. Squaraine Dyes: a mine of Functional Molecular Materials  
Sreejith, S.; Carol, P.; Chithra, P.; Ajayaghosh, A.  
*J. Mater. Chem.* **2007**, *18*, 264.
4. Low Band Gap Squaraine Dyes and Polysquaraines: Role of Aromatic Bridging Units in Optical and Conducting Properties (*under preparation*)
5. Synthesis, Characterization and Aggregation Properties of a few Bispyrrole Derived Squaraine Dyes: Effect of Alkyl Side Chains on the Aryl Bridging Moiety (*under preparation*)

---

**POSTERS PRESENTED AT CONFERENCES**

1. Ratiometric Sensing Of  $\text{Cu}^{2+}$  and  $\text{Zn}^{2+}$  Using Fluorescent Bispyrrole Based Ion Probes.  
**Priya Carol** and Ayyappanpillai Ajayaghosh.  
7<sup>th</sup> National Symposium in Chemistry, IACS, Kolkatha, India, February 4-6, 2005.
2. Near Infrared Absorbing Conjugated Polymers: Controlling Optical Band Gap in Polysquaraines by Structural Modification.  
**Priya Carol**, Joby Eldo and Ayyappanpillai Ajayaghosh  
International Conference on Polymers for Advanced Technologies, MACRO 2004, Trivandrum, India, December 14-17, 2004.
3. Towards Near Infrared Absorbing  $\pi$ -Conjugated Systems: Tuning Optical Properties in Polysquaraines.  
**Priya Carol** and Ayyappanpillai Ajayaghosh  
6<sup>th</sup> National Symposium In Chemistry, IIT Kanpur, Utter Pradesh, India, February 6-8, 2004.
4.  $\pi$ -Extended Squaraine Dyes: Control Of Aggregation By Side Chain Interactions.  
**Priya Carol** and Ayyappanpillai Ajayaghosh  
3<sup>rd</sup> Trivandrum International Symposium on Recent Trends in Photochemical Sciences, NIIST, Trivandrum, India, January 5-7, 2004.